Dissertations, Master's Theses and Master's Reports - Open

Dissertations, Master's Theses and Master's Reports

2006

Exploration of Ground Penetrating Radar and Time Domain Reflectometry Methods for the Determination of Pavement Dielectric Constant

Baron W. Colbert
Michigan Technological University

Follow this and additional works at: https://digitalcommons.mtu.edu/etds

Part of the Geophysics and Seismology Commons

Recommended Citation

Exploration of Ground Penetrating Radar and Time Domain Reflectometry Methods
for the Determination of Pavement Dielectric Constant

By

Baron W. Colbert

A THESIS

Submitted in partial fulfillment of the requirements

For the degree of

MASTER OF SCIENCE IN GEOPHYSICS

MICHIGAN TECHNOLOGICAL UNIVERSITY

2006
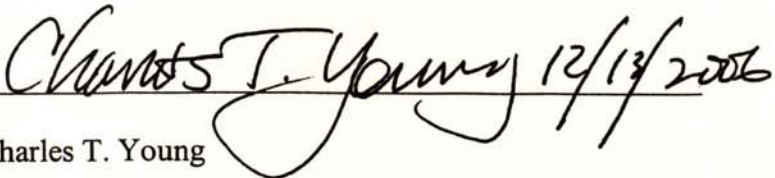
This thesis, "Exploration of Ground Penetrating Radar and Time Domain Reflectometry Methods for the Determination of Pavement Dielectric Constant," is hereby approved in partial fulfillment of the requirements for the Degree of MASTER OF SCIENCE IN APPLIED GEOPHYSICS

DEPARTMENT:

Geological and Mining Engineering and Sciences

Signatures:

Thesis Advisor: _Charles T. Young_   12/13/2006

Charles T. Young

Department Chair: _Wayne P_____

Wayne D. Pennington

Date: 13 December 2006

ABSTRACT

Traditionally, densities of newly built roadways are checked by direct sampling (cores) or by nuclear density gauge measurements. For roadway engineers, density of asphalt pavement surfaces is essential to determine pavement quality. Unfortunately, field measurements of density by direct sampling or by nuclear measurement are slow processes. Therefore, I have explored the use of rapidly-deployed ground penetrating radar (GPR) as an alternative means of determining pavement quality. The dielectric constant of pavement surface may be a substructure parameter that correlates with pavement density, and can be used as a proxy when density of asphalt is not known from nuclear or destructive methods. The dielectric constant of the asphalt can be determined using ground penetrating radar (GPR).In order to use GPR for evaluation of road surface quality, the relationship between dielectric constants of asphalt and their densities must be established. Field measurements of GPR were taken at four highway sites in Houghton and Keweenaw Counties, Michigan, where density values were also obtained using nuclear methods in the field. Laboratory studies involved asphalt samples taken from the field sites and samples created in the laboratory. These were tested in various ways, including density, thickness, and time domain reflectometry (TDR).

In the field, GPR data was acquired using a 1000 MHz air-launched unit and a ground-coupled unit at 200 and 400 MHz. The equipment used was owned and operated by the Michigan Department of Transportation (MDOT) and available for this study for a total of four days during summer 2005 and spring 2006. The analysis of the reflected waveforms included "routine" processing for velocity using

commercial software and direct evaluation of reflection coefficients to determine a dielectric constant. The dielectric constants computed from velocities do not agree well with those obtained from reflection coefficients. Perhaps due to the limited range of asphalt types studied, no correlation between density and dielectric constant was evident.

Laboratory measurements were taken with samples removed from the field and samples created for this study. Samples from the field were studied using TDR, in order to obtain dielectric constant directly, and these correlated well with the estimates made from reflection coefficients. Samples created in the laboratory were measured using 1000 MHz air-launched GPR, and 400 MHz ground-coupled GPR, each under both wet and dry conditions.

On the basis of these observations, I conclude that dielectric constant of asphalt can be reliably measured from waveform amplitude analysis of GJPR data, based on the consistent agreement with that obtained in the laboratory using TDR. Because of the uniformity of asphalts studied here, any correlation between dielectric constant and density is not yet apparent.

Table of Contents

List of Figures

List of Tables

ACKNOWLEDGEMENTS

my like. Most of all I want to thank the Lord Jesus Christ who has been with me

through everything.

CHAPTER 1. INTRODUCTION

This thesis describes a series of three electromagnetic experiments applied to asphalt pavement to develop a process of obtaining consistent dielectric constant data. The results in principle could then be used to correlate with other physical properties of the pavement. The first experiment involved obtaining Ground Penetrating Radar (GPR) data from newly paved roadways in Houghton County, MI with ground-coupled and air-launched GPR antennas. The second experiment involved creating pavement samples manufactured at Michigan Technological University. These samples then were analyzed by ground coupled and air launched GPR antennas to determine their dielectric constant under variable moisture conditions. The final experiment involved calculating dielectric constant with a time domain reflectometer on various pavement samples provided by the Civil Engineering program at Michigan Tech. These methods were used to determine if dielectric constant can consistently be determined by GPR surveys when compared to actual roadway core information. For this study the research plan was significantly affected by the availability of ground penetrating equipment; the radar equipment and interpretation software was only available for four days since it was owned by the Michigan Department of Transportation.

CHAPTER 2. BACKGROUND

Ground penetrating radar has emerged as a developing technology in evaluating roadway conditions. An engineer using GPR can quickly identify defects within the pavement surface nondestructively and propose the best repair strategy (Saarenketo & Scullion, 2000). Using GPR waveforms, dielectric constant, density, void ratio, and pavement moisture content can be determined (Saarenketo & Scullion, 2000).

The use of ground penetrating radar for roadways started in the mid 1970's to scan for tunnels; GPR was used later to scan bridge decks (Saarenketo & Scullion, 2000). In 1985, the Federal Highway Administration first implemented a GPR system for roadways (Morey, 1998). Today, GPR surveys are performed on roadways in order to collect information about the condition of a given pavement area (Morey, 1998). By providing the engineer a continuous profile of the pavement subsurface, more information about the roadway is known than just pavement cores alone (Morey, 1998). GPR has been successful in detecting moisture in hot mix asphalt layers, finding moisture in the base layer of pavement, and evaluation of geosynthethic material performance used within pavement layers (Lahouar et al., 2002). GPR survey crew usually includes a van driver, a radar operator/interpreter, and a drill and core operator (Morey, 1998). GPR data can be collected at a rate of 100 scans/second and survey speeds can take place up to 100 km/hr (Morey, 1998). Finally, GPR surveys can take place at any time except under wet or rainy surface conditions (Morey, 1998).

Three topics of interest to experts in the roadway industry relating to GPR use are: First, developing standard specifications for pavement performance and measurements for producing consistent results (Morey, 1998). Second, understanding how electrical parameters of roadway materials correlate to moisture, strength, and deformation conditions in roadways (Saarenketo & Scullion, 2000). And thirdly, determining dielectric constant of roadway pavements. The dielectric constant is of major importance in determining the correlation between GPR data and pavement conditions. Interest in correlating dielectric constant in pavement materials to physical properties of geological and pavement materials was led by researchers such as Maser (1992), Olhoeft (1999), Martinez & Byrnes (2001), and Saarenketo & Scullion (1996) in the mid 1980's through the early 2000's.

More recently, Saarenketo (2000), Scullion (2000), Rmeili (1997), and Wimsatt (1998) from the Texas Transportation Institute have conducted studies of GPR applications in the use of pavement evaluation. They focused on identifying roadway evaluation applications with air launched and ground coupled GPR antennas. For example, Maser & Scullion (1992) detailed the continuous profiling ability of GPR to predict pavement thickness and pavement properties at strategic highway research locations in Texas (Maser & Scullion, 1992). These studies predicted pavement thickness within .32 inches with GPR data alone and thickness to within .11 inches with a calibration core (Maser & Scullion, 1992).

The topic of determining the velocity of radar waves in pavement with GPR was also studied at this time. Lahouar(2002) adapted the common midpoint method used in seismology to calculate an in-situ dielectric constant of pavements on

3

Interstate 81 in Virginia, and concluded that the dielectric constant determined from GPR when compared to asphalt cores yielded an average error of 6.8% (Lahouar, 2002). Reppert (2000) presented a method to calculate GPR layer velocities using Brewster angles with a common midpoint survey. This study resulted in reasonable dielectric constant values using Brewster angles as compared to determining dielectric constant values from known velocities. Finally Lanbo Liu (2002) determined the dielectric constant to laboratory samples of pavement materials. He placed 30 pavement samples under various moisture conditions and then correlated the results with the sample void ratio and binder content (Liu, 2002). This study concluded that: the electromagnetic wave velocities were greatest in dry conditions and slowest in wet conditions, electromagnetic wave velocities increased slightly with an increase of void ration in dry samples, and that pavement electromagnetic wave velocity and dielectric constant can be predicted using the effective medium theory (Liu, 2002).

Currently research is focused on predicting the conditions where GPR is effective (Morey, 1998). Future research areas for GPR include establishing techniques in road analysis and rehabilitation (Saarenketo, and Scullion, 2002).

CHAPTER 3. Ground Penetrating Radar Road Surveys

Ground Penetrating Radar Principles

Ground Penetrating radar systems rely on various principles of electromagnetism which helps one to understand how GPR can scan the roadway subsurface. The GPR systems send electromagnetic pluses from the antenna onto the roadway and then records the pulse reflected from the surface and subsurface (Al-

Qadi et al., 2005). The electromagnetic wavelet is described as the reflected pulse from the initial generation of the GPR signal with a central maximum and two local signal minima approximately one nanosecond apart (Serbin & Or, 2004). Another definition of a *wavelet* is a brief wave pulse which contains many frequencies and is time limited, meaning that this wave only is in existence for a given period of time instead of oscillating forever (Liner, 2004). Figure 3.1 shows a typical GPR wavelet along with the wavelets from the surface and bottom of the first pavement layer.
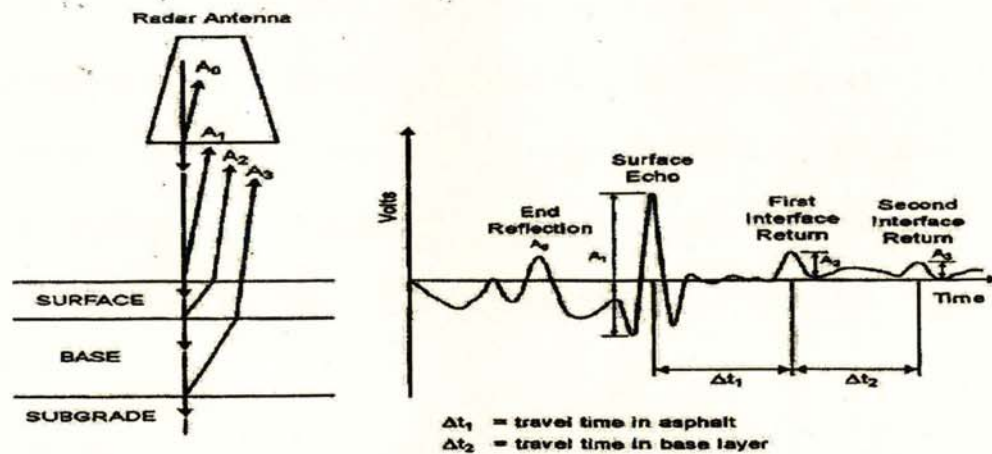
Figure 3.1: GPR wavelet example showing wavelet reflection returns depicting the principles of GPR where the incident wave is reflected at each layer interface and plotted as return voltage against time of arrival in nanoseconds

Factors which affect GPR signal propagation include the dielectric constant and electrical conductivity of a given layer (Saarenketo & Scullion, 1996). The reflected signal of the GPR wavelets are recorded from the subsurface, and the resulting GPR signal results due to the contrasts in the dielectric properties of the subsurface pavement system (Al-Qadi et al., 2005). The amplitude of the reflected signal at each layer interface is a function of dielectric constant contrast between pavement layers (Saarenketo & Scullion, 1994). For flexible asphalt pavement

surfaces these contrasts rely primarily on the moisture contrast between pavement layers (Saarenketo & Scullion, 1994).

GPR systems typically have 3 components: a pulse generator, a transmitter-receiver, and a sampler/recorder (Saarenketo & Scullion, 2000). Common assumptions associated with GPR analysis include that the subsurface materials are homogenous, that the subsurface materials are lossless, and that the relative permeability of air is unity (Alongi et al., 1982).

Ground Penetrating Radar surveys gather vast amounts of roadway data per survey. GPR roadway surveys can generate a continuous profile of the roadway which provides more information on the roadway condition than roadway cores alone (Morey, 1998). Varying the GPR vehicle speed only affects the trace spacing of the collected data; typically, GPR is able to collect traces every 1 to 3 ft (Maser & Scullion, 1998).

The personnel for the roadway evaluation team include the GPR operator/interpreter and driller who take cores from the roadway (Morey, 1998). Typical techniques used within the survey include the reflection technique with an air launched horn antenna, common depth point method, and Radar Surface Arrival Detection method, and TDR and electric measurements based on capacitance measurements (Saarenketo & Scullion, 1994). The dielectric constant is related to the velocity of radar waves in the material and the velocity of radar waves in free space by: $\varepsilon = \left(C/V \right)^{2}$ with c as the speed of light and v as layer velocity (Lahouar et al., 2002). With the common depth point method dielectric constant is determined also by the amplitudes of reflected pulses with an air launched antenna (Al-Qadi et al., 2005).

6

GPR interpretations consist of detecting roadway layer interfaces and using electromagnetic wavelet traveling through the pavement subsurface (Saarenketo & Scullion, 2000). These interpretations result in pavement subsurface profiles indicating pavement depth on a time scale (Saarenketo & Scullion, 2000). GPR waveforms indicate two-way travel for wavelets to travel from the GPR transmitter to receiver (Saarenketo & Scullion, 1996). In order to change from the time scale to depth scale the roadway layer dielectric constant has to be estimated. Software is provided with the GPR to allow the interpreter to acquire, process, interpret, visualize, and integrated GPR data (Saarenketo & Scullion, 2000).

For the typical GPR survey two types of GPR antenna are used, an "air-launched" horn antenna which is suspended about 30 cm about the roadway, and a ground coupled GPR antenna which is placed directly on the pavement surface shown in Figure 3.2.
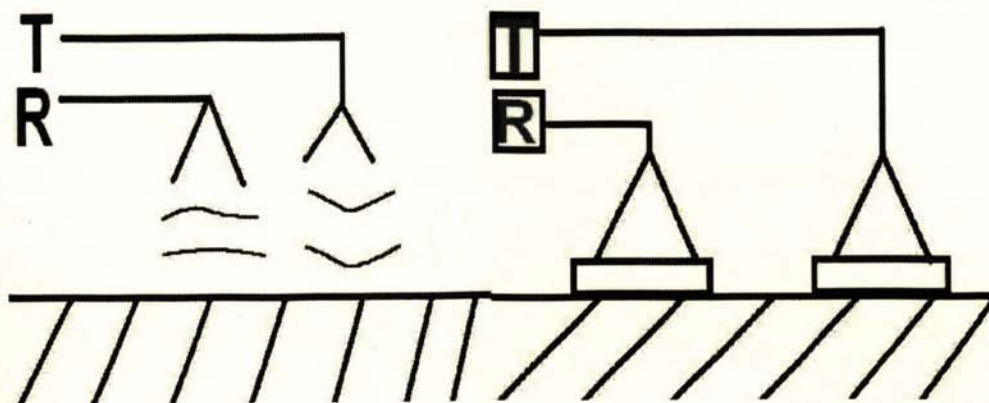
Figure 3.2: Air Launched Antenna (left) transmitter T and receiver R & Ground Coupled GPR antenna transmitter T and receiver R (right)

The air launched horn antenna allows the radar to be used at a high speed and provides well defined directional footprint and subsurface visualization

capabilities for the pavement engineer (Serbin and Or, 2004). Ground coupled

antennae operated from 80 – 1500 MHz (Saarenketo and Scullion, 2000), and provide

a greater depth of penetration than air-launched antennae (Saarenketo and Scullion,

2000). The major disadvantage of using an air launched horn antenna is that its depth

of penetration is only a few inches as most of the electromagnetic signal is reflected

at the air/roadway interface (Al-Qadi et al., 2005). Additionally, air launched GPR

antennae must be subjected to calibration procedures using a large metal plate to

normalize reflected signals (Morey, 1998). One difficulty of using the ground coupled

antennae is the surface coupling and ringing (Saarenketo & Scullion, 2000). In order

to overcome these difficulties, signal processing may be needed (Saarenketo &

Scullion, 2000). Another disadvantage of using ground coupled antennae is the

slower rate of collecting data versus air launched antennae (Al-Qadi et al., 2005).

The ground coupled antenna must move at a slower rate than the air launched antenna

to avoid self destruction of the antenna on the pavement surface.

The equipment for the GPR survey in 2005 used equipment manufactured by

Geophysical Survey Systems, Inc. (GSSI), which includes the GPR antennas,

software, and a controller data logger. With the air launched antennas, this GPR

system is capable of obtaining subsurface images of the pavement layers from a

frequency range of 400 MHz to 1 GHz, corresponding to depths of a few inches to

several feet.

8

Reflection Coefficient Basics

The reflection coefficient is an important concept in GPR data analysis. The definition of the reflection coefficient is the ratio of the amplitudes of the reflected wave and incident wave (Reynolds, 1997). The assumption for the reflection in GPR work is the wave is a vertically incident wave involving no spreading. The reflection coefficient is also a related to relative dielectric constant at the layer boundary (Morey, 1998). This thesis assumes that the reflection coefficient is defined to be normally incident only. Understanding the reflection coefficient behavior at pavement boundaries is important for understanding GPR images and interpretation limits (Martinez & Byrnes, 2001). The reflection coefficient is calculated from layer to layer

by the formula
$$RC = \frac{\sqrt{\varepsilon_{r_1}} - \sqrt{\varepsilon_{r_2}}}{\sqrt{\varepsilon_{r_1}} + \sqrt{\varepsilon_{r_2}}}$$
(Al-Qadi et al., 2005). Where ε_{r_1} and

ε_{r_2} are the dielectric constant values of the first medium and second media, respectively. Typically, reflection coefficients range from .2 for sand and -1 for metal. Thus returning echoes for GPR depend on the material (Alongi et al., 1982). Finally reflection coefficients are valid only at vertical normal incidences but in practice, angles of incidence within 20 degrees of normal are used (Serbin & Or, 2004).

Dielectric Constant Basics

Dielectric constant is an important parameter in GPR analysis. A simple definition of the dielectric constant is the factor κ which increases capacitance of a capacitor when a dielectric material is inserted in place of a vacuum (Serway and Belcher, 2000). This factor helps the pavement engineer estimate various physical

9

parameters of pavement, such as layer velocity, thickness, density, and moisture content. Dielectric constant is an important parameter because it is linked to the propagation velocity of GPR electromagnetic waves through a given media and the resulting reflection coefficient at the pavement layer interface (Martinez & Byrnes, 2001). Moisture significantly affects the bulk dielectric constant value of pavement materials as it has a value of 81(Martinez & Byrnes, 2001). The dielectric constant of water is much higher than any geologic or most roadway materials. Therefore small changes in pavement moisture content have a great effect on pavement dielectric constant or reflection coefficient values. Dielectric constant values are related to

reflection amplitudes by the following formula:

$$\varepsilon_{r_1} = \left(\frac{1 + \dfrac{A_0}{A_p}}{1 - \dfrac{A_0}{A_p}} \right)$$

where A_0 is

the pavement surface amplitude and A_p is the metal plate amplitude (Al-Qadi et al., 2005). The metal plate is used as a calibration reference for complete reflection when the air launched GPR is scanned over the plate.

The dielectric constant of the pavement surfaces can vary according to aggregate type and moisture conditions (Lahouar et al., 2002). Signal attenuation (due to scattering) upon the pavement surface can also create errors in dielectric constant calculations (Saarenketo, 1996). Attenuation is not a major factor affecting pavement dielectric constant in good quality pavement layers (Saarenketo, 1996). Dielectric constant values vary in value according to the pavement type as shown by Wimsatt(1998): ε for pavement composed of normal aggregate ε ranged from 5 – 6.5.

Pavement composed of lightweight aggregate ε ranged from 3.5-4.5 in the Liu (2002)

study, and for flexible base pavement dielectric constant values ranged from 7-10

(Wimsatt, 1998). In the Wimsatt (1998) study dielectric constant values lower than

3.5 indicated excessive air voids and dielectric constant values higher than 10

indicated excessive pavement moisture (Wimsatt, 1998). In the Al-Qadi(2005) study

laboratory manufactured hot mix asphalt samples were tested with an air launched

horn antenna and network analyzer resulted in dielectric constant values of 3.7-5.2 for

dry samples and 4.1 to 5.3 for water saturated samples(Al-Qadi & Lahouar, 2005).

For pavement quality control applications Saarenketo's (2000) study showed that the

pavement dielectric constant was around 5.5 in the center of the pavement slabs, and

approximately 4.5 at the pavement joints.

Dielectric constant "mixing" models are used as a tool to calculate pavement

dielectric constant of pavement layers from a known mixture. Mixing models express

the bulk dielectric constant of a medium as a function of the dielectric constants of

the constituent materials. Dielectric constant models can be used to understand

recorded travel times and amplitudes obtained from GPR traces (Martinez & Byrnes,

2001). One type of dielectric constant mixing models is based on time propagation

accounting for the bulk volume fraction of the pavement material V and ε of the

pavement material (Martinez & Byrnes, 2001). This formula is:

$$\varepsilon_{Composite} = \left[\sum V_i \sqrt{\varepsilon_{r_i}} \right]^2$$ where i is the ith component of the model and

is valid at the specific frequency where ε is represented and for predicting the

dielectric constant of low conductivity non magnetic materials (Martinez & Byrnes,

2001). Generally this mixing model formula can be expressed assuming asphalt is composed of air voids, aggregates, binder, and moisture is:

$$\sqrt{\varepsilon_{HMA}} = V_{air} i \sqrt{\varepsilon_{air_i}} + V_{agg} i \sqrt{\varepsilon_{agg_i}} + V_{binder} i \sqrt{\varepsilon_{binder_i}} + V_{water} i \sqrt{\varepsilon_{water_i}}$$

(Al-Qadi, 2005). The dielectric constants of asphalt pavement materials correlate to volumes which compose the model, which indicate discontinuities or distress in pavement (Al-Qadi, 2005). In a hot mix asphalt, the dielectric constant correlates with density, air voids, asphalt content, and moisture within the pavement layers (Al-Qadi, 2005). Figure 3.3 shows an example of a conceptual model of the dielectric constant mixing model.

GPR Wave

d is distance and volume fraction
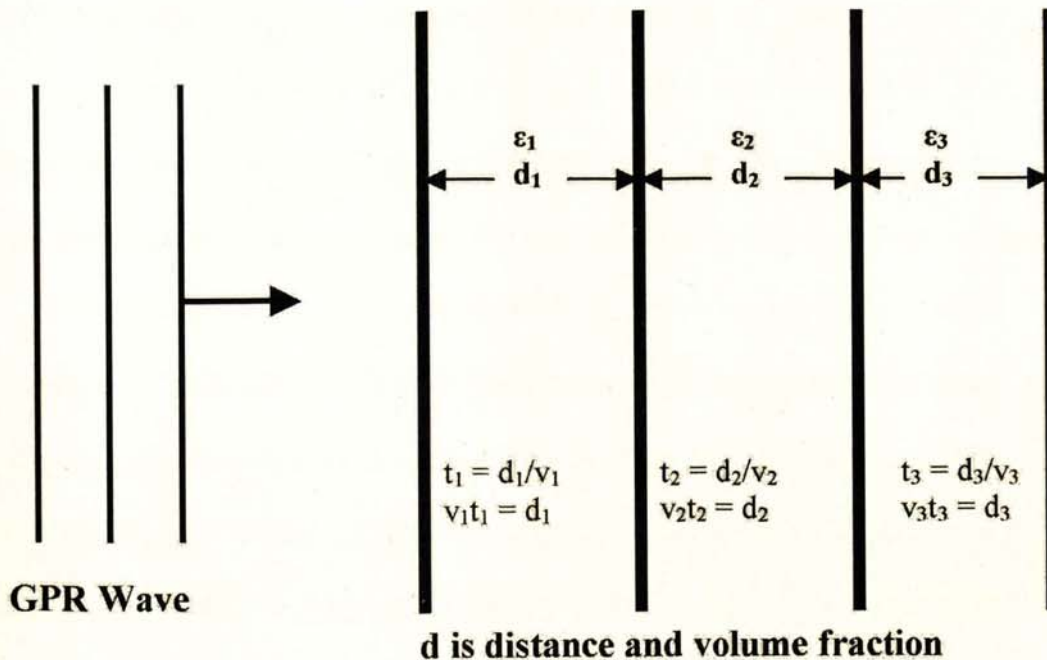
Figure 3.3: Dielectric Constant Mixing Conceptual Model

Total travel time for this model above is related to distance and velocity by the formula:

$$traveltime = t_1 + t_2 + t_3 = \frac{d_1}{v_1} + \frac{d_2}{v_2} + \frac{d_3}{v_3} = \frac{d_1}{c/\sqrt{\varepsilon_1}} + \frac{d_2}{c/\sqrt{\varepsilon_2}} + \frac{d_3}{c/\sqrt{\varepsilon_3}} = \frac{1}{c\sqrt{\varepsilon_{bulk}}}$$

The dielectric constant model formulas assume that the pavement layers are homogeneous, and are composed of lossless materials (Al-Qadi, 2005). Within rocks and sediment the dielectric constant is a function of mineralogy, porosity, pore fluids, frequency, rock geometry, and electrochemical relations between rock components (Martinez & Byrnes, 2001). In general, one should expect the dielectric constant of pavement to be frequency dependant but (Lahouar, 2002) showed that the dielectric constant variation was not significant when compared across the typical GPR operating bandwidth. The typical dielectric constant value regarding frequency is that ε generally decreases with increasing frequency but the values are relatively constant over the typical GPR frequency range of 25 – 1500 MHz (Martinez & Byrnes, 2001).

If the dielectric constant is correctly estimated, then the pavement engineer can use the radar trace data to calculate: pavement layer thickness, pavement layer velocity, and pavement moisture content. To evaluate the pavement thickness from the GPR data the time difference between layer reflections and velocity between pavement layers need to be measured (Morey, 1998). This depends on strong GPR reflections at the layer interfaces which work well on flexible pavements (Morey, 1998). As for thin asphalt layers with different aggregate types small positive reflections will appear on the GPR trace at each interface (Scullion & Rmeili, 1997).

Pavement layer thickness can be calculated by thickness $= \dfrac{c*\Delta t}{2*\sqrt{\varepsilon_r}}$ where c is the

speed of light and ε_r is the dielectric constant at the rth layer (Lahouar et al., 2002). In

the (Morey, 1998) study it was found that pavement thickness using GPR

interpretation programs versus pavement cores were accurate to within +- 7.5% for

finding asphalt thickness.

Water saturation is a variable that is important for accurate GPR interpretation

(Martinez & Byrnes, 2001). From the Martinez and Byrnes (2001) study it was shown

that water exerted a first order influence on bulk dielectric constant values (Martinez

& Byrnes, 2001). High amplitudes in reflected GPR wavelets correlate to moisture

filled voids (Saarenketo & Scullion, 1994). If the pavement base layer moisture

content increases then the amplitude of the reflection from the top of the base layer

will also increase (Scullion & Rmeili, 1997). The dielectric constant value of water is

81(Wimsatt, 1998).

Site Location and Conditions

Ground Penetrating Radar Field Survey

Four sites were selected for the May 2005 GPR field survey to conduct air

launched and ground coupled GPR experiments:

1. US-41 in Allouez, MI M-26 in

2. Houghton County, MI near Twin Lakes State Park,

3. Five Mile Point Road in Keweenaw County, MI

4. Lac La Belle Road in Keweenaw County, MI near the Little Betsy River.

The weather conditions on the 11th of May were mostly cloudy with a temperature of 40 °F. The weather on the 12th of May was partly sunny with a slight breeze and a temperature of 42 °F.

Equipment and Calibration

The 2005 GPR survey was carried out by using GSSI 4108 1000 MHz air-launched horn antenna, a metal sheet which provided unity reflection coefficients for the survey, with the GSSI SIR 10 data collection system.

Data Collection

For the 2005 and 2006 GPR surveys data was acquired by the GSSI Radan Roadway software and stored on a laptop computer provided by the Michigan Department of Transportation. Also GPR data was acquired on one channel for the 1 GHz air launched GPR survey in 2005 and for the ground coupled GPR data in 2005.

Preliminary Roadway Setup

Core locations and distance marks were placed at each roadway site. Core locations were marked every 30 feet beginning at the start of the roadway location and ending 300 feet from the start of the roadway site. In order to address safety concerns about collecting GPR data at each of the roadway sites it was decided that the GPR data would be collected along the shoulder of the roadway to avoid extensive lane closures.

GPR Data Collection

After securing the roadway sites for data collection, the process of generating roadway scans from the GPR antennas begun. The steps that involve roadway GPR collection for this survey are the calibration of the air launched GPR antenna, positioning personnel for electronically marking the roadway core locations, and placing the ground coupled antenna in position for use with the GPR survey van. Data collection for the air launched antenna survey took place at a rate of approximately 39 nanoseconds/sample. This survey phase started with a bounce test. The bounce test calibrates the air launched antenna with a standard aluminum roadway construction sign. The bounce test or "rocking the van" calibrates the air launched antenna by providing the reference amplitude for a reflection coefficient of unity at various heights above the road. Afterward the van driver and helper marked the core location and were placed into position at the starting location for the survey. Finally the van driver and helper would mark core locations and scan the roadway surface with the GPR antenna.

Comparison of MATLAB Wavelet Results vs. Pavement Density

In order to explore the capabilities of GPR to determine the dielectric constant of pavement and its relationship to density, a series of calibration procedures were performed. For the 2005 GPR survey it was decided that the relationship between pavement density and waveform amplitude A_o would be tested. A_o is the pavement surface amplitude calculated from the GPR wavelet. The following figures 3.4

16

through 3.9 show A_o plotted vs. core density and nuclear density of the pavement as well as core density versus nuclear density at each of the sites.
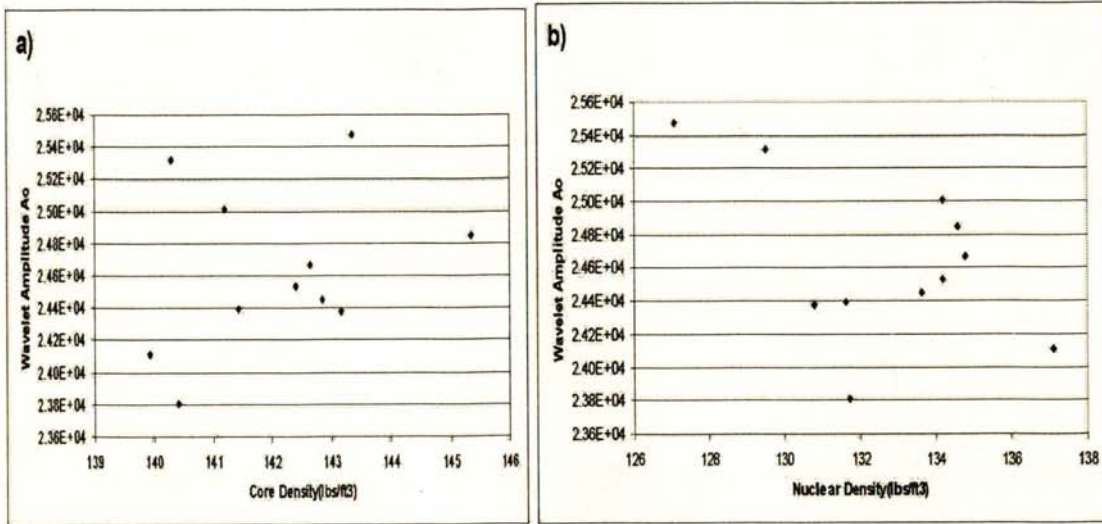
Figure 3.4: Lac La Belle Waveform Amplitude vs. Core Density(a) and Amplitude vs. Nuclear Density Graphs (b)
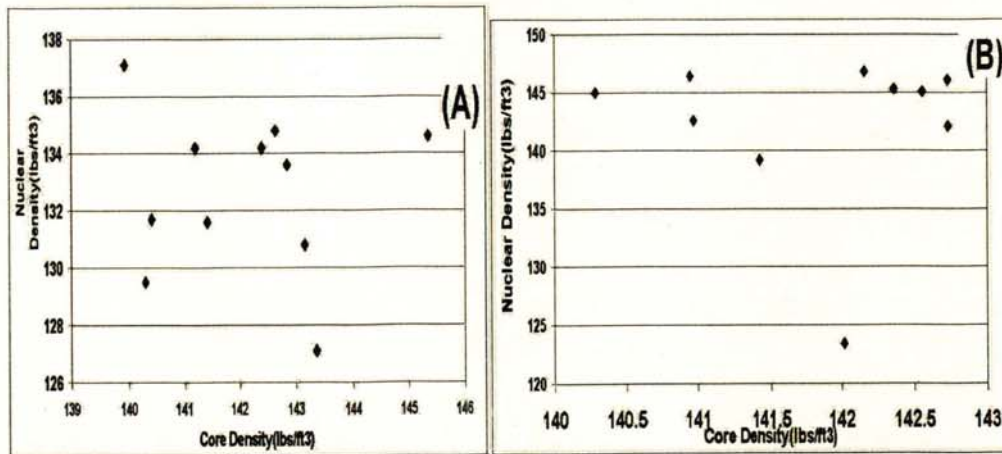
Figure 3.5: Core Density vs. Nuclear Density for (a)Lac La Belle and (b) M-

26

17
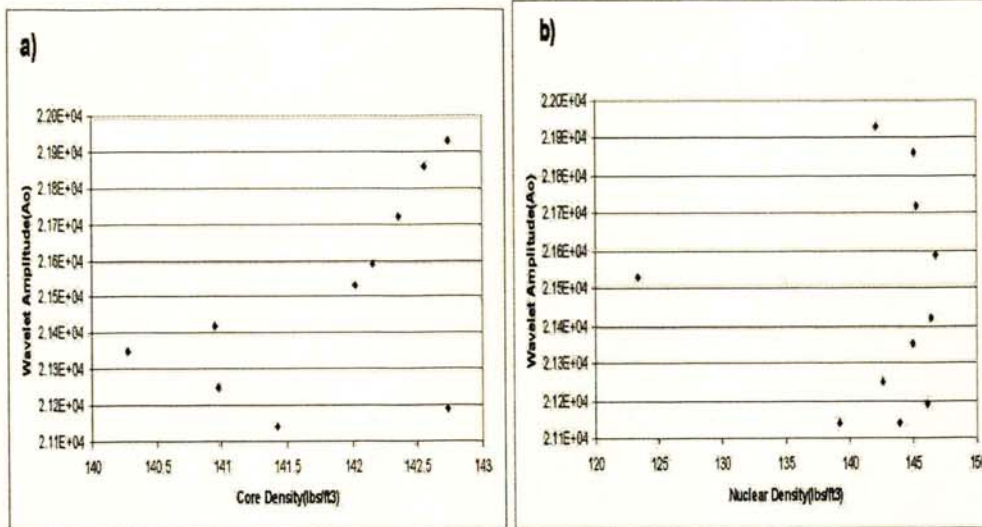
Figure 3.6: M-26 Waveform Amplitude vs. Core Density(a) and Amplitude vs. Nuclear Density Graphs (b)
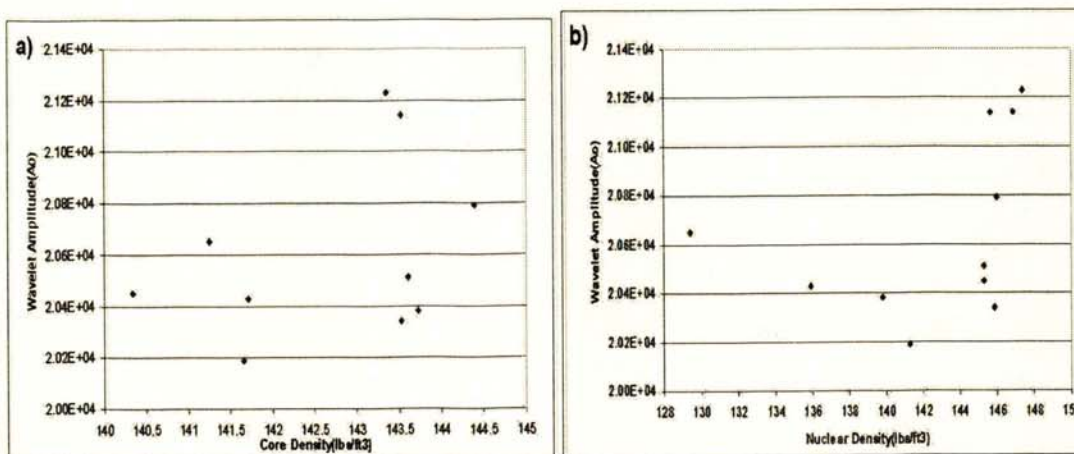
Figure 3.7: US 41 Waveform and Amplitude vs. Core Density(a) and Amplitude vs. Nuclear Density Graphs (b)
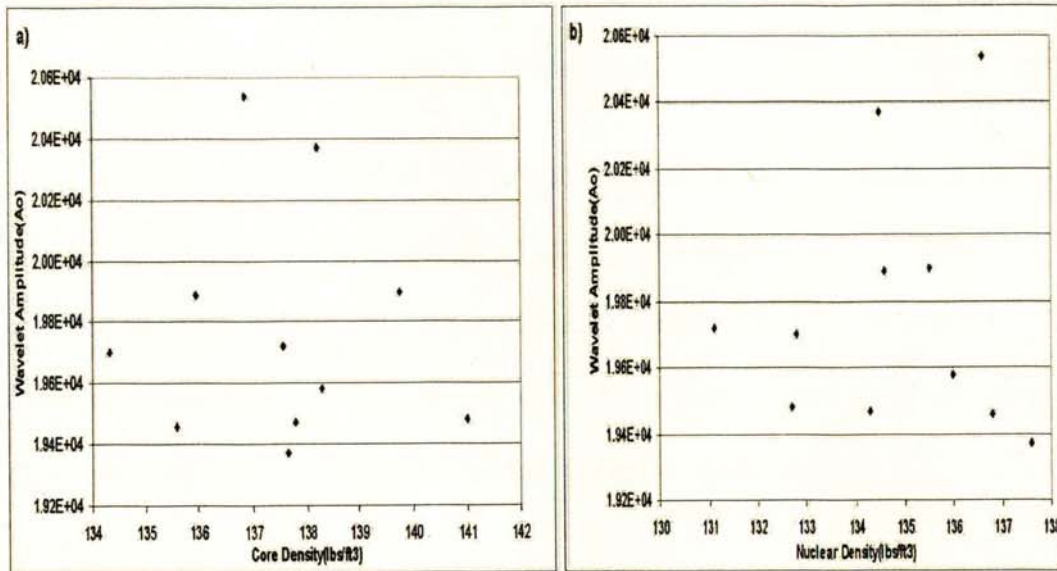
Figure 3.8: 5 Mile Point Road Waveform Amplitude vs. Core Density(a) and Amplitude vs. Nuclear Density Graphs (b)
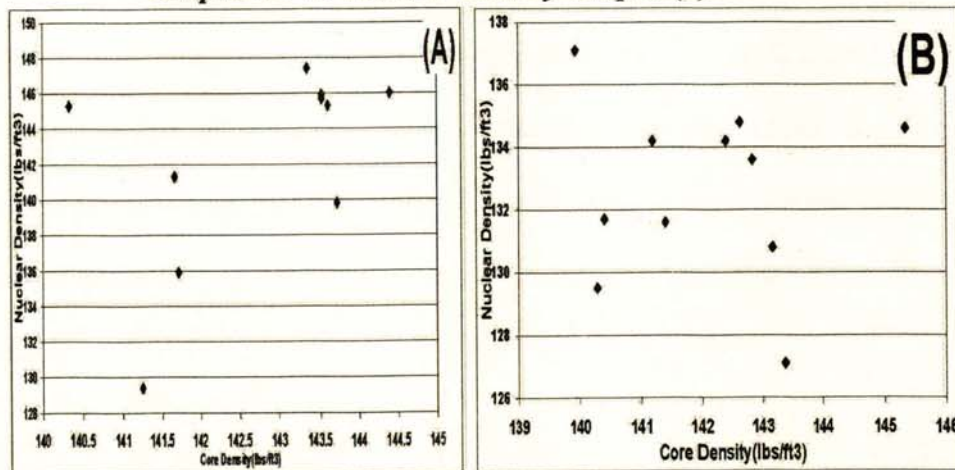
Figure 3.9: Core Density vs. Nuclear Density for (a) US-41 and (b) Five Mile Point Road

Based on the graph of waveform amplitudes vs. density there does not appear to be a direct correlation that between A_o and density. One possible explanation for this is an inadequate spread of densities to gather A_o values from, because many of

the charts above show a density spread of 10 lbs/ft^3 or less are dominated by random

fluctuations Thus, due to a lack of density spread, calibrations using samples of

known densities were attempted to be implemented in the GPR laboratory study.

As a result, the data from the GPR study produced mixed results. From this

survey the author desired a better understanding of the relationship of dielectric

constant and GPR waveforms. This understanding was obtained by measuring

dielectric constants with manufactured pavement samples indirectly with the radar

equipment, and more directly with the time domain reflectometer.

MATLAB Data Analysis Methods

In order to gather dielectric constant and GPR waveform amplitude data, a

series of MATLAB programs were used to analyze the Radan Roadway software

data. The cllickerplot program is listed in Appendix C. In order to read Radan

Roadway software files the MATLAB program gssi3 was used (Baradello, 2006).

Gssi3 in combination with program 'cllickerplot' were used to analyze GPR wavelets

at each core location. Figure 3.9 below shows a wavelet at Core Location 1 in the US-

41 GPR survey.
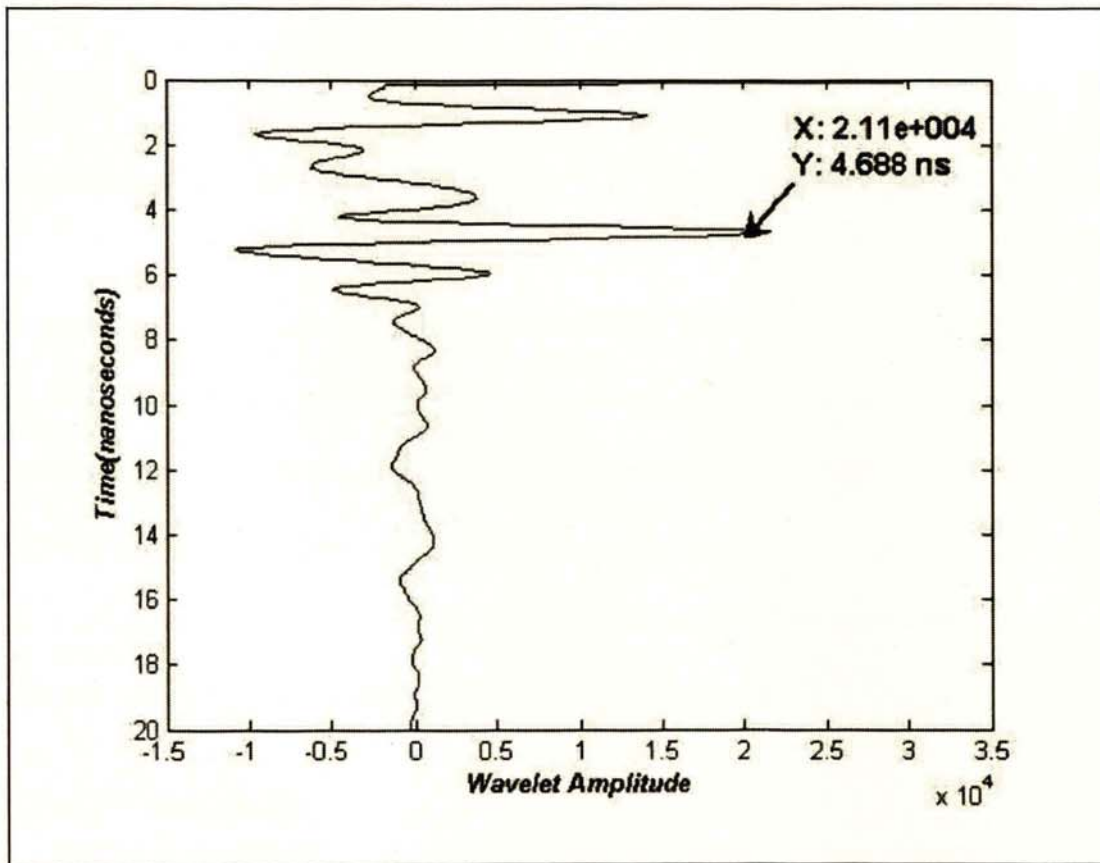
Figure 3.10 GSSI3 waveform analysis of US 41 Scan 114 at core location one and pointing to the value of A_o

Figure 3.10 shows the location where the location where A_o is picked on each GPR trace. It usually is the maximum positive amplitude of each wavelet; in this case it is $2.11 * 10^4$. The maximum plate amplitude A_p is taken from the GSSI calibration files and it is the maximum positive amplitude value. From the GPR calibration files A_p is $3.28 * 10^4$. Finally dielectric constant at the pavement surface r1 is calculated by

the formula: $\varepsilon_{r1} = \left(\dfrac{1 + \dfrac{A_0}{A_p}}{1 - \dfrac{A_0}{A_p}} \right)$. Given A_o and A_p the dielectric constant value for

21

core location 1 at the US 41 site is $\varepsilon_{core1} = \left(\dfrac{1 + \dfrac{2.11*10^4}{32767}}{1 - \dfrac{2.11*10^4}{32767}} \right)$ resulting in a dielectric

constant of 4.64. In order to compare the calculated dielectric constant values with the

Radan Roadway software values identical GPR scan are used. For this example scan

114 was used in MATLAB to get a dielectric constant value of 4.64; scan 114 on the

Radan Roadway software was used for comparison which resulted in a value of 5.44.

The dielectric constant values are compared with the Radan Roadway software

calculated values using the calculation procedure explained above.

Further Procedures

In order to complement the data collected by the GPR software, various

techniques were used to gather more information about the pavement surface at each

roadway site. First, core densities were measured at each roadway site. This data was

collected by a nuclear gauge operator from the Michigan Department of

Transportation. Nuclear density gauges are advantageous to use because the results

can be determined non-destructively and relatively quickly at the site (Roberts et al.,

1996). Nuclear density gauges determine the average density within the top several

inches of the pavement; and was collected at each core location with an additional

reading collected at a random adjacent location to estimate the variability of readings

at each site. Also six-inch diameter pavement cores were obtained at each marked

location to determine asphalt thickness measurements, and asphalt densities. Finally

the asphalt core samples removed from the roadway were analyzed in the Michigan

Tech University Asphalt Pavement Laboratories for thickness, moisture content, and

density. This information was passed on to the Michigan Department of
Transportation Laboratories in Lansing, Michigan. The asphalt data along with the
GPR data was analyzed by John Belcher (the MDOT GPR technician) before being
sent back to Michigan Technological University for final analysis. Finally, Belcher
calculated GPR wavelet velocities for the US-41, M-26, and 5 Mile Point sites. With
these files dielectric constant was directly calculate from these velocities using the
formula: $\varepsilon = (C/V)^2$. For example, core location two was calculated in this fashion
using Radan Roadway software velocities. At

this location a velocity of $8.63 * 10^7$ was calculated, C is $3 * 10^8$ therefore

$$\varepsilon = \left(\frac{3*10^8}{9.02*10^7}\right)^2 = 11.06.$$ All Radan Roadway Software values with calculated

velocities were calculated in this manner.

GPR Road Survey Results and Discussion

Dielectric constant, was determined at the eleven pavement core locations at
the four sites in this survey. A sample calculation for finding the dielectric constant of
core location 1 for the M 26 scan in Table 3.1 is as follows. Using equation

$$\varepsilon_{r1} = \left(\frac{1+\dfrac{A_0}{A_p}}{1-\dfrac{A_0}{A_p}}\right)$$ where $A_o = 2.11 * 10^4$ and $A_p = 3.28 * 10^4$. Placing the

23

amplitudes in the dielectric constant equation $\varepsilon_{r1} = \left(\dfrac{1 + \dfrac{2.11*10^4}{32767}}{1 - \dfrac{2.11*10^4}{32767}} \right) = 4.64$. The results

of the M-26, US 41, and Five Mile Point Road surveys are listed in Appendix A. The

typical dielectric constant value was 5.1 with a maximum dielectric constant value of

7.99 at Core Location 3 at the Lac La Belle site. The lowest dielectric constant value

occurred at Core Location 9 at the 5 Mile Point site. The results of the M-26 and Lac

La Belle sites are shown in Table 3.1. When comparing these two methods the

MATLAB method used surface and metal plate reflection data to calculate dielectric

constants. Also the amplitude for unity reflection from the metal plate was the same

for all tests, regardless of height above the plate. The exact method on how Radan

Roadway software calculated velocities is proprietary, and thus not available, but it is

obvious from using the program that this software makes velocity interpretations

based on core thickness from the roadway samples. With thin or poor quality cores,

velocity interpretation for the Radan Roadway software can lead to unrealistic

dielectric constant values as is the case at the M-26 site.

Table 3.1 MATLAB Calculated Dielectric Constant Values for M-26 & Lac La Belle Road computed from Radan Roadway software and MATLAB Using

Equation $\varepsilon_{r1} = \left(1 + \dfrac{A_0}{A_p} \middle/ 1 - \dfrac{A_0}{A_p}\right)$

LacLaBelle
GPR Scan

Core Locaton	Scan	Wavelet Amplitude		dielectric Constant		thickness (cm)	Calculation Method
		Ap	Ao	MATLAB	RADAN		
1	73	3.28E+04	2.50E+04	7.45	*NC	1.80	Al Plate & Amplitude
2	132	3.28E+04	2.53E+04	7.80	*NC	1.50	Al Plate & Amplitude
3	192	3.28E+04	2.55E+04	7.99	*NC	2.50	Al Plate & Amplitude
4	254	3.28E+04	2.49E+04	7.28	*NC	2.70	Al Plate & Amplitude
5	313	3.28E+04	2.45E+04	6.96	*NC	1.60	Al Plate & Amplitude
6	374	3.28E+04	2.45E+04	6.88	*NC	2.20	Al Plate & Amplitude
7	434	3.28E+04	2.44E+04	6.81	*NC	2.00	Al Plate & Amplitude
8	496	3.28E+04	2.44E+04	6.82	*NC	2.10	Al Plate & Amplitude
9	555	3.28E+04	2.47E+04	7.09	*NC	2.40	Al Plate & Amplitude
10	616	3.28E+04	2.38E+04	6.32	*NC	1.90	Al Plate & Amplitude
11	676	3.28E+04	2.41E+04	6.57	*NC	1.50	Al Plate & Amplitude

*NC = not calculated

M26
GPR Scan

Core Locaton	Scan	Wavelet Amplitude		dielectric Constant		thickness (cm)	Radan Software Calculation Method
		Ap	Ao	MATLAB	RADAN		
1	58	3.28E+04	2.11E+04	4.64	1.28	*NC	Core Thickness
2	121	3.28E+04	2.11E+04	4.64	1.28	3.61	Core Thickness
3	179	3.28E+04	2.15E+04	4.83	1.39	3.73	Core Thickness
4	239	3.28E+04	2.13E+04	4.69	1.43	3.93	Core Thickness
5	301	3.28E+04	2.14E+04	4.74	1.41	3.50	Core Thickness
6	359	3.28E+04	2.12E+04	4.66	1.20	3.66	Core Thickness
7	419	3.28E+04	2.14E+04	4.78	1.12	3.57	Core Thickness
8	480	3.28E+04	2.17E+04	4.93	1.11	2.17	Core Thickness
9	540	3.28E+04	2.19E+04	5.05	1.00	4.19	Core Thickness
10	601	3.28E+04	2.19E+04	5.01	1.00	4.16	Core Thickness
11	663	3.28E+04	2.16E+04	4.86	1.21	3.74	Core Thickness

Radan Roadway software used either core thickness data or GPR amplitude data to calculate dielectric constant. The type of analysis performed depended on the availability of core samples data for the GPR technician to use. The availability of core sample data allowed the technician to use asphalt thickness to help interpret

25

pavement velocities to calculate dielectric constants. Pavement core thickness data was used for the M-26, and Five Mile Point sites. GPR amplitude data was used for the US- 41 pavement section. Pavement cores obtained from the US-41 site were not used due to time constraints. Also pavement cores obtained from the Lac La Belle site were unreliable as they crumbled when removed from the sampling tube making their thickness determinations unreliable. Therefore, GPR amplitudes were used to interpret the Lac La Belle site within the Radan Roadway software.

US 41 Site Analysis

The average dielectric constant for the US 41 data is 4.4 with a maximum value of 4.68 at Core Location 7 and a minimum value of 4.21 at Core Location 8. Using the Radan Roadway software calculated velocities, the average dielectric constant value is 11.39. The maximum value of 12.28 occurred at Core Location 9 and the minimum value of 10.41 occurred and Core Location 8. These values are consistent with the broad range of values from Wimsatt (1998), for flexible pavements. The Matlab results correspond to flexible pavements for lightweight aggregates and the Radan results correspond to flexible pavements made with course grained aggregates Wimsatt (1998). The quality of this survey was affected by the amount of moisture within the first two inches of the roadway and the lack of core thickness data that the GPR technician could use to analyze US 41.

M-26 Site Analysis

Radan Roadway software and pavement thicknesses at the core locations were used to determine pavement velocities and dielectric constant values of the M-26 site. Radan Roadway software calculations of dielectric constant at this site were very low

compared with typical pavement dielectric constant values, and averaged 1.22 with a maximum value of 1.443 at Core Location 4 and minimum value of 1.00 at Core Locations 9 & 10. These values are not realistic for pavement and thus should not be accepted. These values compared to Wimsatt (1998) are not valid for any pavement type. This discrepancy may be explained by the core sample may not have contained the entire first layer of pavement.
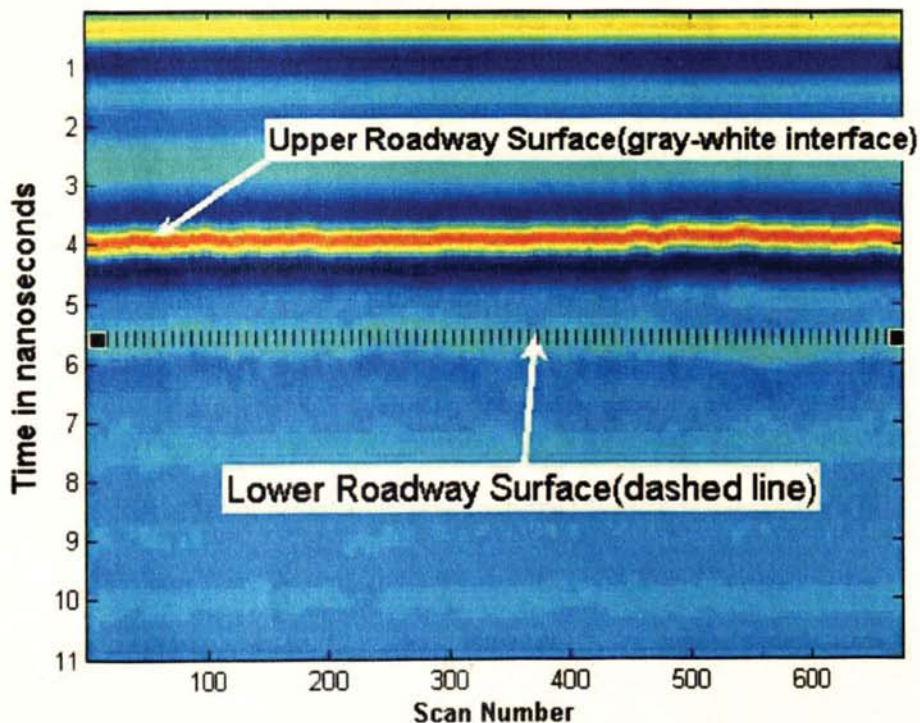
Figure 3.11: GPR Air Launched GPR scan of M-26 roadway site

Figure 3.11 clearly shows where the first layer throughout the scan, as shown by the light horizontal line crossing Figure 3.11, contradicting the idea that the pavement layer was too thin to be traced by the GPR scan. The low value for dielectric constant may be due to the fact that the core samples many not have

contained the full thickness of the top asphalt layer. The core samples used from M-26 for the GPR interpretation were thin. Table 3.2 shows the average height and diameter of the M-26 core samples. Average height and diameter characteristics were calculated using three measurements on each sample.

Table 3.2: Thickness of M-26 Cores for 2005 GPR Survey

	Corelock									
Project Number	M 26/Twin Lake									
Sample	2	3	4	5	6	7	8	9	10	11
Average Height(mm)	3.61	3.73	3.93	3.50	3.66	3.57	2.17	4.19	4.16	3.74
Average Diameter(mm)	15.16	15.20	15.25	15.10	14.75	14.82	14.66	14.54	14.72	13.57

The M-26 core samples have an average thickness of 3.63 cm with core location 10 being the thickest at 4.2 cm and core 8 being the thinnest core at 2.1 cm. Of the four road surveys the M-26 site had on average the thinnest road cores to use for GPR interpretation. Due to the thin pavement, it's difficult to obtain realistic dielectric constant from GPR pavement amplitudes. By only observing the pavement thickness alone, the character of reflections is unidentifiable for beds less than $\lambda/8$ thick according the Widess (1973) or about 3.75 cm. The point of his paper is that with extremely thin bed sections destructive interference of the wavelet modifies or extinguishes the reflection making it impossible to calculate dielectric constant using the GPR wavelet (Widess, 1973). Given these conditions it wasn't possible to determine and obtain reasonable dielectric constant values because the roadway core thicknesses were too thin.

Five Mile Point Road Site Analysis

Dielectric constant values were calculated using the Radan Roadway software velocities had an average value of 7.91, a maximum value of 9.58 at Core Location 11, and a minimum value of 6.84 at Core Location 10. Comparing this average value to Wimsatt (1998), the results indicate this roadway is a flexible pavement. MATLAB calculated dielectric constant values had an average value of 4.05 with a maximum value at Core Location 1 of 4.36 and a minimum value at 3.89 at Core Location 9. This roadway also consistent with values for flexible pavements according to Wimsatt (1998). Generally, the difference in values fall within the range of flexible pavement but may indicate area of higher concentration of aggregate or asphalt binder used at a given core location.

Lac La Belle Road Site Analysis From Surface Reflections

For this site dielectric constant values were solely calculated and interpreted using GPR surface and subsurface wavelet amplitudes along with the MATLAB software. Because of crumbly cores, actual thickness of the pavement could not be determined and thus Radan Roadway software velocities were not calculated. Radan Roadway software determined the following dielectric constant values at the core locations shown in Table 3.1. Dielectric Constant values were determined by the following formula where A_o is the GPR wavelet amplitude and A_p

is the aluminum plate amplitude $\varepsilon_{r1} = \left(\dfrac{1 + \dfrac{A_o}{A_p}}{1 - \dfrac{A_o}{A_p}} \right)$. When comparing the Lac La Belle

Road dielectric constant values to Wimsatt (1998) this pavement is indicated to be a flexible pavement due to the dielectric constant values ranging from 6.5-7.8. A

29

concern for interpreting this site is the very thin pavement at this site, which made it impossible to use core samples to help interpret pavement conditions in the Radan Roadway software.

Comparison of MATLAB Results vs. Radan Roadway Software

A comparison between dielectric constants calculated using the Radan Roadway software with those calculated in this study are shown in Tables 3.3, 3.4, and 3.5. Due to the instability of the roadway cores and lack of time in interpreting the roadway at the Lac La Belle site the GPR data was not analyzed by Radan Roadway software. Table 3.3 compares the MATLAB calculated dielectric constant results with the Radan Roadway software. The results that are compared are the US 41, M-26, and 5 Mile Point Sites.

Table 3.3: MATLAB Vs. Radan Roadway software Dielectric Constant Comparison of US 41 Site from the 2005 GPR Survey

US41 GPR Scan							Radan Software	
		Wavelet Amplitude		**dielectric Constant**		**thickness**	**Calculation Method**	
Core						(cm)		
Locaton	Scan	Ap	Ao	MATLAB	RADAN			
2	114	3.28E+04	2.11E+04	4.64	12.08	6.34	Al Plate & Amplitude	
3	175	3.28E+04	2.05E+04	4.35	11.06	7.18	Al Plate & Amplitude	
4	234	3.28E+04	2.03E+04	4.27	11.36	4.79	Al Plate & Amplitude	
5	295	3.28E+04	2.07E+04	4.41	10.66	4.73	Al Plate & Amplitude	
6	356	3.28E+04	2.04E+04	4.31	10.94	4.83	Al Plate & Amplitude	
7	415	3.28E+04	2.12E+04	4.68	12.05	6.76	Al Plate & Amplitude	
8	476	3.28E+04	2.02E+04	4.21	10.41	8.63	Al Plate & Amplitude	
9	537	3.28E+04	2.08E+04	4.47	12.28	7.10	Al Plate & Amplitude	
10	598	3.28E+04	2.04E+04	4.29	11.98	7.25	Al Plate & Amplitude	
11	658	3.28E+04	2.05E+04	4.32	11.11	6.61	Al Plate & Amplitude	

Table 3.4: MATLAB Vs. Radan Roadway software Dielectric Constant Comparison of M-26 Site from the 2005 GPR Survey

M26 GPR Scan		Wavelet Amplitude		dielectric Constant		thickness (cm)	Radan Software Calculation Method
Core Locaton	Scan	Ap	Ao	MATLAB	RADAN		
1	58	3.28E+04	2.11E+04	4.64	1.28	N/A	Core Thickness
2	121	3.28E+04	2.11E+04	4.64	1.28	3.61	Core Thickness
3	179	3.28E+04	2.15E+04	4.83	1.39	3.73	Core Thickness
4	239	3.28E+04	2.13E+04	4.69	1.43	3.93	Core Thickness
5	301	3.28E+04	2.14E+04	4.74	1.41	3.50	Core Thickness
6	359	3.28E+04	2.12E+04	4.66	1.20	3.66	Core Thickness
7	419	3.28E+04	2.14E+04	4.78	1.12	3.57	Core Thickness
8	480	3.28E+04	2.17E+04	4.93	1.11	2.17	Core Thickness
9	540	3.28E+04	2.19E+04	5.05	1.00	4.19	Core Thickness
10	601	3.28E+04	2.19E+04	5.01	1.00	4.16	Core Thickness
11	663	3.28E+04	2.16E+04	4.86	1.21	3.74	Core Thickness

Table 3.5: MATLAB Vs. Radan Roadway software Dielectric Constant Comparison of 5 Mile Point Road Site from the 2005 GPR Survey

5 Mile Pt GPR Scan		Wavelet Amplitude		dielectric Constant		thickness (cm)	Radan Software Calculation Method
Core Locaton	Scan	Ap	Ao	MATLAB	RADAN		
1	62	3.28E+04	2.05E+04	4.36	7.84	4.84	Core thickness
2	121	3.28E+04	1.95E+04	3.93	7.92	4.61	Core thickness
3	182	3.28E+04	1.99E+04	4.09	8.81	3.98	Core thickness
4	241	3.28E+04	1.99E+04	4.09	8.27	4.31	Core thickness
5	302	3.28E+04	1.96E+04	3.97	7.77	4.87	Core thickness
6	362	3.28E+04	1.95E+04	3.93	7.63	4.51	Core thickness
7	422	3.28E+04	1.97E+04	4.02	7.39	4.56	Core thickness
8	485	3.28E+04	1.97E+04	4.02	7.58	4.73	Core thickness
9	544	3.28E+04	1.94E+04	3.89	7.35	4.81	Core thickness
10	605	3.28E+04	1.95E+04	3.92	6.84	4.76	Core thickness
11	663	3.28E+04	2.04E+04	4.29	9.58	4.01	Core thickness

Table 3.6 MATLAB vs. Radan Roadway software Value Comparison

Site	MATLAB	Radan
US 41	Realistic	~ 2 x MATLAB
M 26	Realistic	Too Low
5 Mile Pt.	Realistic	~ 2 x MATLAB

Tables 3.3 and 3.5 show that the dielectric constants calculated from the MATLAB and Radan Roadway software disagreed by a factor of two to three therefore the author turned to the methods of TDR and creating manufactured pavement sample to better determine values of dielectric constant. Furthermore, the Radan Roadway software is proprietary software, and it was not available for further trials at that time.

Chapter 4. Ground Penetrating Radar Laboratory Measurements

The author and his thesis advisor decided to have six pavement samples with known physical parameters manufactured to better understand the relationship between dielectric constant and pavement amplitude, A_o, the amplitude of the surface reflection. In particular, the goals of this survey included the following five goals:

1. First, creating a calibration curve using samples of known densities to relate pavement surface reflection amplitude A_o to a single value of density.

2. Second, designing an experiment which has a greater range of densities greater than 20 lbs/ft^3 in order to calibrate A_o for dielectric constant and density.

3. Third, analyzing and isolating the effects of moisture using complete dry asphalt samples and calculated the velocity of and dielectric constant of GPR waves traveling within each pavement sample for wet and dry conditions.

4. Fourth, determining whether the direction of scanning the pavement samples has an effect on the dielectric constant of the sample when collecting raw data using the air-launched GPR antenna.

5. Finally, determining whether the manufactured samples produce dielectric constant values consistent with those of Wimsatt (1998) typical flexible pavement values.

In order to understand and analyze the relationship between dielectric constant and A_o, the author wrote a series of MATLAB programs specifically designed to interpret pavement surface interfaces and calculate GPR wavelet velocities within the asphalt samples. Unfortunately, for the final analysis of the raw data Belcher was not able to produce all of the raw data from this survey due to Radan Roadway software difficulties and his professional workload. The manufactured sample GPR survey was conducted at the Michigan Technological University campus.

Equipment and Setup

The Michigan Technological University Civil Engineering Department

created six asphalt pavement samples of varying densities, with physical properties

shown in Table 4.1. The pavement sample dimensions were approximately 8 inches

by 15 inches by 3 inches. The samples have an average thickness of 2.93 inches.

Table 4.1: Physical Parameters of Manufactured Asphalt Samples

Sample Number	Density(lbs/ft^3)	Dry Weight(g)	SSD Weight(g)	Thickness(inches)
1	180.90	13961.60	13977.40	2.84
2	183.60	13996.60	14023.50	2.91
3	186.20	14047.90	14087.70	3.00
4	187.00	13709.00	13792.20	3.02
5	181.50	13993.90	14042.10	2.87
6	185.00	13559.70	13645.50	2.95

The 1 GHz air-launched antenna was used to conduct GPR scans across each

pavement sample parallel and perpendicular direction to the long of the sample as

shown in Figures 4.1 and 4.2. A hand held ground coupled 1 GHz antenna from the

Michigan Department of Transportation was used to provide GPR scans over each

pavement sample as shown in Figure 4.3. Calibrations for unity reflection coefficient

using the air-launched antenna were conducted with a two person team manually

raising and lowering the antenna over a standard aluminum construction sign, to

simulate the bounce test as used in a typical roadway GPR survey. Finally the raw

data from the GPR was analyzed using MATLAB programs created by the author.

GPR Data Collection

The GPR antenna was held approximately 17 inches above the ground. The

antenna scanned over each sample as it was placed with its long axis perpendicular or

parallel to the direction of motion, as shown in Figure 4.1. The purpose for having the GPR antenna traverse the samples in a parallel and perpendicular manner determine if direction of traverse makes a recognizable difference in determining pavement dielectric constants values. For this experiment the finite "footprint" of the radar block was not infinitesimal in size, therefore the purpose of this experiment is to experimentally understand and reduce the effect of the edge of the pavement blocks, if possible.
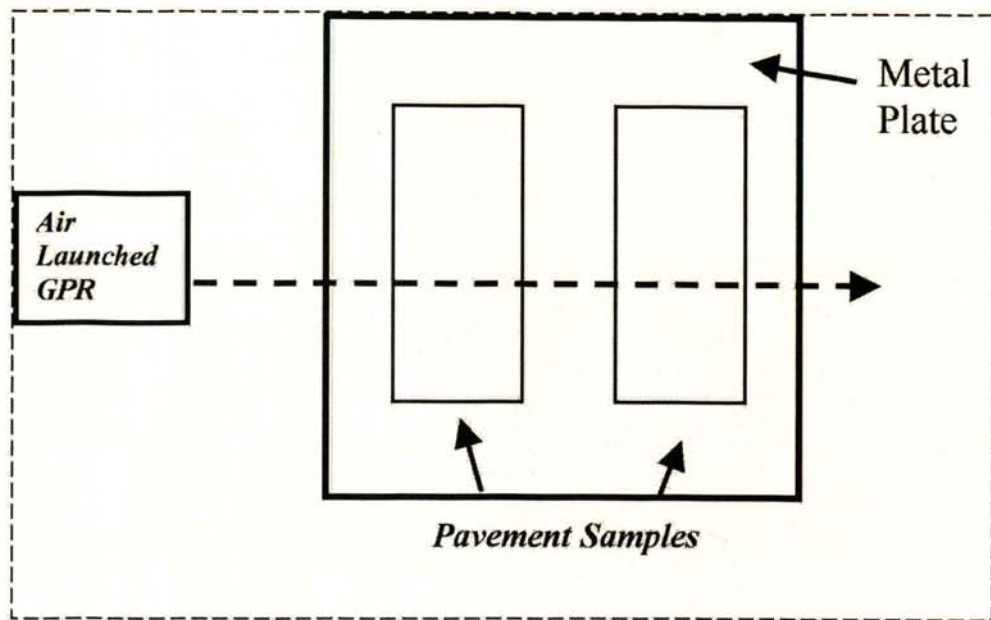
Figure 4.1: 2006 GPR laboratory experimental setup for perpendicular direction of motion

Pavement Samples

Air Launched GPR

Metal Plate
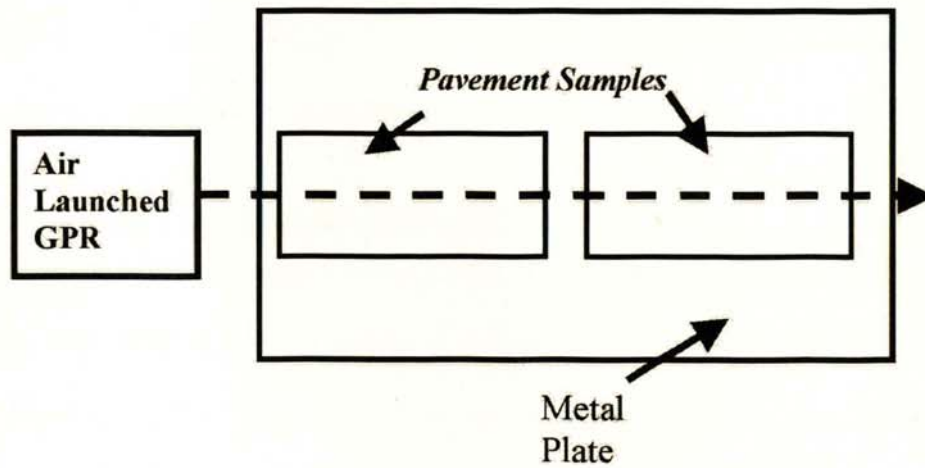
Figure 4.2: 2006 GPR laboratory experimental setup for parallel direction of motion

The ground-coupled antenna used in this experiment is shown in Figure 4.3.

~ 8 inches

asphalt sample
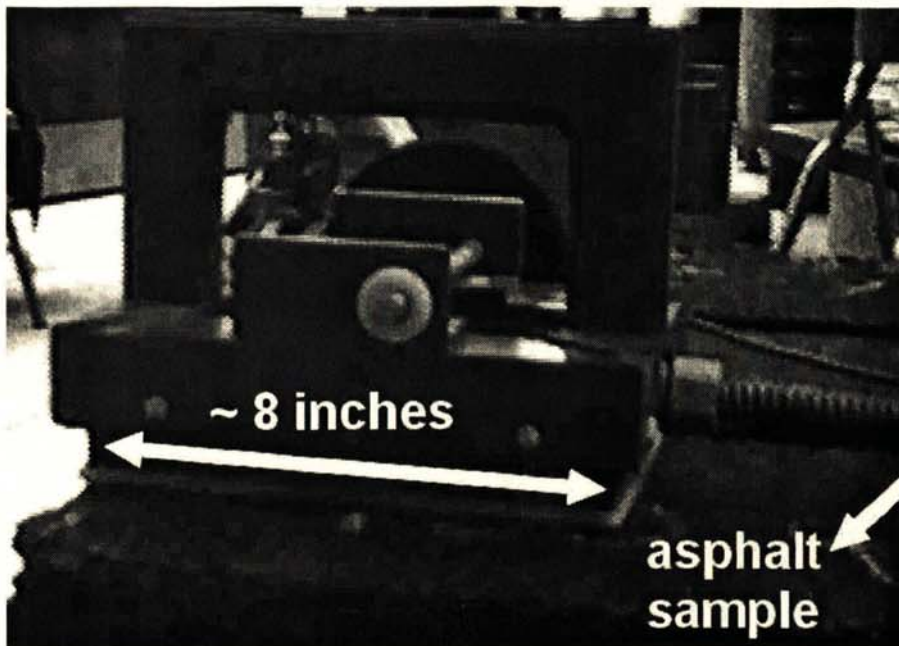
Figure 4.3: Ground Coupled Antenna gliding across pavement sample

The sample interval for the waveforms was 39 picoseconds/sample. In order to obtain GPR data of the pavement samples in a surface saturated dry condition each sample was submerged in a water bath for an hour and a half in the Michigan

Technological University Pavement laboratory. After the samples were submerged in the water bath for nearly an hour and a half, they were weighed and then scanned by both GPR antennas according to the procedures above.

GPR Survey Data Analysis with MatLab

MATLAB was the primary program used to analyze raw data files obtained from John Belcher from MDOT. A MATLAB program, gssi3, autopicklayers3, plus additional programs written by Baron Colbert, were used to analyze the GPR wavelet velocities in pavement samples.

The MATLAB programs by the author were used to determine the amount of travel time that the GPR waves used to reach the top and bottom surface of each sample. Program autopicklayers3 served as a semi-automatic function selector in determining the top and bottom pavement sample interfaces based on the minimum amplitude from each GPR trace from a given raw data file scan. Given an initial time window and trace number, program "autopicklayers3" will pick the time of the most negative portion of the waveform and proceed to automatically pick the most negative points on adjacent traces. Thus, a reflection may be traced across a radar cross section. It is crucial to examine the data set carefully to obtain valid times for reflections from the metal plate, and the top of the asphalt block. This program also converted the time depth scale on a GPR trace to a specific trace number based of the raw data file's scan/second interval. This allowed the author to easily select the appropriate trace number to select pavement interfaces. The following description will explain how the pavement surface interfaces were selected for each pavement sample and how the dielectric constant values were calculated, using data from

37

samples 5 and 6 from the air-launched GPR for wet samples in the experimental setup as shown in Figure 4.1.

Autopicklayers3 asks the user to select a raw data file and input the number of traces and scans of the file. After entering the required information, the program then begins to interpret the location of the aluminum plate layer of the GPR trace. For the file including Samples 5 and 6, the author interprets the aluminum layer as the dark region within the GPR trace. For this example the aluminum layer is below scan 155 at trace 450 as shown in Figure 4.4.
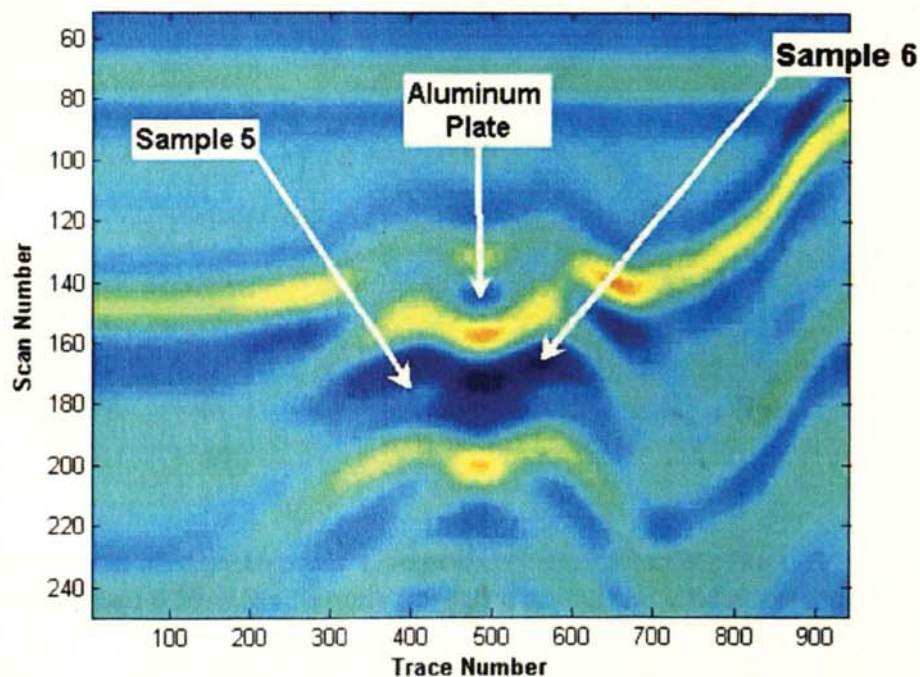
Figure 4:4: Air-Launched GPR Scan of Saturated Samples 5 & 6

After making the selection, autopicker3 will go through every GPR trace searching for the minimum amplitude for trace number 1 through 912 with the minimum amplitude being chosen at any scan number greater than 155 as shown in Figure 4.4. The program will stop occasionally to allow for manual input of the

38

location of the minimum trace in instances of multiple scan number locations having the same minimum amplitude at a particular trace number. After the program is finished, the output will be a combination plot of amplitude, first layer interpretation, and GPR image of samples 5 & 6 as shown in
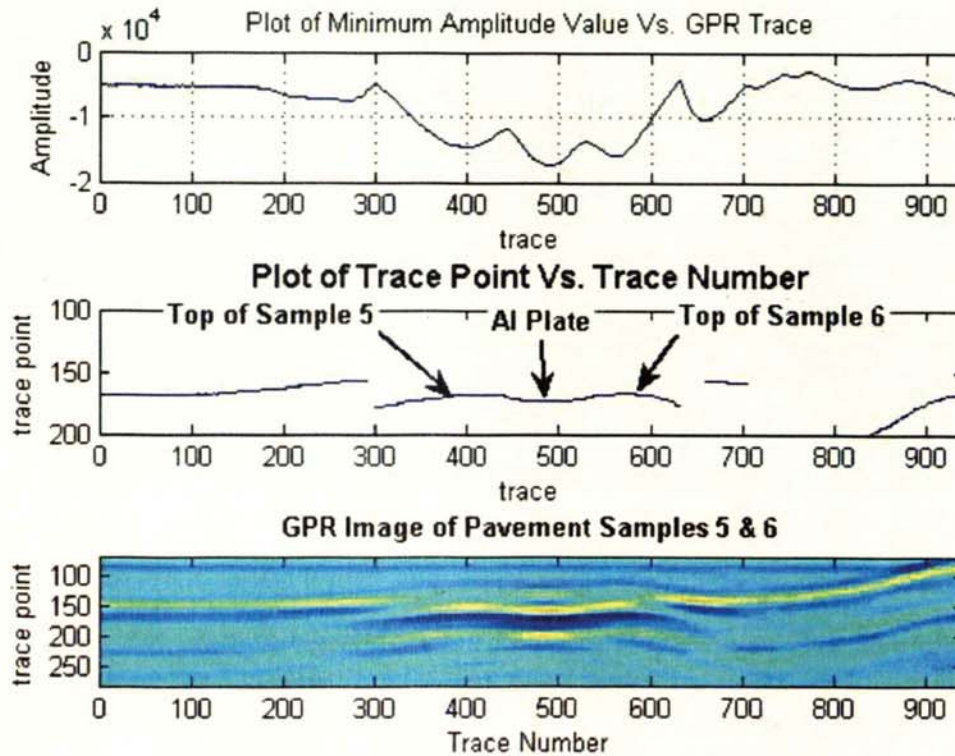
Figure 4.5: Autopicklayers3 Composite Output Showing the GPR Scan of Sample 5 and 6 Plus the Sample Surface Layer Picks and Amplitudes

Figure 4.5. Afterward, autopicklayers3 will interpret the location of the top layer of samples 5 & 6. Figure 4.5 displays the selection process of picking the

surface layer for samples 5 & 6.
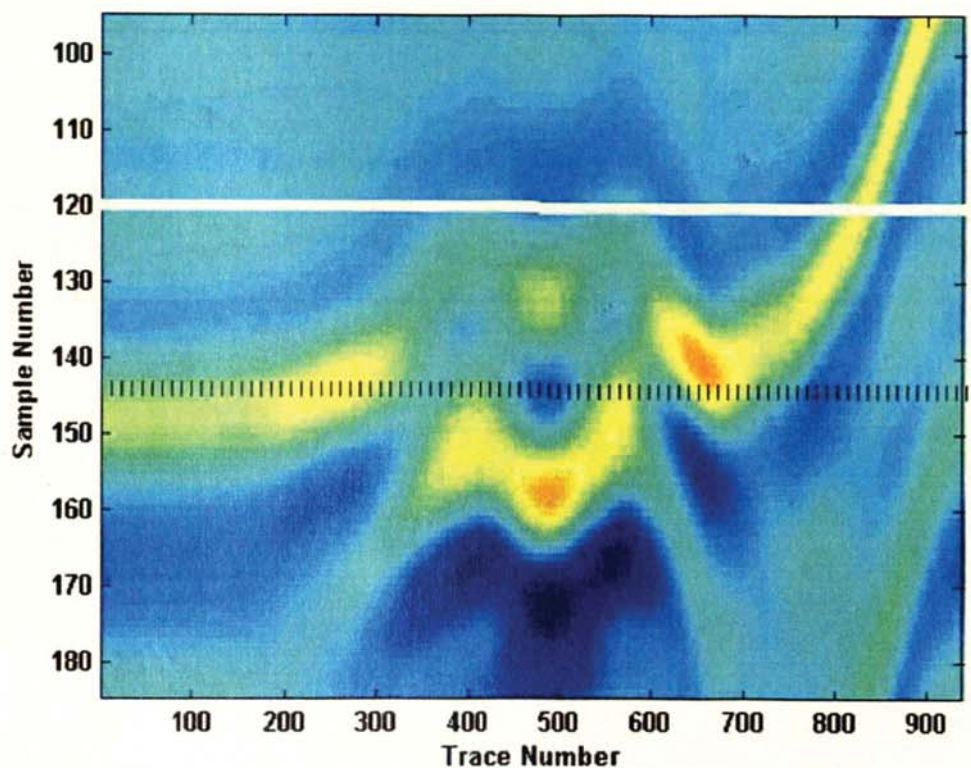
Figure 4:6: Autopicklayer3 Output Showing Upper Layer Pick Boundary Parameters for Samples 5 and 6. Proposed boundary range for upper layer boundary for samples 5 & 6 with the solid line @ trace 120 being the upper range and the dashed line @ 145 being the lower range.

As shown in Figure 4.6, autopicklayers3 allows the user to select the boundary

of the surface layer for samples 5 and 6. In this case scan number 120 was the upper

boundary as shown by the solid line in Figure 4. 6 and scan number 145 was the

lower boundary for surface layer interpretation shown by the dashed line in Figure

4.6. After autopicklayers3 interprets the upper and lower sample interfaces it's

displayed as shown in Figure 4.7.
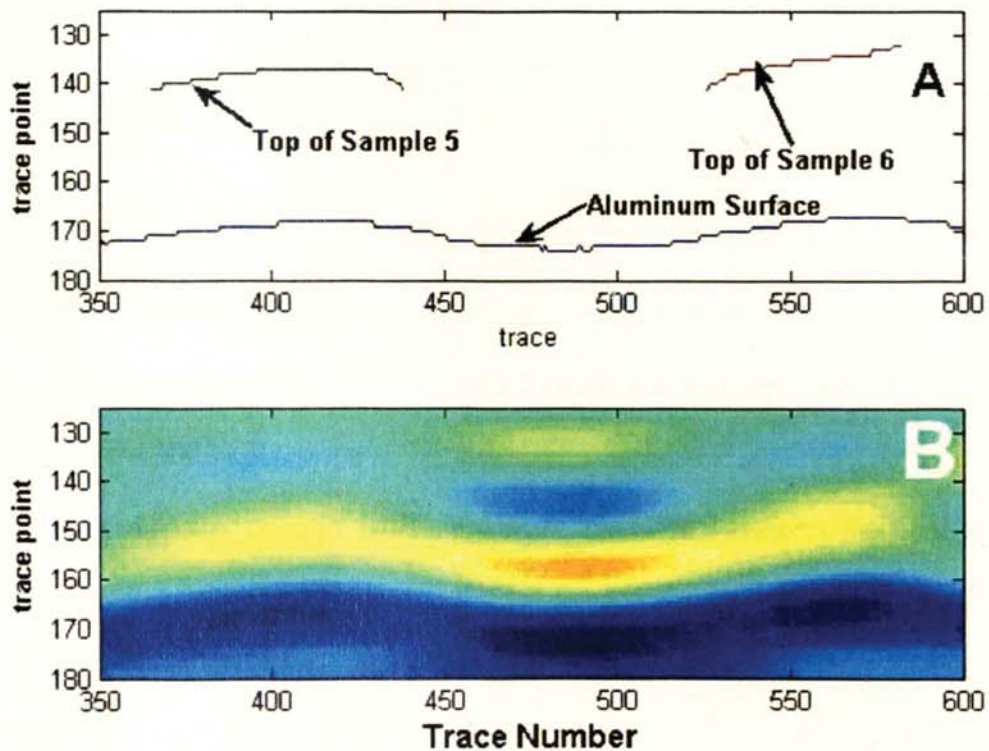
Figure 4:7: Autopicklayers3 Upper and Lower Boundary Layer Picks A is the top surface plot of samples 5 and 6 and the aluminum plate surface and B is a GPR image of pavement samples 5 and 6.

At this point velocities and dielectric constants are ready to be calculated. For Sample 5 velocities were calculated by taking the difference between the bottom and top scan number from the sample and multiplying the difference by the sampling time. The top scan number for sample 5 is 169 and the bottom scan number is 137. The sample rate is $3.91 * 10^{-11}$ seconds`. The one-way travel time for the GPR wave to travel through Sample 5 is:

$$TT_{oneway} = (169 - 137) * 3.91 * 10^{-11} * \frac{1}{2} = 6.25 * 10^{-10} \text{ seconds.}$$

41

With a thickness of $7.3 * 10^{-2}$ meters the velocity is:

$$Velocity_{samples} = thickness\Big/traveltime = \frac{7.3 * 10^{-2}\, m}{6.25 * 10^{-10}\, sec} = 1.17 * 10^{8}\, m\Big/sec.$$ The

dielectric constant is calculated using: $\kappa = (c/v)^2 = \left(\dfrac{3 * 10^{8}}{1.17 * 10^{8}}\right)^2 = 6.6$. Where c is

the speed of light and v is the velocity of the radar wave within the pavement. Thus,

using the pavement thickness, and GPR travel time in pavement, and speed of light,

dielectric constant measurements were calculated for the saturated and unsaturated

samples for the 2006 GPR survey.

For the ground coupled GPR experiment, the GPR waveform was used to

calculate the dielectric constant. Figure 4.8 below shows a sample wavelet taken from

sample #1 in the saturated phase of the ground coupled GPR experiment.
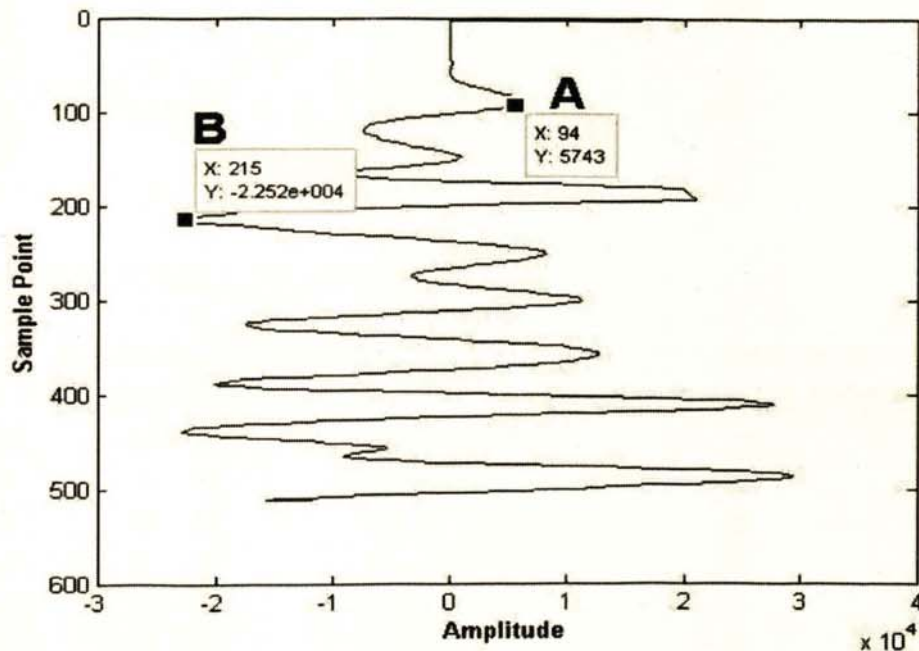
Figure 4.8: Ground Coupled GPR Wet Sample Picking Points for Top A and Bottom Pavement Surface B. The x coordinates are the sample points and the y coordinates are the wavelet amplitudes

The ground coupled GPR typically has a time-depth range of 6 nanoseconds and a sampling rate of nearly 12 picoseconds/sample. For this experiment the asphalt samples are approximately 2 inches. Combined with the sampling rate of 12 picoseconds/sample, MATLAB has a reasonable resolution in determining dielectric constant values for the asphalt samples. As shown in Table 4.2., approximately 120 - 130 samples, are used to calculate GPR wavelet travel time within the pavement samples.

Table 4.2: GPR Wavelet Sample Count for the Calculation of Dielectric Constant Using Ground Coupled GPR Experiment

Unsaturated Sample Trace Locations

	Top Sample Location	Bottom Sample Location	Total Sample Count Used to Determine GPR Wavelet
Sample 1	77	206	129
Sample 2	77	209	132
Sample 3	77	212	135
Sample 4	77	208	131
Sample 5	77	207	130
Sample 6	77	210	133

Saturated Sample Trace Locations

	Top Sample Location	Bottom Sample Location	Total Sample Count Used to Determine GPR Wavelet
Sample 1	94	215	
Sample 2	94	220	126
Sample 3	94	222	128
Sample 4	94	218	124
Sample 5	94	215	121
Sample 6	94	220	126

Single Density Calibration Results and Discussion

Also as a part of the 2006 GPR survey an attempt to calibrate GPR wavelet

amplitudes we according to their densities were performed. Numerical values are

given in Table 4.3, 4.4, and 4.5, and the data are plotted in Figures 4.9 and 4.10.

Table 4.3: Amplitude and Dielectric Constant Results for Wavelet Calibration Test for Unsaturated Pavement samples 1 & 2 Using Air Launched GPR Antenna Ap is metal plate reflection amplitude, Ao is pavement surface amplitude

Core Locaton	Scan	Ap	Ao	dielectric Constant	Density(lbs/ft^3)	Motion Relative to sample
1	430	3.28E+04	1.89E+04	3.72	180.90	parallel
1	450	3.28E+04	1.98E+04	4.06	180.90	parallel
1	470	3.28E+04	2.08E+04	4.46	180.90	parallel
1	490	3.28E+04	2.05E+04	4.32	180.90	parallel
2	640	3.28E+04	1.95E+04	3.93	183.60	parallel
2	660	3.28E+04	2.11E+04	4.63	183.60	parallel
2	680	3.28E+04	2.19E+04	5.01	183.60	parallel
2	700	3.28E+04	2.11E+04	4.59	183.60	parallel
Core Locaton	Scan	Ap	Ao		Density(lbs/ft^3)	Motion Relative to sample
1	460	3.28E+04	1.57E+04	2.83	180.90	perpendicular
1	500	3.28E+04	2.04E+04	4.32	180.90	perpendicular
1	540	3.28E+04	2.09E+04	4.50	180.90	perpendicular
1	580	3.28E+04	1.59E+04	2.89	180.90	perpendicular
2	780	3.28E+04	1.34E+04	2.39	183.60	perpendicular
2	800	3.28E+04	1.91E+04	3.79	183.60	perpendicular
2	820	3.28E+04	2.03E+04	4.25	183.60	perpendicular
2	840	3.28E+04	1.92E+04	3.84	183.60	perpendicular

Table 4.4: Amplitude and Dielectric Constant Results for Wavelet Calibration Test for Unsaturated Pavement samples 3 & 4 Using Air Launched GPR Antenna

Core Locaton	Scan	Ap	Ao	dielectric Constant	Density(lbs/ft³)	Motion Relative to sample
3	460	3.28E+04	1.74E+04	3.27	186.20	parallel
3	480	3.28E+04	1.82E+04	3.49	186.20	parallel
3	500	3.28E+04	1.85E+04	3.60	186.20	parallel
3	520	3.28E+04	1.85E+04	3.59	186.20	parallel
4	660	3.28E+04	1.76E+04	3.32	187.00	parallel
4	680	3.28E+04	1.81E+04	3.46	187.00	parallel
4	700	3.28E+04	1.90E+04	3.77	187.00	parallel
4	720	3.28E+04	1.77E+04	3.35	187.00	parallel
Core Locaton	Scan	Ap	Ao	dielectric Constant	Density(lbs/ft³)	Motion Relative to sample
3	370	3.28E+04	1.24E+04	2.22	186.20	perpendicular
3	390	3.28E+04	1.64E+04	3.00	186.20	perpendicular
3	410	3.28E+04	1.74E+04	3.28	186.20	perpendicular
3	430	3.28E+04	1.41E+04	2.51	186.20	perpendicular
4	590	3.28E+04	1.44E+04	2.57	187.00	perpendicular
4	610	3.28E+04	1.83E+04	3.51	187.00	perpendicular
4	630	3.28E+04	1.85E+04	3.60	187.00	perpendicular
4	650	3.28E+04	1.48E+04	2.65	187.00	perpendicular

Table 4.5: Amplitude and Dielectric Constant Results for Wavelet Calibration Test for Unsaturated Pavement samples 5 & 6 Using Air Launched GPR Antenna

Core Locaton	Scan	Ap	Ao	dielectric Constant	Density(lbs/ft³)	Motion Relative to sample
5	500	3.28E+04	1.86E+04	3.61	181.50	parallel
5	520	3.28E+04	2.06E+04	4.39	181.50	parallel
5	540	3.28E+04	2.13E+04	4.73	181.50	parallel
5	560	3.28E+04	2.02E+04	4.20	181.50	parallel
6	700	3.28E+04	1.92E+04	3.82	185.00	parallel
6	720	3.28E+04	2.11E+04	4.61	185.00	parallel
6	740	3.28E+04	2.02E+04	4.21	185.00	parallel
6	760	3.28E+04	1.77E+04	3.34	185.00	parallel
Core Locaton	**Scan**	**Ap**	**Ao**	**dielectric Constant**	**Density(lbs/ft³)**	**Motion Relative to sample**
5	480	3.28E+04	1.39E+04	2.47	181.50	perpendicular
5	500	3.28E+04	1.69E+04	3.12	181.50	perpendicular
5	520	3.28E+04	1.70E+04	3.17	181.50	perpendicular
5	540	3.28E+04	1.40E+04	2.50	181.50	perpendicular
6	680	3.28E+04	1.47E+04	2.63	185.00	perpendicular
6	700	3.28E+04	1.68E+04	3.10	185.00	perpendicular
6	720	3.28E+04	1.58E+04	2.86	185.00	perpendicular
6	740	3.28E+04	1.29E+04	2.31	185.00	perpendicular

In tables 4.3 − 4.5 the dielectric constant was calculated using A_p, A_o,

and $\varepsilon_{r1} = \left(\dfrac{1 + \dfrac{A_0}{A_p}}{1 - \dfrac{A_0}{A_p}} \right)$. The single calibration phase of this study consisted of taking A_o

from each of the core scans and comparing it with the sample density. Surface wave

46

amplitudes were plotted vs. densities to visualize the statistical behavior. Figures 4.9

and 4.10 below show the calibration for the single density for sample waveform

amplitude vs. density.
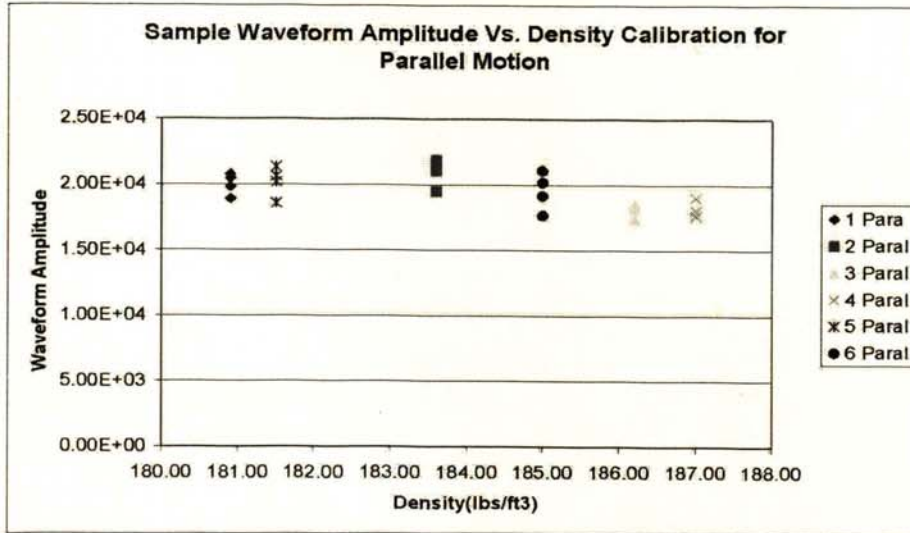
Figure 4.9: Sample Waveform Amplitude Vs. Density Calibration for Radar Traverse Parallel to Long Axis of Block.
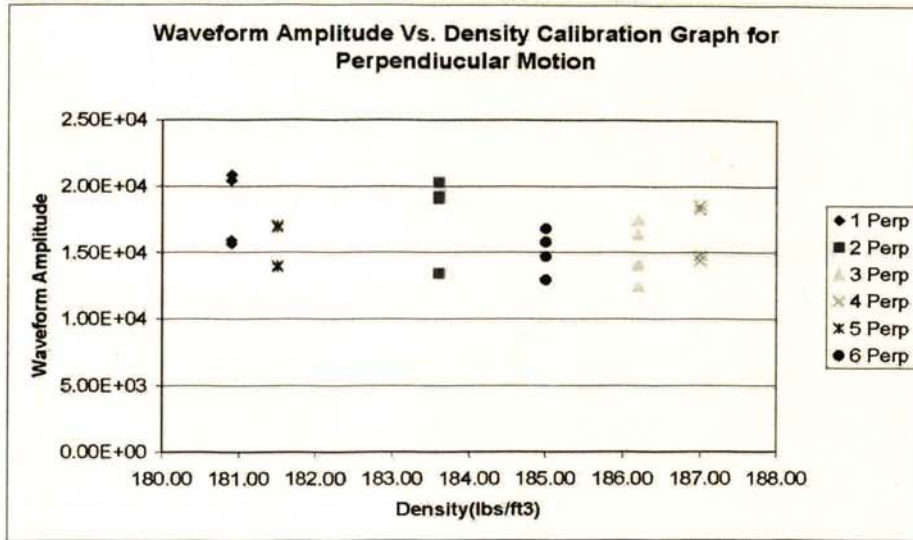
Figure 4.10: Sample Waveform Amplitude Vs. Density Calibration for Radar Traverse Perpendicular to Long Axis of Block.

In order to determine the error of the calibrations for the parallel and

perpendicular motions, a standard deviation was calculated for each sample in both

directions of motion. The results for the standard deviation are shown in Table 4.6.

Table 4.6: Core Density and A_o Calibration Standard Deviation Using $A_o = 3.28*10^4$

Core Locaton	Density(lbs/ft3)	Motion Relative to sample	Standard Deviation of A_o	Percent Error
1	180.90	parallel	828.39	2.5
1	180.90	perpendicular	2813.48	8.6

Core Locaton	Density(lbs/ft3)	Motion Relative to sample	Standard Deviation of A_o	Percent Error
2	183.60	parallel	1009.07	3.1
2	183.60	perpendicular	3103.59	9.5

Core Locaton	Density(lbs/ft3)	Motion Relative to sample		
3	186.20	parallel	504.54	1.5
3	186.20	perpendicular	2257.44	6.9

Core Locaton	Density(lbs/ft3)	Motion Relative to sample	Standard Deviation of A_o	Percent Error
4	187.00	parallel	651.84	2.0
4	187.00	perpendicular	2190.96	6.7

Core Locaton	Density(lbs/ft3)	Motion Relative to sample	Standard Deviation of A_o	Percent Error
5	181.50	parallel	1174.77	3.6
5	181.50	perpendicular	1734.25	5.3

Core Locaton	Density(lbs/ft3)	Motion Relative to sample	Standard Deviation of A_o	Percent Error
6	185.00	parallel	1466.57	4.5
6	185.00	perpendicular	1647.85	5.0

Table 4.6 shows that when the air launched GPR antenna is run in a parallel direction along the pavement sample there is significantly less deviation from the mean of A_o as shown for cores 1-4. As for cores 5 and 6 running the GPR in a parallel direction across the samples produces slightly less deviation in surface amplitude

48

values. As a result of this study the calibration of pavement amplitude A_o vs. density provided better results that the dielectric constant vs. density results of the 2005 survey. These results indicate a small linear dependence of A_o with density. Although the A_o vs. density provided a trend that was linear, the result contradicted in theory that as pavement amplitude increased density or dielectric constant would increase. The calibration results from this experiment showed that as density increased A_o slightly decreased. This result indicates that again an increase in the range of densities still will be needed in order to validate this result. Despite attempts to increase the density range of asphalt samples, a density range of greater than 20 lbs/ft^3 could not be obtained.

GPR LABORATORY RESULTS AND DISCUSSION

Wavelet amplitude data was collected with the air-launched antenna data and used to calculate dielectric constant by using MATLAB along with sample thickness data. The thickness information of each sample was used to analyze each sample except for samples five and six. Due to faulty software, these samples could not be analyzed with their thickness data using Radan Roadway software. Pavement layer interface data determined from the ground coupled GPR antenna was used to calculate dielectric constant using $\varepsilon = (C/V)^2$, where C is the speed of light, and V is the GPR wave velocity within the sample.

The results for the air-launched GPR data for the saturated and unsaturated manufactured asphalt samples are displayed in Table 4.7. The results of the ground coupled GPR data for dry and wet samples are shown in Table 4.8.

Table 4.7: 1GHz Air-Launched GPR Dielectric Constant Results from the GPR Laboratory Measurements

Unsaturated Samples

Files	Trace Locations			(Surface to	Thickness meters	Velocity (m/s) sample bottom	ε
	Top	Bottom	Sample	Sample Bottom)		Velocity	Dielectric Const.
1&2Perp.dzt	167	196	1	5.66E-10	7.21E-02	1.27E+08	5.6
	166	197	1	6.05E-10	7.21E-02	1.19E+08	6.4
	167	196	1	5.66E-10	7.21E-02	1.27E+08	5.6
	165	196	2	6.05E-10	7.39E-02	1.22E+08	6.0
	166	195	2	5.66E-10	7.39E-02	1.30E+08	5.3
	167	196	2	5.66E-10	7.39E-02	1.30E+08	5.3
1&2PARAL.DZT Top Bottom	171	203	1	6.25E-10	7.21E-02	1.15E+08	6.8
	170	204	1	6.64E-10	7.21E-02	1.09E+08	7.6
	171	205	1	6.64E-10	7.21E-02	1.09E+08	7.6
	170	204	2	6.64E-10	7.39E-02	1.11E+08	7.3
	169	203	2	6.64E-10	7.39E-02	1.11E+08	7.3
	168	202	2	6.64E-10	7.39E-02	1.11E+08	7.3
3&4PARAL.DZT	173	206	3	6.45E-10	7.61E-02	1.18E+08	6.4
	173	206	3	6.45E-10	7.61E-02	1.18E+08	6.4
	174	206	3	6.25E-10	7.61E-02	1.22E+08	6.1
	171	206	4	6.84E-10	7.67E-02	1.12E+08	7.1
	171	206	4	6.84E-10	7.67E-02	1.12E+08	7.1
	172	206	4	6.64E-10	7.67E-02	1.16E+08	6.7
3&4PERP.DZT	171	201	3	5.86E-10	7.61E-02	1.30E+08	5.3
	171	201	3	5.86E-10	7.61E-02	1.30E+08	5.3
	171	201	3	5.86E-10	7.61E-02	1.30E+08	5.3
	171	201	4	5.86E-10	7.67E-02	1.31E+08	5.3
	171	201	4	5.86E-10	7.67E-02	1.31E+08	5.3
	173	201	4	5.47E-10	7.67E-02	1.40E+08	4.6
5&6PARAL.DZT	170	203	5	6.45E-10	7.30E-02	1.13E+08	7.0
	170	204	5	6.64E-10	7.30E-02	1.10E+08	7.4
	169	203	5	6.64E-10	7.30E-02	1.10E+08	7.4
	170	202	6	6.25E-10	7.50E-02	1.20E+08	6.2
	170	203	6	6.45E-10	7.50E-02	1.16E+08	6.6
	169	204	6	6.84E-10	7.50E-02	1.10E+08	7.5
5&6PERP.DZT	173	203	5	5.86E-10	7.30E-02	1.25E+08	5.8
	173	202	5	5.66E-10	7.30E-02	1.29E+08	5.4
	172	202	5	5.86E-10	7.30E-02	1.25E+08	5.8
	169	199	6	5.86E-10	7.50E-02	1.28E+08	5.5
	170	200	6	5.86E-10	7.50E-02	1.28E+08	5.5
	171	201	6	5.86E-10	7.50E-02	1.28E+08	5.5

Files	Trace Locations			Time(seconds) (Surface to Sample Bottom)	Thickness meters	Velocity (m/s) sample bottom Velocity	t Dielectric Const.
	Top	Bottom	Sample				
1&2Perp2.dzt	147	178	1	6.05E-10	7.21E-02	1.19E+08	6.4
	147	178	1	6.05E-10	7.21E-02	1.19E+08	6.4
	148	177	1	5.66E-10	7.21E-02	1.27E+08	5.6
	141	174	2	6.45E-10	7.39E-02	1.15E+08	6.8
	141	174	2	6.45E-10	7.39E-02	1.15E+08	6.8
	141	175	2	6.64E-10	7.39E-02	1.11E+08	7.3
1&2PARA2.DZT	Top	Bottom					
	126	158	1	6.25E-10	7.21E-02	1.15E+08	6.8
	126	158	1	6.25E-10	7.21E-02	1.15E+08	6.8
	126	158	1	6.25E-10	7.21E-02	1.15E+08	6.8
	127	159	2	6.25E-10	7.39E-02	1.18E+08	6.4
	127	159	2	6.25E-10	7.39E-02	1.18E+08	6.4
	127	159	2	6.25E-10	7.39E-02	1.18E+08	6.4
3&4PARA2.DZT	129	163	3	6.64E-10	7.61E-02	1.15E+08	6.8
	130	163	3	6.45E-10	7.61E-02	1.18E+08	6.4
	131	163	3	6.25E-10	7.61E-02	1.22E+08	6.1
	127	158	4	6.05E-10	7.67E-02	1.27E+08	5.6
	125	157	4	6.25E-10	7.67E-02	1.23E+08	6.0
	124	157	4	6.45E-10	7.67E-02	1.19E+08	6.4
3&4PERP2.DZT	141	172	3	6.05E-10	7.61E-02	1.26E+08	5.7
	141	173	3	6.25E-10	7.61E-02	1.22E+08	6.1
	140	173	3	6.45E-10	7.61E-02	1.18E+08	6.4
	141	173	4	6.25E-10	7.67E-02	1.23E+08	6.0
	141	173	4	6.25E-10	7.67E-02	1.23E+08	6.0
	141	173	4	6.25E-10	7.67E-02	1.23E+08	6.0
5&6PARA2.DZT	140	173	5	6.45E-10	7.30E-02	1.13E+08	7.0
	141	174	5	6.45E-10	7.30E-02	1.13E+08	7.0
	141	174	5	6.45E-10	7.30E-02	1.13E+08	7.0
	138	170	6	6.25E-10	7.50E-02	1.20E+08	6.2
	139	172	6	6.45E-10	7.50E-02	1.16E+08	6.6
	140	173	6	6.45E-10	7.50E-02	1.16E+08	6.6
5&6PERP2.DZT	137	168	5	6.05E-10	7.30E-02	1.21E+08	6.2
	137	169	5	6.25E-10	7.30E-02	1.17E+08	6.6
	138	169	5	6.05E-10	7.30E-02	1.21E+08	6.2
	135	168	6	6.45E-10	7.50E-02	1.16E+08	6.6
	136	169	6	6.45E-10	7.50E-02	1.16E+08	6.6
	134	167	6	6.45E-10	7.50E-02	1.16E+08	6.6

Table 4.8: Ground Coupled GPR Dielectric Constant Results from the laboratory GPR survey

Files DRY	Sample	Time(seconds) one way travel time	Thickness	Velocity (m/s)	
			meters	sample bottom Velocity	Dielectric Constant
01.dzt	1	7.559E-10	0.07	9.54E+07	9.90
02.dzt	2	7.734E-10	0.07	9.56E+07	9.85
03.dzt	3	7.910E-10	0.08	9.63E+07	9.71
04.dzt	4	7.676E-10	0.08	9.99E+07	9.01
05.dzt	5	7.617E-10	0.07	9.58E+07	9.80
06.dzt	6	7.793E-10	0.08	9.63E+07	9.71
Files WET		**Time(seconds)** one way travel time	**Thickness**	**Velocity (m/s)**	
			meters	sample bottom Velocity	Dielectric Constant
012.dzt	1	7.09E-10	0.07	1.02E+08	8.71
022.dzt	2	7.38E-10	0.07	1.00E+08	8.98
032.dzt	3	7.50E-10	0.08	1.02E+08	8.73
042.dzt	4	7.27E-10	0.08	1.06E+08	8.07
052.dzt	5	7.09E-10	0.07	1.03E+08	8.49
062.dzt	6	7.38E-10	0.08	1.02E+08	8.72

From the results of the GPR survey in Table 4.8 the dielectric constant

values for the saturated samples are generally lower then their unsaturated sample

counterparts using the ground-coupled GPR antenna. Explanations for this

discrepancy may be that the samples weren't fully saturated or due to human error in

determining where the upper and lower pavement surface interfaces are located using Autopicklayers3. As for the air-launched GPR antenna, the dielectric constant ranges for the unsaturated samples are from 4.6-7.6 and for saturated samples dielectric constant ranges from 5.6-7.0 as shown in Figure 4.3. Looking at the results of Table 4.9, the author's MATLAB program calculated GPR wave velocities using the autopicklayers3 program using processed raw data files provided by John Belcher using Radan Roadway software. The dielectric constant measurements determined from the saturated samples using the ground-coupled GPR antenna as shown in Table 4.8 were generally greater than the results from the unsaturated samples. Therefore, the results from the saturated/wet samples should be discarded and only the velocity values from the unsaturated samples should be used. Table 4.9 shows that the dielectric constant values ranged from 10.78-12.76 as shown below using the GPR wave velocities obtained from Belcher's processed raw data files and sample thickness (core data).

Table 4.9: Dielectric constant values of the air launched GPR survey using Radan Roadway Software and $\varepsilon=(c/v)^2$

Air Launched GPR 2006 using Radan Roadway Software						
Sample	**Dielectric Constant**	**type**				
1	10.78	core data				
2	9.75	core data				
3	12.76	core data				
4	12.76	core data				
5	N/A	core data				
6	N/A	core data				

When comparing all values to Wimsatt(1998), the results generally indicate that the samples consistent with his flexible pavement values and are similar to the results for the 2005 GPR study results for flexible pavements. Also with all the samples thicker than seven centimeters there doesn't appear to be any problem with GPR analysis in terms of thin pavement sections. Some problems that were raised from the 2006 GPR analysis was the faulty Radan Roadway software, resulting not

obtaining process raw data for each sample from the GPR technician. Other results from this survey include that using the air-launched GPR antenna on the wet sample indicated an increase in the average value of the dielectric constant in general when compared to the dry samples. Using the results from Lanbo Liu's 2002 study the results indicated that little moisture absorbed into the pavement samples and testing the samples with a ground coupled antenna. Due to the limited amount of time to conduct this survey the sample were only put into a water bath for only an hour and a half. This time may not have been sufficient enough to fully saturate the samples properly and therefore didn't yield the proper results for a ground coupled GPR study. Although with the air-launched GPR antenna reasonable results were obtained that were consistent with flexible pavements and resulted in ε values increasing with increasing moisture conditions. This problem (Liu & Guo 2002) was also discovered in the Lanbo Liu study resulting in their pavement samples not being fully saturated for their experiment. Finally, the dielectric constant measurement are sensitive to survey direction, where dielectric constant values are generally greater when the GPR antenna scans the samples along the length of the samples as shown in Figure 4.3. For instance, the pavement samples in the parallel motion setup had dielectric constant values greater than the samples in a perpendicular motion setup to within a factor of two.

Chapter 5. Time Domain Reflectometry Experiments

Time Domain Reflectometry Principles

Time domain reflectometry(TDR) is another electromagnetic technique which can complement results obtained from GPR data. The TDR operates on principles

similar to radar, where the TDR transmits a pulse through a cable and at the end of the cable or at a break in the wire the pulse is reflected back to the TDR unit(Granite Island Group, 2002). The TDR then measures the time the pulse was transmitted and reflected before converting that time into the two way travel distance of the pulse (Granite Island Group, 2002). The result is then displayed as a distance reading or waveform (Granite Island Group, 2002). GPR measures reflections from voltage pulses from antennas whereas time domain reflectometry measures reflections along transmission lines (Serbin & Or, 2004). TDR can be used to find the capacitance of a foil-asphalt-foil sandwich, and thus allow for estimation of the dielectric constant of the asphalt or concrete sample. The value of using the TDR is that it replaces a more expensive and unavailable network analyzer for finding dielectric constant of a pavement sample. This application for the TDR is appropriate for the time resolution when compared to a 1 GHz air-launched antenna. In contrast, a network analyzer would sweep through frequencies commonly used in GPR applications. This use of the time domain reflectometer is novel.

Time domain reflectometry (TDR) was utilized in order to directly calculate dielectric constant of asphalt pavement samples. TDR applies a step signal to the asphalt sample, and the step response is recorded. The response is identical to that of a RC series circuit suddenly connected to a battery, as shown in Figure 5.1. To the author's knowledge this technique has never been used on pavement samples before. Samples were prepared by cutting an asphalt sample into a thin slice, and gluing aluminum foil to the slice, forming a parallel plate capacitor. The capacitance of the asphalt slice is then measured by time domain reflectometry, and assuming a parallel

plate capacitor is used, dielectric constant is determined by using the formula for a parallel plate capacitor. A conceptual RC circuit analog to a parallel plate capacitor is shown in Figure 5.1.
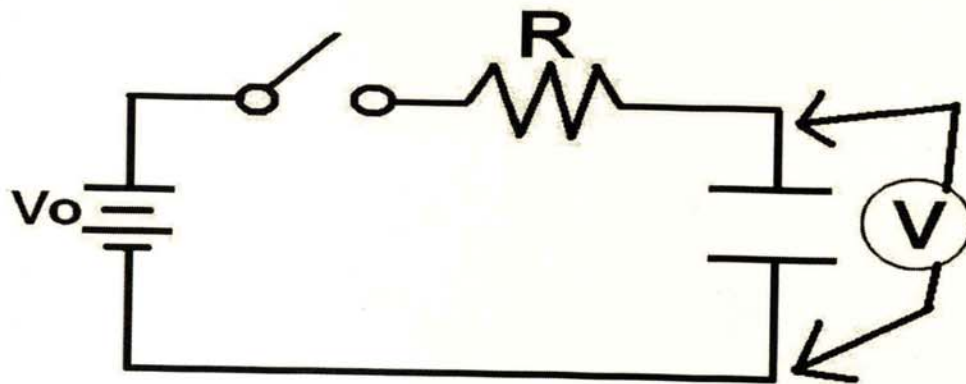
Figure 5.1: Conceptual RC circuit depicting TDR response for asphalt samples

The voltage response of this equivalent circuit is $V_o = V_o(1 - e^{-\frac{t}{RC}})$ where V_o, which is battery voltage and the resistor, is (50 ohms) the internal resistance of the TDR instrument. The MATLAB program created to analyze the step response from the pavement samples appears in the form similar to an ideal resistor voltage step response as shown in Figure 5.2.
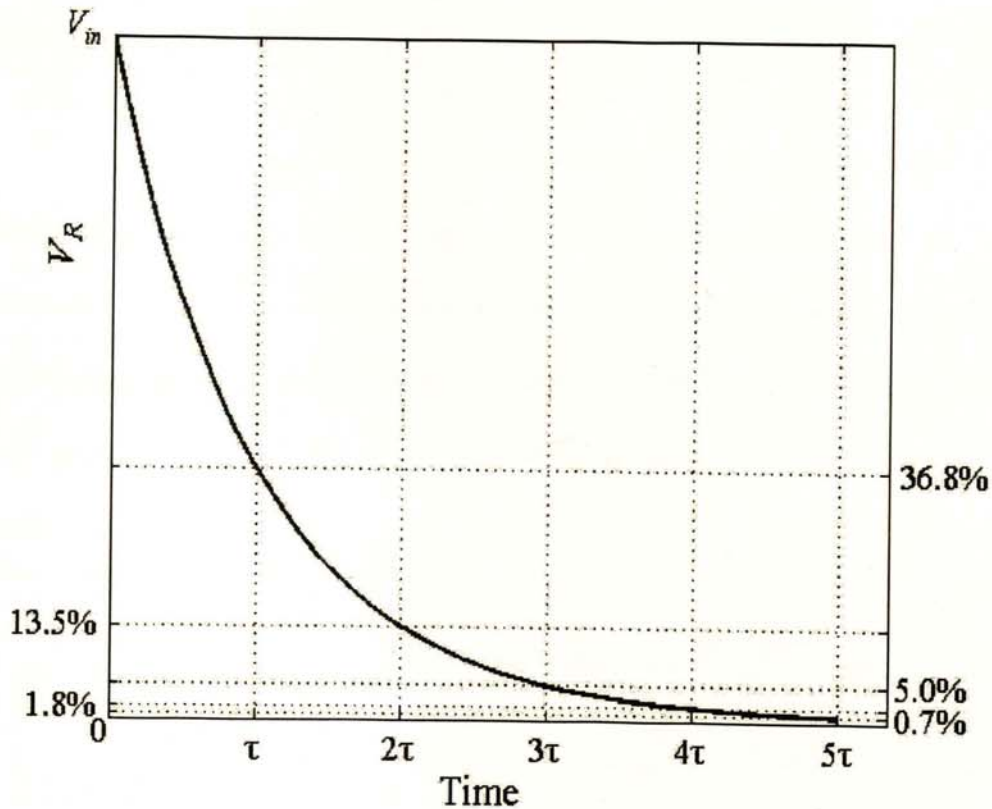
Figure 5.2 Resistor Voltage Step Response

Reference data is obtained from the TDR using an air dielectric capacitor of

the same dimensions as the pavement sample. The time domain reflectometer records

and displays the voltage/capacitor step response of each pavement sample. The

assumptions for these experiments are that asphalt pavement samples acts as a

dielectric within a parallel plate capacitor. A limitation is that the parallel plate

capacitor is finite because the length of the plates are not infinite, but we assume that

the discontinuous parallel plate capacitor the electric field at the edges of the

capacitor plates are negated by the stronger electric field within the center of the

parallel plate setup. The formula used to calculate and the theoretical air capacitance

of the pavement samples as shown in Figure 5.6 is $C_{theory} = \dfrac{A\varepsilon}{d}$ where C is

capacitance, A is plate area, ε is dielectric constant, and d is plate distance.

Laboratory Setup

Aluminum foil covered the top and bottom of the core sample where this experiment was conducted at room temperature in March 2006. A Tektronix 1502 Time Domain Reflectometer which used to determine capacitance of pavement cores that are covered with aluminum foil at the top and bottom of each sample. Figure 5.3 below illustrates the actual TDR setup used to calculate pavement capacitance measurements.
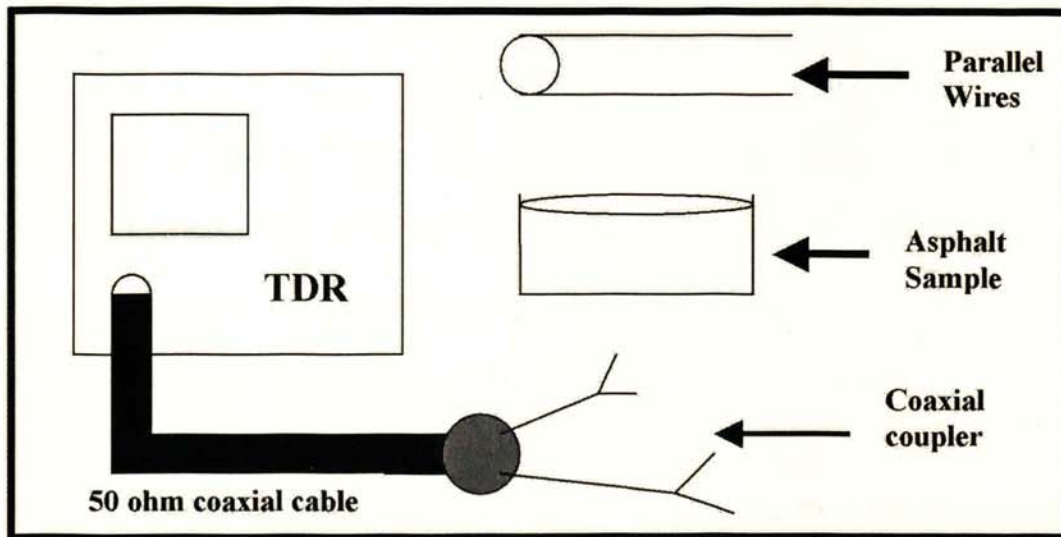
Figure 5.3: Time Domain Reflectometry Experimental Setup Showing Parallel Wires used for oscilloscope calibration the asphalt sample used as a dielectric and a coaxial coupler used to clamp to the aluminum foil plate attached to the asphalt sample

The TDR experiments used two types of pavement samples. The first type of pavement sample consisted of 6 inch diameter cores with circular shaped aluminum foil attached to the top and bottom of each (Figure 5.4).
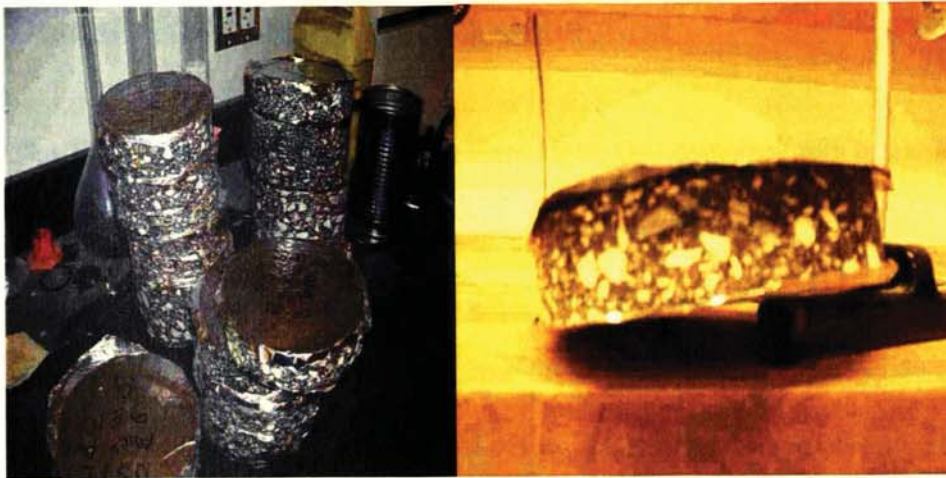
Figure 5.4: Six inch diameter pavement samples used in TDR experiment (left) and a close up of aluminum foil-asphalt-aluminum foil asphalt sandwich (right).

The second type of pavement sample used thinly cut rectangular asphalt pavement samples with aluminum foil attached to the top and bottom of each sample as shown in Figure 5.5 below. Appendix A lists the core diameter and thicknesses of each sample used in this study.

Figure 5.5: Thin rectangular pavement sample used in TDR experiment

Time Domain Reflectometry Data Collection

The TDR was an older model (Tektronix 1502) that provided only an analog chart recorder output, no digital storage, so it was necessary to experimentally determine the time duration of the digitized data. The TDR was calibrated for horizontal time scale before recording data from the sample. The horizontal time scale was calculated from the TDR by the following steps. First the sample waveform was recorded on the TDR and the analog data was transferred by wire to the Agilent digital oscilloscope. The waveform used for time scale calibration was the TDR test using the 16.3 cm straight wire apparatus as shown in Figure 5.6 below. TDR data was collected by attaching voltage clips from the TDR to the top and bottom aluminum foil plate on the asphalt sample.
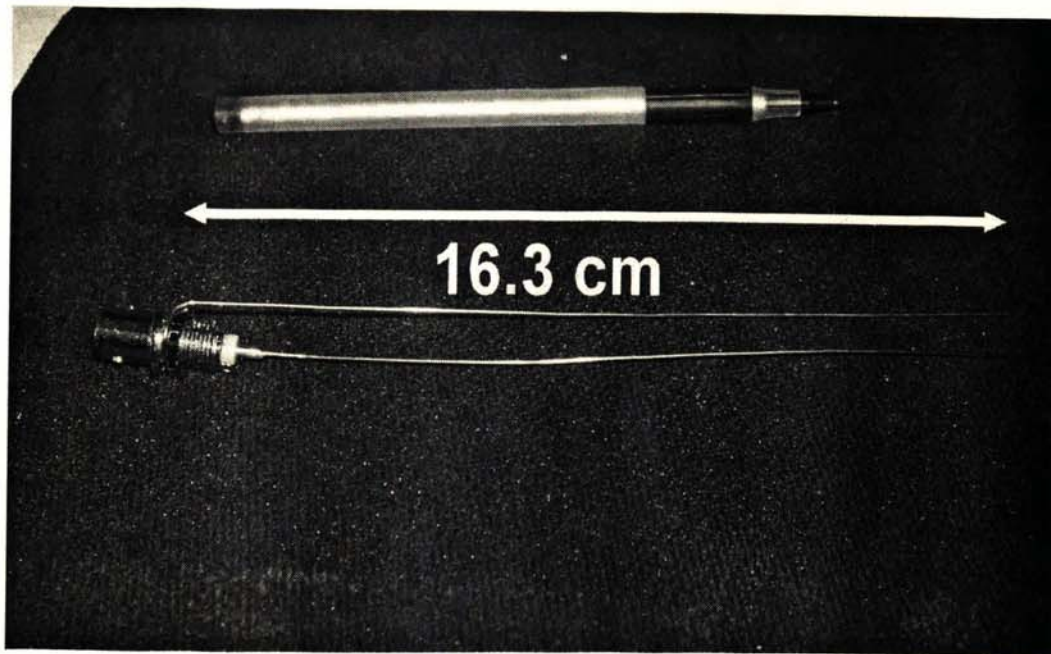
Figure 5.6 TDR open-end wire calibration device

The TDR recorded the step response of this apparatus and the results were transferred to the oscilloscope. Figure 5.7 shows the results of the TDR step response for the double wire apparatus.
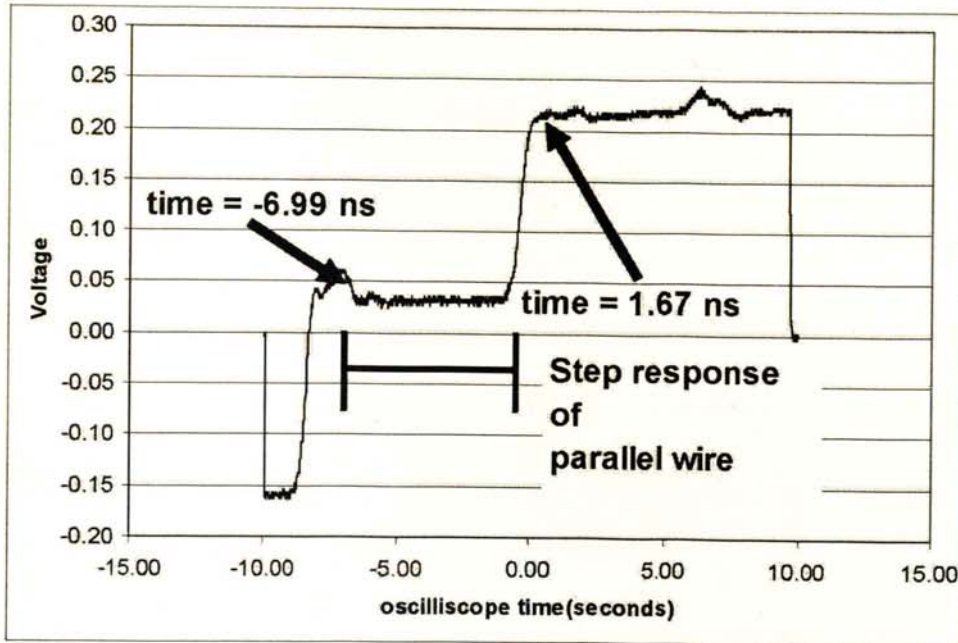
Figure 5.7: TDR Graph Showing Step Response of Double Wire Device Used for TDR Time Scale Calibration

The arrows in Figure 5.7 show the beginning and end of the step response for the double wire. The horizontal axis is time recorder on the digital oscilloscope measured in seconds. The figure shows that the TDR will complete its step response in (1.67 - -6.99) seconds or 8.66 seconds on the oscilloscope. Now the oscilloscope time is corrected to the amount of time it takes to generate the waveform step response on the TDR. The formula used to calculated the TDR step response time

is $time = \dfrac{2 * length}{c}$,

where the length is .163 cm, the length of the parallel wire apparatus in Figure 5.7. meters and c is the speed of light. With these values there are .92 TDR

62

nanoseconds for every 8.66 seconds of oscilloscope time. Since all of the TDR

sample data is transferred to the oscilloscope the oscilloscope time must be converted

to TDR time with the ratio $conversion = X_{\substack{scope \\ time}} * \dfrac{.92_{\substack{TDR \\ Time}}}{8.66_{\substack{Scope \\ Time}}}$. Finally to convert into

oscilloscope time the conversion factor is multiplied by $1 * 10^{-9}$ seconds.

The data collection process was performed for all of the circular and

rectangular asphalt pavement samples. For calibration, a capacitor with an air

dielectric was also tested. This was created by stacking two aluminum-clad pavement

samples on top of one another separated by a spacer, as shown in Figure 5.8 below.

***Figure 5.8: Setup for asphalt samples for calculating air dielectric in TDR
experiment***
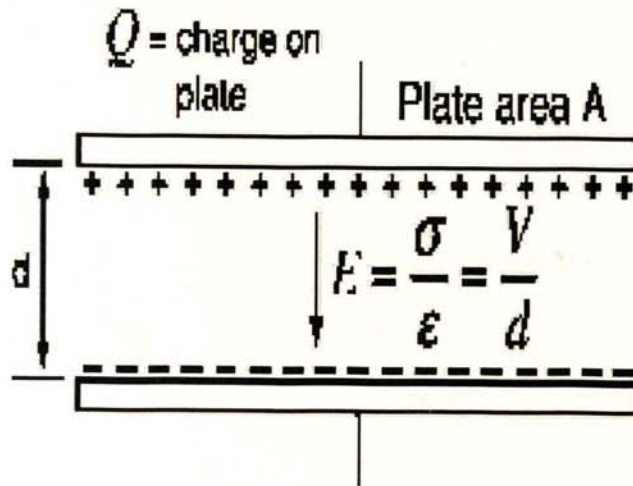
Figure 5.9 Setup for Ideal Parallel Plate Capacitor

The method used in calculating dielectric constant from the original TDR waveform

as follows. First, the MATLAB program TDRDATA2 was used to load the sample

waveform for manipulation as shown in Figure 5.10 below.
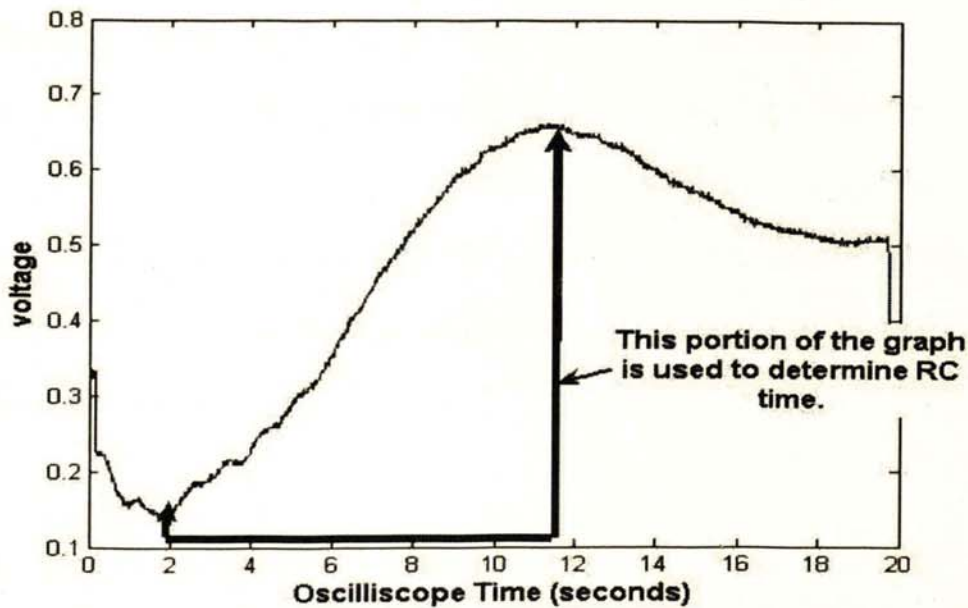
Figure 5.10: Original TDR Plot of US-21 Michigan Ave.

TDR Plot of Data for US 21 - Michigan Ave

Truncate Graph between the arrows
approximately between data numbers
0-1100
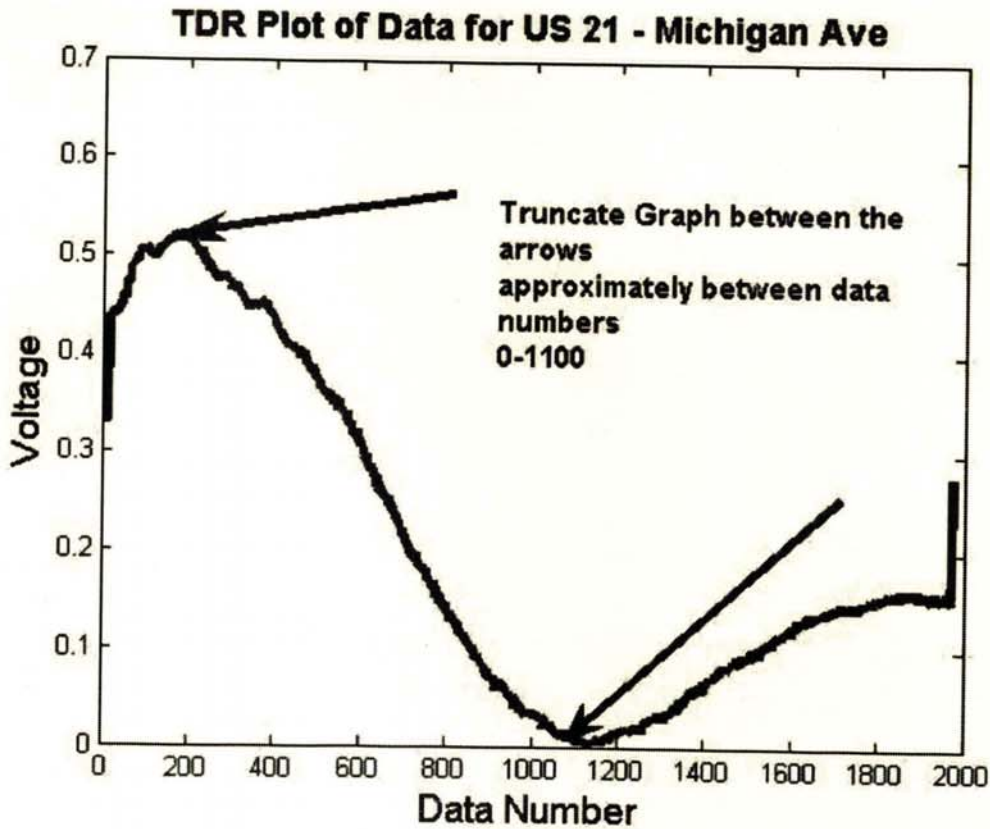
Figure 5.11 : TDR Waveform Plot of Sample US 21- Michigan Ave A Inverted and Raised by the Maximum Voltage Value

In Figure 5.10 shows a portion of the original waveform being used to compute RC time. In order to avoid having infinite values when the natural log of waveform is taken, the maximum voltage value of the original waveform is added to all values of the original waveform to create Figure 5.11.so that all values of the reconstructed waveform are above zero. The steepest part of the truncated TDR sample plot is selected as shown in Figure 5.12 below

Truncated TDR Plot of US 21-Michigan Ave with Time Scale and Ln Voltage

Select Shallowest part of Truncated TDR Plot for capacitance calculations
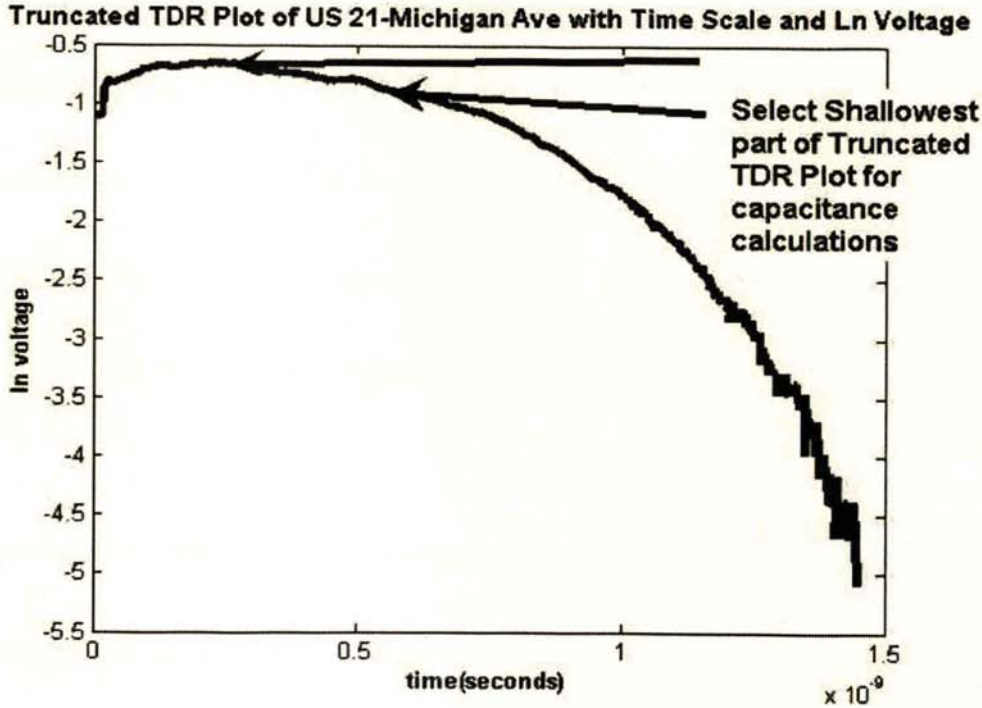
Figure 5.12 : Reconstructed TDR Waveform Plot of US 21-Michigan A

Truncated TDR Plot of US 21-Michigan Ave A Sample with Linear Fit

US 21 A
linear fit

$y = -7.46e+008*x - 0.468$
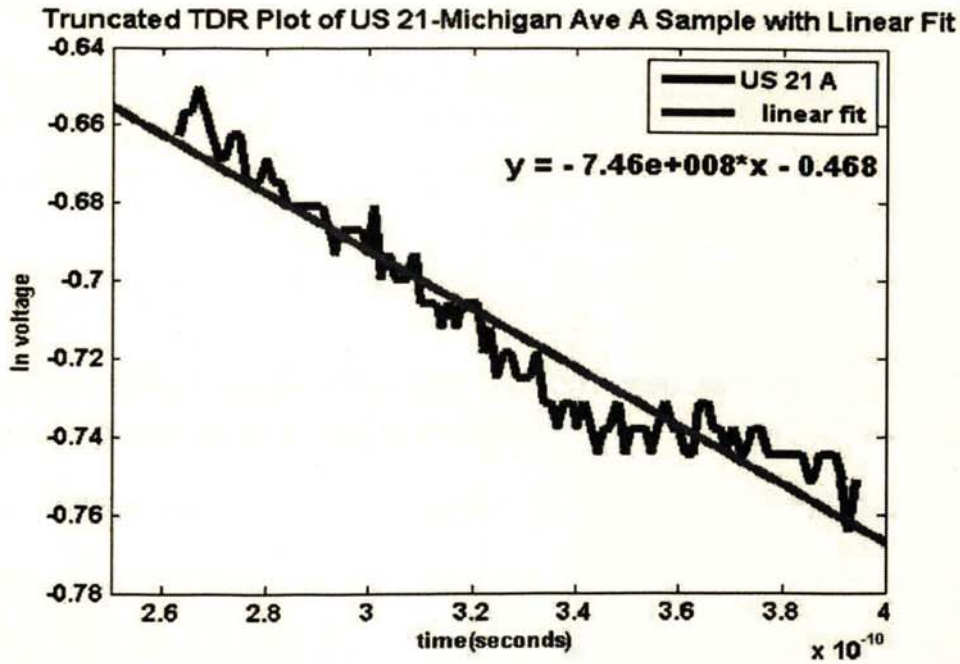
Figure 5.13 : Selected part of TDR Waveform Plot of US 21 with a linear fit applied.

After the steepest part of the TDR wavelet is selected as shown in Figure 5.12 above.

A linear fit is applied to the truncated wavelet as shown in Figure 5.13. A linear fit is

used because it's assumed that the slope of the linear fit is $\frac{1}{\tau} = Slope_{TDR}$ where τ is

the time constant. Capacitance is calculated using $\tau = RC$ where R is 50 ohms & $\tau = $

$\frac{1}{Slope_{TDR}}$. Finally in order to find dielectric constant values the capacitance values of

the asphalt dielectric samples are compared to TDR calculated capacitance using the

air dielectric configurations of the same sample thickness as shown in Figure 5.8.

Using the formula $\kappa = \frac{C_{TDRSample}}{C_{TDRair}}$ dielectric constant for the sample is calculated where

the air dielectric is assumed to have a dielectric constant value of one.

From the linear fit. the slope of the linear formula is taken and used to calculate the

capacitance of sample six. For example, the absolute value of the slope given from

Figure 5.14 is $|-7.46 * 10^8|$. Given a TDR slope value of $7.46 * 10^8$ the capacitance

is $C = \frac{\tau}{50}$ where $C = \frac{1}{50 * 7.46 * 10^8} = 26.8$ pf. All of the TDR capacitance samples

are calculated in this manner.

Time Domain Reflectometer Results and Discussion

The method of calculating the dielectric constants for each of the roadway

core samples involved using the shallowest part of the TDR waveform generating a

linear fit to negative natural log for the TDR trace. The TDRDATA2 program created

to calculate the linear equations for capacitances is shown in Appendix C. Appendix

E lists the results of the dielectric constant values calculated from the TDR

experiments. As seen in Appendix E there are a range of dielectric constant values

for the pavement samples. The values ranged from a dielectric constant value of 1.61 for the 1 cm thick samples, to a value of 10.4 for the US-131 E pavement sample. The majority of the samples have values of 4 to 5 with most samples having values of above unity. Thus, the values are reasonable for pavement dielectric constant. Although when one compares the pavement dielectric constant values obtained with the TDR using air as a dielectric with the TDR values calculated using a pavement dielectric, the majority of dielectric constant values have a dielectric constant of 2.0 with the exception of a few asphalt pavement samples being above 3.0. As for the thin rectangular samples, their dielectric constant value averaged 2.29. From these results it is the writer's opinion that reasonable dielectric constant values can be obtained from roadway cores by calculating capacitance from the TDR and comparing it to the theoretical capacitance formula for air dielectrics for a parallel plate capacitor $\kappa = \dfrac{C_{TDR}}{C_{theory}}$. TDR measurements can provide reasonable results from varying pavement mixes as shown from this study in Appendix E.

Consistency for this survey is subjective in deciding where to place the linear slope at the shallowest point of the TDR log voltage vs. time graph. The selection of the slope should not include any value past one time constant or the dielectric constant results will become unreasonable for pavement samples. This problem may be overcome with also recording multiple TDR voltage scans to get an average linear slope of the capacitance function.

CHAPTER 6. SUGGESTIONS FOR FUTURE WORK

Several refinements can be made on the methods of collecting GPR data and calculating dielectric constants for pavement sections. For the manufactured pavement sample survey one should submerge the pavement samples in a water-filled vacuum chamber to eliminate any air pockets within the samples similar to the Lanbo Liu study. Also these samples should be in the vacuum chamber for a one-day period. Also pavement samples need to be created that range in densities between 100 lbs/ft^3 to 200 lbs/ft^3 For the time domain reflectometer survey one should create at least 30 thin pavement cores of less than 1.5 cm of similar pavement mixes and density to test the stability of the TDR measurements. Also an apparatus that would accurately model an air dielectric with a dielectric constant as close to unity would need to be created for use in future tests. This study would help determine if the TDR measurements of pavement dielectric constant measurement are repeatable and if pavement thickness is a factor in this measurement.

Future studies suggestions would include collecting pavement GPR scans and dielectric constant calculations from the center of the roadway, and wheel pathway scans.

In the ideal situation, the author estimates, would be to have air and ground coupled GPR antenna traces along the edges, middle and along the wheel pathway on the roadway at each site. Also in the ideal situation 30 thin pavement samples made with the same pavement mix as the pavement tested with the GPR antenna would be made. These samples would be tested with a TDR for dielectric constant calculations.

Chapter 7. CONCLUSIONS

Using the techniques of GPR road surveys, scanning manufactured pavement samples, and time domain reflectometry has been demonstrated here that the use of GPR wavelets can be used within a short-term comprehensive road radar plan to determine dielectric constants in a variety of asphalt pavement conditions. The procedures used to collect and calculate dielectric constant data ranged from passive methods such as field radar experiments, to more direct measurements with Time Domain Reflectometry. "Theoretical" values of dielectric constant from mixing models were also considered in this study. For the field GPR study, GPR wavelets were used to calculate dielectric constants of pavement material using both the air launched and ground coupled GPR antennas. Time domain reflectometry used in conjunction with roadway cores and GPR scans can also help to determine asphalt dielectric constants. Limitations encountered in the GPR study included the type of Radan Roadway Software interpretation, more consistent results were produced using roadway core samples, but poor quality or thin cores resulted in unrealistic dielectric constant and roadway velocity values. Using the amplitude of surface reflection resulted in fairly accurate dielectric constant data, even when the roadway is relatively thin or of poor quality. This investigation was severely limited by the small amount of time the MDOT operator were available, primarily leading to the lack of opportunity to repeat experiments and develop efficient procedures directed by experience. Therefore, this study tested initial survey design, on the basis of which refinements could be made to make measurements more reliable and accurate for GPR studies.

Dielectric constant measurements estimated using the manufactured samples gave consistent measurements when compared to the air launched and ground coupled GPR scans. Limitations to this experiment involved determining dielectric constant data under surface saturated conditions using ground coupled antennas. This experiment required that the samples being soaked under long-term conditions possibly a day or more with a vacuum to fully saturate the samples.

The capacitance measurement of the asphalt samples using TDR provided consistent results for samples with similar thicknesses and asphalt mix type. This experiment also produced dielectric constant data consistent with actual pavement values. Limitations for this experiment are that this experiment did not work well when testing for the air dielectrics and comparing these results to the actual pavement capacitance values. This resulted in errors on the order of 2 -3 times greater than an air dielectric of 1.0. Also this experiment did not work well the comparing the TDR computed dielectric constant values of the 1.0 cm pavement samples with their theoretical capacitances. These values were not realistic for pavement samples.

The major conclusions that can be drawn from this study are that dielectric constant values that were obtained from these 3 experiments were in general agreement. This conclusion provides evidence that the dielectric constant values obtained in the 2005 GPR field study were accurate. The general groundwork has been laid for conducting more efficient comprehensive GPR surveys that gather the most amount of information on a short-term basis. With some extra time and expense it would be possible to develop a procedure which creates pavement conditions found

71

on actual roadway and use a time domain reflectometer along with GPR to develop

methods which detect defects in roadways in an efficient manner.

REFERENCES CITED

Alongi, A.V., et al. "Concrete Evaluation by Radar Theoretical Analysis." *Transportation Research Record* 853 (1982): 31-37.

Al-Qadi, Imad L., and Lahouar, Samer. "Detection of Asphalt Binder Aging in Flexible Pavement by Ground Penetrating Radar." *Materials Evaluation* 63.9 (2005): 921-925.

Baradello, L., GPR Tips e Tricks Georadar, http://digilander.libero.it/lucabaradello/uk_tipstricks.html, 2006.

Granite Island Group, TDR Tutorial - Introduction to Time Domain Reflectometry, 2002, http://www.tscm.com/riprcop.html.

Lahouar, Samer, et al. "Approach to Determining In Situ Dielectric Constant of Pavements: Development and Implementation at Interstate 81 in Virginia." *Transportation Research Record* 1806 (2002): 81-87.

Liner, Christopher L. Elements of 3D Seismology 2nd Ed, PennWell Corporation, Tulsa, Oklahoma, USA, 2004.

Liu, Lanbo, Guo, T. "Dielectric Property of Asphalt Pavement Specimens in Dry, Water-Saturated, and Frozen Conditions." *Ninth International Conference on Ground Penetrating Radar* (2002): 410-415.

Martinez, Alex, and Byrnes, Alan P. "Modeling Dielectric-Constant Values of Geologic Materials: An Aid to Ground-penetrating Radar Data Collection and Interpretation." *Kansas Geological Survey, Current Research in Earth Sciences* 247.1 (2001): http://www.kgs.ku.edu/Current/2001/martinez/martinez1.html.

Maser, Kenneth R. "Automated Interpretation for Sensing In Situ Conditions." *Journal of Computing in Civil Engineering* 2.3 (1998): 215-238.

Maser, Kenneth R., and Scullion, Tom. "Automated Pavement Subsurface Profiling Using Radar: Case Studies of Four Experimental Field Sites" *Transportation Research Record* 1344 (1992): 148-154.

Morey Rexford M. "Synthesis of Highway Practice 255, Ground Penetrating Radar for Evaluating Subsurface Conditions for Transportation Facilities." *Transportation Research Board* (1998).

Olhoeft, Gary R. "Maximizing the information return from ground penetrating radar." *Journal of Applied Geophysics* 43 (2000): 175-187.

Reppert, Philip M., Morgan, F. Dale., and Toksöz, M. Nafi. "Dielectric constant determination using ground-penetrating radar reflection coefficients." *Journal of Applied Geophysics* 43 (2000): 189-197.

Reynolds, John M. An <u>Introduction to Applied and Environmental Geophysics</u>, John Wiley & Sons, New York, 1997,

Roberts, Freddy L. et al., <u>Hot Mix Asphalt Materials, Mixture Design, and Construction</u>, NAPA Research and Education Foundation, Lanham, MD, 2nd Ed., 1996, p. 585.

Saarenketo, T., and Scullion, T. "Road Evaluation with ground penetrating radar." *Journal of Applied Geophysics* 43 (2000):119-138.

Saarenketo, Timo, and Scullion, T. "Using Electrical Properties to Classify the Strength Properties of Base Course Aggregates." *Texas Transportation Institute* FHWA/TX-97/1341-2 (1996): p. 87.

Saarenketo, Timo, and Scullion, T. "Ground Penetrating Radar Applications on Roads and Highways." *Texas Transportation Institute* TX-95/1923-2F (1994): p. 52.

Scullion, T., and Saarenketo T. "Use of Ground Penetrating Radar for Site Investigation of Low-Volume Roadways and Design Recommendations." *Texas Transportation Institute* TX-02/4906-1 (2002): p. 58.

Scullion Tom, et al. "Applications of Ground-Coupled GPR to Pavement Evaluation." *Texas Transportation Institute* TX-98/2947-S (1997): p. 54.

Scullion, Tom, and Rmeili, E. "Detecting Stripping in Asphalt Concrete Layers Using Ground-Penetrating Radar." *Texas Transportation Institute* TX-98/2964-S (1997): p. 38.

Serbin, Guy, and Or, Dani. "Ground-Penetrating Radar Measurement of Soil Water Content Dynamics Using a Suspended Horn Antenna." *IEEE Transactions on Geoscience and Remote Sensing* 42.8 (2004): 1695-1705.

Serway, Raymond A., and Beichner, Robert J., <u>Physics: For Scientists and Engineers with Modern Physics.</u> Saunders College Publishing, Orlando, Fl, 5th Ed. 2000.

Widess, M. B. "How Thin is a Thin Bed?" *Geophysics* 38.6 (1973):1176-1180.

Wimsatt, Andrew J., et al. "The Use of Ground Penetrating Radar Data In Pavement Rehabilitation Strategy Selection and Pavement Condition Assessment," *SPIE proceedings series* 3400 (1998):372-383.

APPENDIX A

Appendix A contains the physical parameters for the pavement cores from the 2005 GPR survey

Project Number	AM									
Location	US-41									
Sample	AM2	AM3	AM4	AM5	AM6	AM7	AM8	AM9	AM10	AM11
Average Height	63.42	71.75	47.89	47.31	48.31	67.61	86.30	70.99	72.47	66.05
Average Diameter	146.42	146.87	146.59	146.81	146.37	147.16	147.25	147.09	147.01	147.48

	Corelock									
Project Number	M 26/Twin Lake									
Sample	2	3	4	5	6	7	8	9	10	11
Average Height(mm)	3.61	3.73	3.93	3.50	3.66	3.57	2.17	4.19	4.16	3.74
Average Diameter(mm)	15.16	15.20	15.25	15.10	14.75	14.82	14.66	14.54	14.72	13.57

	Corelock									
Location	Five Mile Pt									
Sample	FM 1	FM 2	FM 3	FM 4	FM 5	FM 6	FM 7	FM 8	FM 9	FM 10	FM 11
Average Height	48.44	46.12	39.82	43.13	48.69	45.05	45.62	47.26	48.05	47.62	40.08
Average Diameter	146.74	146.59	146.66	146.71	146.72	146.79	146.80	147.21	146.89	147.02	146.70

LAC LA BELLE Cores					LLB Cores					
Sample Number	1	2	3	4	5	6	7	8	9	10	11
Height (cm)	1.8	1.5	2.5	2.7	1.6	2.2	2	2.1	2.4	1.9	1.5

APPENDIX B

Appendix B contains the continuous dielectric constant values taken from the Radan Road software for the 2005 and 2006 GPR surveys

WARNING: Modification of this ASCII file outside of RADAN may cause unpredictable
Version = 5   behavior when this file is reloaded into RADAN.
Data Filename = M41 LAYER PICK.DZT
Layer threshold distance = 32.807999 ft
Number of layers = 1
Amplitude Units = Decibels with correction applied for spreading and transmission
Last Pick Settings:
Layer 1   Automatic   150   0   1   3
Calibration file = C:\DATA\MTU RESEARCH\M-41 PROCESSED FILES\M41 CALIBRATION.CZT

File	Ch#	Scan#	x(ft)	y(ft)	Layer 1	z(in)	Amp	Dev(ft)
M41 LAYE	1	109	54.602		0 Layer 1	1.938	-5.12	0.2
M41 LAYE	1	110	55.103		0 Layer 1	2.075	-16.79	0.04
M41 LAYE	1	111	55.604		0 Layer 1	2.029	-16.2	0.08
M41 LAYE	1	112	56.105		0 Layer 1	1.908	-4.86	0.16
M41 LAYE	1	113	56.606		0 Layer 1	2.018	-16.81	0.17
M41 LAYE	1	114	57.107		0 Layer 1	2.145	-17.39	0.04
M41 LAYE	1	120	60.113		0 Layer 1	2.095	-16.74	0.06
M41 LAYE	1	121	60.614		0 Layer 1	2.003	-4.95	0.15
M41 LAYE	1	127	63.619		0 Layer 1	2.049	-18.18	0.05
M41 LAYE	1	128	64.12		0 Layer 1	2.044	-17.11	0.04
M41 LAYE	1	129	64.621		0 Layer 1	2.061	-16.5	0.02
M41 LAYE	1	169	84.659		0 Layer 1	2.21	-5.31	0.29
M41 LAYE	1	170	85.16		0 Layer 1	2.245	-5.39	0.33
M41 LAYE	1	172	86.162		0 Layer 1	2.411	-5.46	0.5
M41 LAYE	1	173	86.662		0 Layer 1	2.355	-5.32	0.45
M41 LAYE	1	174	87.163		0 Layer 1	2.286	-5.33	0.38
M41 LAYE	1	175	87.664		0 Layer 1	2.242	-5.39	0.34
M41 LAYE	1	176	88.165		0 Layer 1	2.185	-5.24	0.28
M41 LAYE	1	177	88.666		0 Layer 1	2.08	-5.32	0.18
M41 LAYE	1	178	89.167		0 Layer 1	2.107	-5.22	0.21
M41 LAYE	1	179	89.668		0 Layer 1	2.089	-5.35	0.2
M41 LAYE	1	180	90.169		0 Layer 1	2.02	-5.35	0.13
M41 LAYE	1	229	114.715		0 Layer 1	1.736	-5.57	0.02
M41 LAYE	1	230	115.216		0 Layer 1	1.646	-5.26	0.07
M41 LAYE	1	231	115.717		0 Layer 1	1.714	-5.49	0.01
M41 LAYE	1	232	116.218		0 Layer 1	1.634	-5.22	0.07
M41 LAYE	1	233	116.719		0 Layer 1	1.678	-5.37	0.02
M41 LAYE	1	234	117.22		0 Layer 1	1.663	-5.32	0.03
M41 LAYE	1	235	117.721		0 Layer 1	1.661	-5.31	0.03
M41 LAYE	1	236	118.222		0 Layer 1	1.71	-5.47	0.03
M41 LAYE	1	237	118.723		0 Layer 1	1.614	-5.39	0.07
M41 LAYE	1	238	119.224		0 Layer 1	1.589	-5.3	0.09
M41 LAYE	1	239	119.724		0 Layer 1	1.627	-5.43	0.05
M41 LAYE	1	240	120.225		0 Layer 1	1.558	-5.43	0.12
M41 LAYE	1	290	145.272		0 Layer 1	1.68	-5.37	0.06
M41 LAYE	1	291	145.773		0 Layer 1	1.71	-5.47	0.09
M41 LAYE	1	292	146.274		0 Layer 1	1.632	-5.45	0.01
M41 LAYE	1	293	146.775		0 Layer 1	1.672	-5.59	0.05
M41 LAYE	1	294	147.276		0 Layer 1	1.574	-5.25	0.05
M41 LAYE	1	295	147.777		0 Layer 1	1.646	-5.5	0.03
M41 LAYE	1	296	148.278		0 Layer 1	1.699	-5.44	0.08

Scan#	x(ft)	% Scans	Vel. Type	v(in/ns)	t(ns)	V(m/s)	ε	thickness(cm)
109	54.602	100	Automatic	3.386	1.141	8.60E+07	12.17	4.92
110	55.103	100	Automatic	3.504	1.18	8.90E+07	11.36	5.27
111	55.604	100	Automatic	3.543	1.141	9.00E+07	11.11	5.15
112	56.105	100	Automatic	3.224	1.18	8.19E+07	13.42	4.85
113	56.606	90.77	Automatic	3.299	1.219	8.38E+07	12.82	5.13
114	**57.107**	**90.77**	**Automatic**	**3.398**	**1.258**	**8.63E+07**	**12.08**	**5.45**
120	60.113	90.77	Automatic	3.319	1.258	8.43E+07	12.66	5.32
121	60.614	90.77	Automatic	3.276	1.219	8.32E+07	13.00	5.09
127	63.619	93.85	Automatic	3.461	1.18	8.79E+07	11.65	5.20
128	64.12	93.85	Automatic	3.343	1.219	8.49E+07	12.48	5.19
129	64.621	93.85	Automatic	3.48	1.18	8.84E+07	11.52	5.23
169	84.659	98.46	Automatic	3.5	1.258	8.89E+07	11.39	5.61
170	85.16	100	Automatic	3.555	1.258	9.03E+07	11.04	5.70
172	86.162	100	Automatic	3.594	1.336	9.13E+07	10.80	6.12
173	86.662	100	Automatic	3.512	1.336	8.92E+07	11.31	5.98
174	87.163	100	Automatic	3.512	1.297	8.92E+07	11.31	5.81
175	**87.664**	**100**	**Automatic**	**3.551**	**1.258**	**9.02E+07**	**11.06**	**5.69**
176	88.165	100	Automatic	3.461	1.258	8.79E+07	11.65	5.55
177	88.666	100	Automatic	3.512	1.18	8.92E+07	11.31	5.28
178	89.167	100	Automatic	3.445	1.219	8.75E+07	11.75	5.35
179	89.668	100	Automatic	3.528	1.18	8.96E+07	11.21	5.31
180	90.169	100	Automatic	3.528	1.141	8.96E+07	11.21	5.13
229	114.715	100	Automatic	3.657	0.945	9.29E+07	10.43	4.41
230	115.216	100	Automatic	3.469	0.945	8.81E+07	11.59	4.18
231	115.717	100	Automatic	3.61	0.945	9.17E+07	10.70	4.35
232	116.218	100	Automatic	3.445	0.945	8.75E+07	11.75	4.15
233	116.719	100	Automatic	3.535	0.945	8.98E+07	11.16	4.26
234	**117.22**	**100**	**Automatic**	**3.604**	**0.945**	**8.90E+07**	**11.36**	**4.22**
235	117.721	100	Automatic	3.5	0.945	8.89E+07	11.39	4.22
236	118.222	100	Automatic	3.602	0.945	9.15E+07	10.75	4.34
237	118.723	100	Automatic	3.547	0.906	9.01E+07	11.09	4.10
238	119.224	100	Automatic	3.492	0.906	8.87E+07	11.44	4.04
239	119.724	100	Automatic	3.575	0.906	9.08E+07	10.91	4.13
240	120.225	100	Automatic	3.579	0.867	9.09E+07	10.89	3.96
290	145.272	100	Automatic	3.539	0.945	8.99E+07	11.14	4.27
291	145.773	100	Automatic	3.602	0.945	9.15E+07	10.75	4.34
292	146.274	100	Automatic	3.587	0.906	9.11E+07	10.84	4.15
293	146.775	100	Automatic	3.673	0.906	9.33E+07	10.34	4.25
294	147.276	100	Automatic	3.461	0.906	8.79E+07	11.65	4.00
295	**147.777**	**100**	**Automatic**	**3.618**	**0.906**	**9.19E+07**	**10.66**	**4.18**
296	148.278	100	Automatic	3.579	0.945	9.09E+07	10.89	4.32

M41 LAYE	1	297	148.779	0 Layer 1	1.596	-5.32	0.02
M41 LAYE	1	298	149.28	0 Layer 1	1.627	-5.2	0.01
M41 LAYE	1	299	149.781	0 Layer 1	1.581	-5.52	0.04
M41 LAYE	1	300	150.282	0 Layer 1	1.619	-5.4	0
M41 LAYE	1	301	150.783	0 Layer 1	1.586	-5.53	0.03
M41 LAYE	1	351	175.83	0 Layer 1	1.583	-5.27	0.05
M41 LAYE	1	352	176.331	0 Layer 1	1.506	-5.24	0.13
M41 LAYE	1	353	176.832	0 Layer 1	1.665	-5.56	0.02
M41 LAYE	1	354	177.332	0 Layer 1	1.525	-5.31	0.13
M41 LAYE	1	355	177.833	0 Layer 1	1.58	-5.26	0.08
M41 LAYE	**1**	**356**	**178.334**	**0 Layer 1**	**1.555**	**-5.42**	**0.1**
M41 LAYE	1	357	178.835	0 Layer 1	1.655	-5.53	0.01
M41 LAYE	1	358	179.336	0 Layer 1	1.63	-5.44	0.04
M41 LAYE	1	359	179.837	0 Layer 1	1.556	-5.18	0.12
M41 LAYE	1	360	180.338	0 Layer 1	1.581	-5.27	0.1
M41 LAYE	1	361	180.839	0 Layer 1	1.781	-5.47	0.1
M41 LAYE	1	406	203.381	0 Layer 1	2.598	-18.87	0.4
M41 LAYE	1	411	205.886	0 Layer 1	2.395	-15.47	0.08
M41 LAYE	1	412	206.387	0 Layer 1	2.434	-15.14	0.1
M41 LAYE	1	413	206.888	0 Layer 1	2.51	-16.81	0.15
M41 LAYE	1	414	207.389	0 Layer 1	2.656	-28.69	0.28
M41 LAYE	**1**	**415**	**207.89**	**0 Layer 1**	**2.614**	**-22.05**	**0.21**
M41 LAYE	1	419	209.894	0 Layer 1	2.595	-17.82	0.11
M41 LAYE	1	422	211.396	0 Layer 1	2.778	-23.59	0.24
M41 LAYE	1	423	211.897	0 Layer 1	2.706	-19.76	0.15
M41 LAYE	1	426	213.4	0 Layer 1	2.931	-37.22	0.32
M41 LAYE	1	428	214.402	0 Layer 1	2.651	-18.41	0
M41 LAYE	1	471	235.942	0 Layer 1	3.242	-17.41	0.09
M41 LAYE	1	472	236.443	0 Layer 1	3.163	-15.23	0.01
M41 LAYE	1	473	236.944	0 Layer 1	3.203	-15.85	0.05
M41 LAYE	1	474	237.445	0 Layer 1	3.283	-17.36	0.1
M41 LAYE	1	475	237.946	0 Layer 1	3.163	-15.2	0.02
M41 LAYE	**1**	**476**	**238.447**	**0 Layer 1**	**3.163**	**-15.19**	**0.03**
M41 LAYE	1	477	238.948	0 Layer 1	3.282	-17.59	0.15
M41 LAYE	1	478	239.449	0 Layer 1	3.123	-18.28	0
M41 LAYE	1	479	239.95	0 Layer 1	3.163	-15.94	0.04
M41 LAYE	1	481	240.952	0 Layer 1	3.163	-16.14	0.05
M41 LAYE	1	482	241.453	0 Layer 1	3.163	-16.73	0.05
M41 LAYE	1	531	265.999	0 Layer 1	2.32	-14.47	0.01
M41 LAYE	1	532	266.5	0 Layer 1	2.398	-15.01	0.09
M41 LAYE	1	533	267.001	0 Layer 1	2.271	-14.25	0.02
M41 LAYE	1	535	268.003	0 Layer 1	2.11	-17.74	0.15
M41 LAYE	1	536	268.503	0 Layer 1	2.117	-16.85	0.12
M41 LAYE	**1**	**537**	**269.004**	**0 Layer 1**	**2.061**	**-17.07**	**0.16**
M41 LAYE	1	538	269.505	0 Layer 1	2.035	-16.54	0.17
M41 LAYE	1	539	270.006	0 Layer 1	2.066	-16.61	0.12
M41 LAYE	1	540	270.507	0 Layer 1	2.099	-15.78	0.08
M41 LAYE	1	541	271.008	0 Layer 1	1.979	-5.24	0.18
M41 LAYE	1	542	271.509	0 Layer 1	2.009	-5.32	0.13
M41 LAYE	1	593	297.057	0 Layer 1	1.92	-5.26	0.11
M41 LAYE	1	594	297.558	0 Layer 1	1.885	-5.16	0.16

297	148.779	100 Automatic	3.508	0.906	8.91E+07	11.34	4.05
298	149.28	100 Automatic	3.429	0.945	8.71E+07	11.86	4.13
299	149.781	100 Automatic	3.63	0.867	9.22E+07	10.59	4.02
300	150.282	100 Automatic	3.559	0.906	9.04E+07	11.01	4.11
301	150.783	100 Automatic	3.642	0.867	9.25E+07	10.52	4.03
351	175.83	100 Automatic	3.48	0.906	8.84E+07	11.52	4.02
352	176.331	100 Automatic	3.461	0.867	8.79E+07	11.65	3.83
353	176.832	100 Automatic	3.657	0.906	9.29E+07	10.43	4.23
354	177.332	100 Automatic	3.504	0.867	8.90E+07	11.36	3.87
355	177.833	100 Automatic	3.472	0.906	8.82E+07	11.57	4.01
356	**178.334**	**100 Automatic**	**3.571**	**0.867**	**9.07E+07**	**10.94**	**3.95**
357	178.835	100 Automatic	3.638	0.906	9.24E+07	10.54	4.20
358	179.336	100 Automatic	3.583	0.906	9.10E+07	10.87	4.14
359	179.837	100 Automatic	3.421	0.906	8.69E+07	11.92	3.95
360	180.338	100 Automatic	3.476	0.906	8.83E+07	11.55	4.02
361	180.839	100 Automatic	3.602	0.984	9.15E+07	10.75	4.52
406	203.381	83.08 Automatic	3.469	1.492	8.81E+07	11.59	6.60
411	205.886	83.08 Automatic	3.374	1.414	8.57E+07	12.25	6.08
412	206.387	83.08 Automatic	3.429	1.414	8.71E+07	11.86	6.18
413	206.888	83.08 Automatic	3.441	1.453	8.74E+07	11.78	6.38
414	207.389	83.08 Automatic	3.37	1.57	8.56E+07	12.28	6.75
415	**207.89**	**83.08 Automatic**	**3.402**	**1.531**	**8.64E+07**	**12.05**	**6.64**
419	209.894	83.08 Automatic	3.465	1.492	8.80E+07	11.62	6.59
422	211.396	83.08 Automatic	3.524	1.57	8.95E+07	11.23	7.06
423	211.897	83.08 Automatic	3.52	1.531	8.94E+07	11.26	6.87
426	213.4	81.54 Automatic	3.461	1.688	8.79E+07	11.65	7.44
428	214.402	81.54 Automatic	3.449	1.531	8.76E+07	11.73	6.73
471	235.942	90 Automatic	3.661	1.766	9.30E+07	10.41	8.23
472	236.443	90 Automatic	3.74	1.688	9.50E+07	9.97	8.03
473	236.944	90 Automatic	3.701	1.727	9.40E+07	10.18	8.14
474	237.445	90 Automatic	3.819	1.727	9.70E+07	9.56	8.34
475	237.946	80 Automatic	3.661	1.727	9.30E+07	10.41	8.03
476	**238.447**	**80 Automatic**	**3.661**	**1.727**	**9.30E+07**	**10.41**	**8.03**
477	238.948	80 Automatic	3.74	1.766	9.50E+07	9.97	8.34
478	239.449	80 Automatic	3.622	1.727	9.20E+07	10.63	7.93
479	239.95	80 Automatic	3.74	1.688	9.50E+07	9.97	8.03
481	240.952	80 Automatic	3.661	1.727	9.30E+07	10.41	8.03
482	241.453	80 Automatic	3.661	1.727	9.30E+07	10.41	8.03
531	265.999	96.92 Automatic	3.461	1.336	8.79E+07	11.65	5.89
532	266.5	96.92 Automatic	3.575	1.336	9.08E+07	10.91	6.09
533	267.001	96.92 Automatic	3.488	1.297	8.86E+07	11.47	5.77
535	268.003	96.92 Automatic	3.449	1.219	8.76E+07	11.73	5.36
536	268.503	98.46 Automatic	3.461	1.219	8.79E+07	11.65	5.38
537	**269.004**	**98.46 Automatic**	**3.37**	**1.219**	**8.56E+07**	**12.28**	**5.23**
538	269.505	100 Automatic	3.437	1.18	8.73E+07	11.81	5.17
539	270.006	100 Automatic	3.488	1.18	8.86E+07	11.47	5.25
540	270.507	100 Automatic	3.543	1.18	9.00E+07	11.11	5.33
541	271.008	100 Automatic	3.457	1.141	8.78E+07	11.67	5.03
542	271.509	100 Automatic	3.508	1.141	8.91E+07	11.34	5.10
593	297.057	100 Automatic	3.472	1.102	8.82E+07	11.57	4.88
594	297.558	100 Automatic	3.409	1.102	8.66E+07	12.00	4.79

M41 LAYE	1	595	298.059	0 Layer 1	1.885	-5.16	0.16
M41 LAYE	1	596	298.56	0 Layer 1	1.835	-5.21	0.22
M41 LAYE	1	597	299.061	0 Layer 1	2.034	-15.22	0.02
M41 LAYE	**1**	**598**	**299.562**	**0 Layer 1**	**1.954**	**-5.16**	**0.09**
M41 LAYE	1	599	300.063	0 Layer 1	2.068	-15.83	0.01
M41 LAYE	1	600	300.564	0 Layer 1	2.023	-16.11	0.04
M41 LAYE	1	601	301.064	0 Layer 1	2.103	-15.9	0.03
M41 LAYE	1	602	301.565	0 Layer 1	2.044	-15.82	0.02
M41 LAYE	1	603	302.066	0 Layer 1	2.14	-16.39	0.05
M41 LAYE	1	653	327.113	0 Layer 1	2.569	-16.51	0.15
M41 LAYE	1	654	327.614	0 Layer 1	2.609	-16.05	0.18
M41 LAYE	1	655	328.115	0 Layer 1	2.529	-15.43	0.09
M41 LAYE	1	656	328.616	0 Layer 1	2.371	-17.5	0.07
M41 LAYE	1	657	329.117	0 Layer 1	2.451	-14.35	0
M41 LAYE	**1**	**658**	**329.618**	**0 Layer 1**	**2.451**	**-13.47**	**0.01**
M41 LAYE	1	659	330.119	0 Layer 1	2.332	-17.15	0.14
M41 LAYE	1	660	330.62	0 Layer 1	2.45	-13.52	0.03
M41 LAYE	1	661	331.121	0 Layer 1	2.371	-16.46	0.12
M41 LAYE	1	662	331.622	0 Layer 1	2.648	-17.18	0.17
M41 LAYE	1	663	332.123	0 Layer 1	2.57	-14.3	0.33

595	298.059	100 Automatic	3.409	1.102	8.66E+07	12.00	4.79
596	298.56	100 Automatic	3.441	1.063	8.74E+07	11.78	4.66
597	299.061	100 Automatic	3.551	1.141	9.02E+07	11.06	5.17
598	**299.562**	**100 Automatic**	**3.413**	**1.141**	**8.67E+07**	**11.98**	**4.96**
599	300.063	100 Automatic	3.61	1.141	9.17E+07	10.70	5.25
600	300.564	100 Automatic	3.417	1.18	8.68E+07	11.95	5.14
601	301.064	100 Automatic	3.551	1.18	9.02E+07	11.06	5.34
602	301.565	100 Automatic	3.453	1.18	8.77E+07	11.70	5.19
603	302.066	100 Automatic	3.614	1.18	9.18E+07	10.68	5.44
653	327.113	100 Automatic	3.543	1.453	9.00E+07	11.11	6.53
654	327.614	100 Automatic	3.583	1.453	9.10E+07	10.87	6.63
655	328.115	100 Automatic	3.465	1.453	8.80E+07	11.62	6.42
656	328.616	100 Automatic	3.465	1.375	8.80E+07	11.62	6.02
657	329.117	100 Automatic	3.543	1.375	9.00E+07	11.11	6.23
658	**329.618**	**100 Automatic**	**3.543**	**1.375**	**9.00E+07**	**11.11**	**6.23**
659	330.119	100 Automatic	3.504	1.336	8.90E+07	11.36	5.92
660	330.62	100 Automatic	3.465	1.414	8.80E+07	11.62	6.22
661	331.121	100 Automatic	3.465	1.375	8.80E+07	11.62	6.02
662	331.622	100 Automatic	3.543	1.492	9.00E+07	11.11	6.73
663	332.123	95 Automatic	3.622	1.414	9.20E+07	10.63	6.53

WARNING: Modification of this ASCII file outside of RADAN may cause
Version = 5
Data Filename = M26 ADJ SCAN LAYER.DZT
unpredictable behavior when this file is reloaded
into RADAN.
Layer threshold distance = 32.807999 ft
Number of layers = 1
Amplitude Units = Decibels with correction applied for spreading and transmission
Last Pick Settings:
Layer 1   Core Data   150   0   1   3
Calibration file = C:\DATA\MTU RESEARCH\M-26 PROCESSED FILES\M26 CALIB ADJ2.CZT

File	Ch#	Scan#	x(ft)	y(ft)	Layer 1	z(in)	Amp	Dev(ft)
M26 CORE LOCA⌐	1	53	26.55		0 Layer 1	3.909	-15.32	0
M26 CORE LOCA⌐	1	54	27.051		0 Layer 1	3.909	-16.03	0
M26 CORE LOCA⌐	1	55	27.552		0 Layer 1	3.706	-14.65	0
M26 CORE LOCA⌐	1	56	28.053		0 Layer 1	3.909	-15.61	0
M26 CORE LOCA⌐	1	57	28.554		0 Layer 1	3.909	-15.67	0
M26 CORE LOCA⌐	**1**	**58**	**29.054**		**0 Layer 1**	**3.909**	**-16.23**	**0**
M26 CORE LOCA⌐	1	59	29.555		0 Layer 1	3.909	-16.88	0
M26 CORE LOCA⌐	1	60	30.056		0 Layer 1	3.909	-15.06	0
M26 CORE LOCA⌐	1	61	30.557		0 Layer 1	3.706	-14.28	0
M26 CORE LOCA⌐	1	62	31.058		0 Layer 1	3.706	-14.89	0
M26 CORE LOCA⌐	1	63	31.559		0 Layer 1	3.706	-14.64	0
M26 CORE LOCA⌐	1	116	58.109		0 Layer 1	3.706	-15.82	0
M26 CORE LOCA⌐	1	117	58.61		0 Layer 1	3.909	-16.83	0
M26 CORE LOCA⌐	1	118	59.111		0 Layer 1	3.909	-16.24	0
M26 CORE LOCA⌐	1	119	59.612		0 Layer 1	3.706	-15.51	0
M26 CORE LOCA⌐	1	120	60.113		0 Layer 1	3.909	-16.33	0
M26 CORE LOCA⌐	**1**	**121**	**60.614**		**0 Layer 1**	**3.909**	**-16.46**	**0**
M26 CORE LOCA⌐	1	122	61.115		0 Layer 1	3.706	-15.78	0
M26 CORE LOCA⌐	1	123	61.616		0 Layer 1	3.909	-16.17	0
M26 CORE LOCA⌐	1	124	62.116		0 Layer 1	3.909	-15.8	0
M26 CORE LOCA⌐	1	125	62.617		0 Layer 1	3.706	-15.65	0
M26 CORE LOCA⌐	1	126	63.118		0 Layer 1	3.706	-15.39	0
M26 CORE LOCA⌐	1	297	148.779		0 Layer 1	3.541	-15.52	0
M26 CORE LOCA⌐	1	298	149.28		0 Layer 1	3.541	-16.32	0
M26 CORE LOCA⌐	1	299	149.781		0 Layer 1	3.541	-17.01	0
M26 CORE LOCA⌐	1	300	150.282		0 Layer 1	3.541	-15.51	0
M26 CORE LOCA⌐	1	301	150.783		0 Layer 1	3.541	-15.5	0
M26 CORE LOCA⌐	**1**	**302**	**151.284**		**0 Layer 1**	**3.541**	**-15.74**	**0**
M26 CORE LOCA⌐	1	303	151.785		0 Layer 1	3.541	-16.33	0
M26 CORE LOCA⌐	1	304	152.286		0 Layer 1	3.541	-15.67	0
M26 CORE LOCA⌐	1	305	152.786		0 Layer 1	3.541	-15.58	0
M26 CORE LOCA⌐	1	306	153.287		0 Layer 1	3.541	-16.9	0
M26 CORE LOCA⌐	1	307	153.788		0 Layer 1	3.541	-15.47	0
M26 CORE LOCA⌐	1	357	178.835		0 Layer 1	4.039	-16.27	0
M26 CORE LOCA⌐	1	358	179.336		0 Layer 1	4.039	-15.18	0
M26 CORE LOCA⌐	1	359	179.837		0 Layer 1	4.039	-14.92	0
M26 CORE LOCA⌐	1	360	180.338		0 Layer 1	4.039	-15.07	0
M26 CORE LOCA⌐	1	361	180.839		0 Layer 1	4.039	-15.15	0
M26 CORE LOCA⌐	**1**	**362**	**181.34**		**0 Layer 1**	**4.039**	**-16.52**	**0**
M26 CORE LOCA⌐	1	363	181.841		0 Layer 1	4.039	-16.62	0
M26 CORE LOCA⌐	1	364	182.342		0 Layer 1	4.039	-15.77	0

Scan#	x(ft)	% Scans	Vel. Type	v(in/ns)	t(ns)	V(m/s)	ε	thickness (cm)
53	26.55	0	Core Data	10.43	0.75	2.65E+08	1.28	9.93
54	27.051	0	Core Data	10.43	0.75	2.65E+08	1.28	9.93
55	27.552	0	Core Data	10.43	0.711	2.65E+08	1.28	9.41
56	28.053	0	Core Data	10.43	0.75	2.65E+08	1.28	9.93
57	28.554	0	Core Data	10.43	0.75	2.65E+08	1.28	9.93
58	29.054	0	Core Data	10.43	0.75	2.65E+08	1.28	9.93
59	29.555	0	Core Data	10.43	0.75	2.65E+08	1.28	9.93
60	30.056	0	Core Data	10.43	0.75	2.65E+08	1.28	9.93
61	30.557	0	Core Data	10.43	0.711	2.65E+08	1.28	9.41
62	31.058	0	Core Data	10.43	0.711	2.65E+08	1.28	9.41
63	31.559	0	Core Data	10.43	0.711	2.65E+08	1.28	9.41
116	58.109	0	Core Data	10.43	0.711	2.65E+08	1.28	9.41
117	58.61	0	Core Data	10.43	0.75	2.65E+08	1.28	9.93
118	59.111	0	Core Data	10.43	0.75	2.65E+08	1.28	9.93
119	59.612	0	Core Data	10.43	0.711	2.65E+08	1.28	9.41
120	60.113	0	Core Data	10.43	0.75	2.65E+08	1.28	9.93
121	60.614	0	Core Data	10.43	0.75	2.65E+08	1.28	9.93
122	61.115	0	Core Data	10.43	0.711	2.65E+08	1.28	9.41
123	61.616	0	Core Data	10.43	0.75	2.65E+08	1.28	9.93
124	62.116	0	Core Data	10.43	0.75	2.65E+08	1.28	9.93
125	62.617	0	Core Data	10.43	0.711	2.65E+08	1.28	9.41
126	63.118	0	Core Data	10.43	0.711	2.65E+08	1.28	9.41
297	148.779	0	Core Data	9.96	0.711	2.53E+08	1.41	8.99
298	149.28	0	Core Data	9.96	0.711	2.53E+08	1.41	8.99
299	149.781	0	Core Data	9.96	0.711	2.53E+08	1.41	8.99
300	150.282	0	Core Data	9.96	0.711	2.53E+08	1.41	8.99
301	150.783	0	Core Data	9.96	0.711	2.53E+08	1.41	8.99
302	151.284	0	Core Data	9.96	0.711	2.53E+08	1.41	8.99
303	151.785	0	Core Data	9.96	0.711	2.53E+08	1.41	8.99
304	152.286	0	Core Data	9.96	0.711	2.53E+08	1.41	8.99
305	152.786	0	Core Data	9.96	0.711	2.53E+08	1.41	8.99
306	153.287	0	Core Data	9.96	0.711	2.53E+08	1.41	8.99
307	153.788	0	Core Data	9.96	0.711	2.53E+08	1.41	8.99
357	178.835	0	Core Data	10.77	0.75	2.74E+08	1.20	10.26
358	179.336	0	Core Data	10.77	0.75	2.74E+08	1.20	10.26
359	179.837	0	Core Data	10.77	0.75	2.74E+08	1.20	10.26
360	180.338	0	Core Data	10.77	0.75	2.74E+08	1.20	10.26
361	180.839	0	Core Data	10.77	0.75	2.74E+08	1.20	10.26
362	181.34	0	Core Data	10.77	0.75	2.74E+08	1.20	10.26
363	181.841	0	Core Data	10.77	0.75	2.74E+08	1.20	10.26
364	182.342	0	Core Data	10.77	0.75	2.74E+08	1.20	10.26

M26 CORE LOCA⌐	1	365	182.843	0 Layer 1	4.039	-14.77	0
M26 CORE LOCA⌐	1	366	183.344	0 Layer 1	4.039	-15.41	0
M26 CORE LOCA⌐	1	367	183.845	0 Layer 1	4.039	-16.31	0
M26 CORE LOCA⌐	1	417	208.892	0 Layer 1	4.18	-15.43	0
M26 CORE LOCA⌐	1	418	209.393	0 Layer 1	3.962	-14.76	0
M26 CORE LOCA⌐	1	419	209.894	0 Layer 1	4.18	-15.66	0
M26 CORE LOCA⌐	1	420	210.394	0 Layer 1	4.18	-15.86	0
M26 CORE LOCA⌐	1	421	210.895	0 Layer 1	4.18	-14.75	0
M26 CORE LOCA⌐	**1**	**422**	**211.396**	**0 Layer 1**	**4.18**	**-14.74**	**0**
M26 CORE LOCA⌐	1	423	211.897	0 Layer 1	4.18	-15	0
M26 CORE LOCA⌐	1	424	212.398	0 Layer 1	3.962	-14.76	0
M26 CORE LOCA⌐	1	425	212.899	0 Layer 1	4.18	-15.53	0
M26 CORE LOCA⌐	1	426	213.4	0 Layer 1	4.18	-15.55	0
M26 CORE LOCA⌐	1	427	213.901	0 Layer 1	4.18	-15.92	0
M26 CORE LOCA⌐	1	480	240.451	0 Layer 1	4.202	-15	0
M26 CORE LOCA⌐	1	481	240.952	0 Layer 1	4.202	-14.95	0
M26 CORE LOCA⌐	1	482	241.453	0 Layer 1	4.202	-14.39	0
M26 CORE LOCA⌐	1	483	241.954	0 Layer 1	4.202	-15.14	0
M26 CORE LOCA⌐	1	484	242.455	0 Layer 1	4.421	-14.92	0
M26 CORE LOCA⌐	**1**	**485**	**242.956**	**0 Layer 1**	**4.202**	**-15.63**	**0**
M26 CORE LOCA⌐	1	486	243.456	0 Layer 1	4.202	-14.42	0
M26 CORE LOCA⌐	1	487	243.957	0 Layer 1	4.202	-13.87	0
M26 CORE LOCA⌐	1	488	244.458	0 Layer 1	4.202	-14.41	0
M26 CORE LOCA⌐	1	489	244.959	0 Layer 1	4.202	-14.11	0
M26 CORE LOCA⌐	1	490	245.46	0 Layer 1	4.202	-14.57	0
M26 CORE LOCA⌐	1	539	270.006	0 Layer 1	4.42	-14.43	0
M26 CORE LOCA⌐	1	540	270.507	0 Layer 1	4.65	-15.58	0
M26 CORE LOCA⌐	1	541	271.008	0 Layer 1	4.65	-14.37	0
M26 CORE LOCA⌐	1	542	271.509	0 Layer 1	4.42	-14.02	0
M26 CORE LOCA⌐	1	543	272.01	0 Layer 1	4.65	-15.37	0
M26 CORE LOCA⌐	**1**	**544**	**272.511**	**0 Layer 1**	**4.42**	**-14.05**	**0**
M26 CORE LOCA⌐	1	545	273.012	0 Layer 1	4.65	-14.39	0
M26 CORE LOCA⌐	1	546	273.513	0 Layer 1	4.65	-15.69	0
M26 CORE LOCA⌐	1	547	274.014	0 Layer 1	4.42	-14.46	0
M26 CORE LOCA⌐	1	548	274.515	0 Layer 1	4.42	-13.95	0
M26 CORE LOCA⌐	1	549	275.016	0 Layer 1	4.65	-15.51	0
M26 CORE LOCA⌐	1	600	300.564	0 Layer 1	4.65	-15.71	0
M26 CORE LOCA⌐	1	601	301.064	0 Layer 1	4.65	-15.94	0
M26 CORE LOCA⌐	1	602	301.565	0 Layer 1	4.42	-14.95	0
M26 CORE LOCA⌐	1	603	302.066	0 Layer 1	4.65	-16.22	0
M26 CORE LOCA⌐	1	604	302.567	0 Layer 1	4.65	-16.3	0
M26 CORE LOCA⌐	**1**	**605**	**303.068**	**0 Layer 1**	**4.65**	**-15.46**	**0**
M26 CORE LOCA⌐	1	606	303.569	0 Layer 1	4.65	-16.33	0
M26 CORE LOCA⌐	1	607	304.07	0 Layer 1	4.65	-16.42	0
M26 CORE LOCA⌐	1	608	304.571	0 Layer 1	4.65	-15.23	0
M26 CORE LOCA⌐	1	609	305.072	0 Layer 1	4.65	-16.63	0
M26 CORE LOCA⌐	1	610	305.573	0 Layer 1	4.881	-16.09	0
M26 CORE LOCA⌐	1	658	329.618	0 Layer 1	4.02	-14.13	0
M26 CORE LOCA⌐	1	659	330.119	0 Layer 1	4.02	-14.79	0
M26 CORE LOCA⌐	1	660	330.62	0 Layer 1	4.02	-15.57	0
M26 CORE LOCA⌐	1	661	331.121	0 Layer 1	4.23	-16.28	0
M26 CORE LOCA⌐	1	662	331.622	0 Layer 1	4.02	-16.77	0
M26 CORE LOCA⌐	**1**	**663**	**332.123**	**0 Layer 1**	**4.23**	**-16.47**	**0**
M26 CORE LOCA⌐	1	664	332.624	0 Layer 1	4.23	-16.23	0
M26 CORE LOCA⌐	1	665	333.125	0 Layer 1	4.02	-15.26	0
M26 CORE LOCA⌐	1	666	333.626	0 Layer 1	4.02	-15.29	0
M26 CORE LOCA⌐	1	667	334.126	0 Layer 1	4.23	-15.73	0
M26 CORE LOCA⌐	1	668	334.627	0 Layer 1	4.02	-14.67	0

365	182.843	0 Core Data	10.77	0.75	2.74E+08	1.20	10.26
366	183.344	0 Core Data	10.77	0.75	2.74E+08	1.20	10.26
367	183.845	0 Core Data	10.77	0.75	2.74E+08	1.20	10.26
417	208.892	0 Core Data	11.15	0.75	2.83E+08	1.12	10.62
418	209.393	0 Core Data	11.15	0.75	2.83E+08	1.12	10.62
419	209.894	0 Core Data	11.15	0.711	2.83E+08	1.12	10.06
420	210.394	0 Core Data	11.15	0.75	2.83E+08	1.12	10.62
421	210.895	0 Core Data	11.15	0.75	2.83E+08	1.12	10.62
422	**211.396**	**0 Core Data**	**11.15**	**0.75**	**2.83E+08**	**1.12**	**10.62**
423	211.897	0 Core Data	11.15	0.75	2.83E+08	1.12	10.62
424	212.398	0 Core Data	11.15	0.711	2.83E+08	1.12	10.06
425	212.899	0 Core Data	11.15	0.75	2.83E+08	1.12	10.62
426	213.4	0 Core Data	11.15	0.75	2.83E+08	1.12	10.62
427	213.901	0 Core Data	11.15	0.75	2.83E+08	1.12	10.62
480	240.451	0 Core Data	11.21	0.75	2.85E+08	1.11	10.67
481	240.952	0 Core Data	11.21	0.75	2.85E+08	1.11	10.67
482	241.453	0 Core Data	11.21	0.75	2.85E+08	1.11	10.67
483	241.954	0 Core Data	11.21	0.75	2.85E+08	1.11	10.67
484	242.455	0 Core Data	11.21	0.789	2.85E+08	1.11	11.23
485	**242.956**	**0 Core Data**	**11.21**	**0.75**	**2.85E+08**	**1.11**	**10.67**
486	243.456	0 Core Data	11.21	0.75	2.85E+08	1.11	10.67
487	243.957	0 Core Data	11.21	0.75	2.85E+08	1.11	10.67
488	244.458	0 Core Data	11.21	0.75	2.85E+08	1.11	10.67
489	244.959	0 Core Data	11.21	0.75	2.85E+08	1.11	10.67
490	245.46	0 Core Data	11.21	0.75	2.85E+08	1.11	10.67
539	270.006	0 Core Data	11.79	0.75	2.99E+08	1.00	11.23
540	270.507	0 Core Data	11.79	0.789	2.99E+08	1.00	11.81
541	271.008	0 Core Data	11.79	0.789	2.99E+08	1.00	11.81
542	271.509	0 Core Data	11.79	0.75	2.99E+08	1.00	11.23
543	272.01	0 Core Data	11.79	0.789	2.99E+08	1.00	11.81
544	**272.511**	**0 Core Data**	**11.79**	**0.75**	**2.99E+08**	**1.00**	**11.23**
545	273.012	0 Core Data	11.79	0.789	2.99E+08	1.00	11.81
546	273.513	0 Core Data	11.79	0.789	2.99E+08	1.00	11.81
547	274.014	0 Core Data	11.79	0.75	2.99E+08	1.00	11.23
548	274.515	0 Core Data	11.79	0.75	2.99E+08	1.00	11.23
549	275.016	0 Core Data	11.79	0.789	2.99E+08	1.00	11.81
600	300.564	0 Core Data	11.79	0.789	2.99E+08	1.00	11.81
601	301.064	0 Core Data	11.79	0.789	2.99E+08	1.00	11.81
602	301.565	0 Core Data	11.79	0.75	2.99E+08	1.00	11.23
603	302.066	0 Core Data	11.79	0.789	2.99E+08	1.00	11.81
604	302.567	0 Core Data	11.79	0.789	2.99E+08	1.00	11.81
605	**303.068**	**0 Core Data**	**11.79**	**0.789**	**2.99E+08**	**1.00**	**11.81**
606	303.569	0 Core Data	11.79	0.789	2.99E+08	1.00	11.81
607	304.07	0 Core Data	11.79	0.789	2.99E+08	1.00	11.81
608	304.571	0 Core Data	11.79	0.789	2.99E+08	1.00	11.81
609	305.072	0 Core Data	11.79	0.789	2.99E+08	1.00	11.81
610	305.573	0 Core Data	11.79	0.828	2.99E+08	1.00	12.40
658	329.618	0 Core Data	10.72	0.75	2.72E+08	1.21	10.21
659	330.119	0 Core Data	10.72	0.75	2.72E+08	1.21	10.21
660	330.62	0 Core Data	10.72	0.75	2.72E+08	1.21	10.21
661	331.121	0 Core Data	10.72	0.789	2.72E+08	1.21	10.74
662	331.622	0 Core Data	10.72	0.75	2.72E+08	1.21	10.21
663	**332.123**	**0 Core Data**	**10.72**	**0.789**	**2.72E+08**	**1.21**	**10.74**
664	332.624	0 Core Data	10.72	0.789	2.72E+08	1.21	10.74
665	333.125	0 Core Data	10.72	0.75	2.72E+08	1.21	10.21
666	333.626	0 Core Data	10.72	0.75	2.72E+08	1.21	10.21
667	334.126	0 Core Data	10.72	0.789	2.72E+08	1.21	10.74
668	334.627	0 Core Data	10.72	0.75	2.72E+08	1.21	10.21

WARNING: Modification of this ASCII file outside of RADAN may cause
Version = 5 unpredictable behavior when this file is reloaded into RADAN.
Data Filename = MTU5PT1 LAYER.DZT
Layer threshold distance = 32.807999 ft
Number of layers = 1
Amplitude Units = Decibels with correction applied for spreading and transmission
Last Pick Settings:

Layer 1	Core Data	150	0.00	1	3		

Calibration file = C:\DATA\MTU RESEARCH\5 MILE PT PROCESSED FILES\CALIBPT.CZT

File	Ch#	Scan#	x(ft)	y(ft)	Layer 1	z(in)	Amp	Dev(ft)
FINAL RESULTS	1	57	28.55		0 Layer 1	1.911	-19.32	0
FINAL RESULTS	1	58	29.05		0 Layer 1	1.911	-19.76	0.08
FINAL RESULTS	1	59	29.56		0 Layer 1	1.911	-20.12	0.04
FINAL RESULTS	1	60	30.06		0 Layer 1	1.911	-19.07	0
FINAL RESULTS	1	61	30.56		0 Layer 1	1.911	-18.67	0.04
FINAL RESULTS	**1**	**62**	**31.06**		**0 Layer 1**	**1.911**	**-19.08**	**0**
FINAL RESULTS	1	63	31.56		0 Layer 1	1.911	-19.56	0.04
FINAL RESULTS	1	64	32.06		0 Layer 1	1.828	-18.85	0.11
FINAL RESULTS	1	65	32.56		0 Layer 1	1.828	-18.93	0.07
FINAL RESULTS	1	66	33.06		0 Layer 1	1.911	-19.64	0.01
FINAL RESULTS	1	67	33.56		0 Layer 1	1.911	-20.01	0.05
FINAL RESULTS	1	177	88.67		0 Layer 1	1.648	-21.87	0
FINAL RESULTS	1	178	89.17		0 Layer 1	1.57	-21.94	0.12
FINAL RESULTS	1	179	89.67		0 Layer 1	1.57	-22.04	0.04
FINAL RESULTS	1	180	90.17		0 Layer 1	1.57	-22.22	0.08
FINAL RESULTS	1	181	90.67		0 Layer 1	1.57	-21.66	0.08
FINAL RESULTS	**1**	**182**	**91.17**		**0 Layer 1**	**1.648**	**-22.2**	**0**
FINAL RESULTS	1	183	91.67		0 Layer 1	1.57	-21.85	0.12
FINAL RESULTS	1	184	92.17		0 Layer 1	1.648	-22.71	0
FINAL RESULTS	1	185	92.67		0 Layer 1	1.648	-22.67	0.08
FINAL RESULTS	1	186	93.18		0 Layer 1	1.648	-22.99	0.04
FINAL RESULTS	1	187	93.68		0 Layer 1	1.648	-23.44	0
FINAL RESULTS	1	297	148.78		0 Layer 1	1.92	-21.74	0.01
FINAL RESULTS	1	298	149.28		0 Layer 1	1.837	-20.82	0.11
FINAL RESULTS	1	299	149.78		0 Layer 1	1.92	-21.36	0.05
FINAL RESULTS	1	300	150.28		0 Layer 1	1.92	-20.71	0.03
FINAL RESULTS	1	301	150.78		0 Layer 1	1.92	-21.02	0.05
FINAL RESULTS	**1**	**302**	**151.28**		**0 Layer 1**	**1.92**	**-20.38**	**0.05**
FINAL RESULTS	1	303	151.79		0 Layer 1	1.92	-20.27	0.01
FINAL RESULTS	1	304	152.29		0 Layer 1	1.92	-19.82	0.03
FINAL RESULTS	1	305	152.79		0 Layer 1	1.92	-20.1	0.01
FINAL RESULTS	1	306	153.29		0 Layer 1	1.837	-19.81	0.11
FINAL RESULTS	1	307	153.79		0 Layer 1	1.92	-20.01	0.07
FINAL RESULTS	1	357	178.84		0 Layer 1	1.854	-20.41	0.06
FINAL RESULTS	1	358	179.34		0 Layer 1	1.854	-20.03	0.02
FINAL RESULTS	1	359	179.84		0 Layer 1	1.937	-21.41	0.1
FINAL RESULTS	1	360	180.34		0 Layer 1	1.77	-20.5	0.13
FINAL RESULTS	1	361	180.84		0 Layer 1	1.77	-20.42	0.13
FINAL RESULTS	**1**	**362**	**181.34**		**0 Layer 1**	**1.77**	**-20.99**	**0.13**
FINAL RESULTS	1	363	181.84		0 Layer 1	1.77	-21.61	0.17
FINAL RESULTS	1	364	182.34		0 Layer 1	1.854	-21.74	0.01

Scan#	x(ft)	% Scans	Vel. Type	v(in/ns)	t(ns)	V(m/s)	ε	thickness(cm)
57	$28.55	96	Core Data	4.217	0.906	107111800	7.84	4.85
58	$29.05	96	Core Data	4.217	0.906	107111800	7.84	4.85
59	$29.56	96	Core Data	4.217	0.906	107111800	7.84	4.85
60	$30.06	96	Core Data	4.217	0.906	107111800	7.84	4.85
61	$30.56	96	Core Data	4.217	0.906	107111800	7.84	4.85
62	**$31.06**	**96**	**Core Data**	**4.217**	**0.906**	**107111800**	**7.84**	**4.85**
63	$31.56	96	Core Data	4.217	0.906	107111800	7.84	4.85
64	$32.06	96	Core Data	4.217	0.867	107111800	7.84	4.64
65	$32.56	96	Core Data	4.217	0.867	107111800	7.84	4.64
66	$33.06	96	Core Data	4.217	0.906	107111800	7.84	4.85
67	$33.56	96	Core Data	4.217	0.906	107111800	7.84	4.85
177	$88.67	98	Core Data	3.98	0.828	101092000	8.81	4.19
178	$89.17	98	Core Data	3.98	0.789	101092000	8.81	3.99
179	$89.67	98	Core Data	3.98	0.789	101092000	8.81	3.99
180	$90.17	98	Core Data	3.98	0.789	101092000	8.81	3.99
181	$90.67	98	Core Data	3.98	0.789	101092000	8.81	3.99
182	**$91.17**	**98**	**Core Data**	**3.98**	**0.828**	**101092000**	**8.81**	**4.19**
183	$91.67	98	Core Data	3.98	0.789	101092000	8.81	3.99
184	$92.17	98	Core Data	3.98	0.828	101092000	8.81	4.19
185	$92.67	98	Core Data	3.98	0.828	101092000	8.81	4.19
186	$93.18	98	Core Data	3.98	0.828	101092000	8.81	4.19
187	$93.68	98	Core Data	3.98	0.828	101092000	8.81	4.19
297	$148.78	98	Core Data	4.236	0.906	107594400	7.77	4.88
298	$149.28	98	Core Data	4.236	0.867	107594400	7.77	4.67
299	$149.78	98	Core Data	4.236	0.906	107594400	7.77	4.88
300	$150.28	98	Core Data	4.236	0.906	107594400	7.77	4.88
301	$150.78	98	Core Data	4.236	0.906	107594400	7.77	4.88
302	**$151.28**	**98**	**Core Data**	**4.236**	**0.906**	**107594400**	**7.77**	**4.88**
303	$151.79	98	Core Data	4.236	0.906	107594400	7.77	4.88
304	$152.29	98	Core Data	4.236	0.906	107594400	7.77	4.88
305	$152.79	98	Core Data	4.236	0.906	107594400	7.77	4.88
306	$153.29	98	Core Data	4.236	0.867	107594400	7.77	4.67
307	$153.79	98	Core Data	4.236	0.906	107594400	7.77	4.88
357	$178.84	92	Core Data	4.276	0.867	108610400	7.63	4.71
358	$179.34	92	Core Data	4.276	0.867	108610400	7.63	4.71
359	$179.84	92	Core Data	4.276	0.906	108610400	7.63	4.92
360	$180.34	92	Core Data	4.276	0.828	108610400	7.63	4.50
361	$180.84	92	Core Data	4.276	0.828	108610400	7.63	4.50
362	**$181.34**	**92**	**Core Data**	**4.276**	**0.828**	**108610400**	**7.63**	**4.50**
363	$181.84	92	Core Data	4.276	0.828	108610400	7.63	4.50
364	$182.34	92	Core Data	4.276	0.867	108610400	7.63	4.71

FINAL RESULTS	1	365	182.84	0 Layer 1	1.77	-20.16	0.09
FINAL RESULTS	1	366	183.34	0 Layer 1	1.937	-21.77	0.11
FINAL RESULTS	1	367	183.85	0 Layer 1	1.854	-21.38	0.01
FINAL RESULTS	1	417	208.89	0 Layer 1	1.8	-21.05	0.09
FINAL RESULTS	1	419	209.89	0 Layer 1	1.8	-21.23	0.04
FINAL RESULTS	1	421	210.90	0 Layer 1	1.8	-21.16	0.11
FINAL RESULTS	**1**	**422**	**211.40**	**0 Layer 1**	**1.8**	**-21.69**	**0.07**
FINAL RESULTS	1	423	211.90	0 Layer 1	1.8	-21.68	0.06
FINAL RESULTS	1	424	212.40	0 Layer 1	1.8	-20.71	0.07
FINAL RESULTS	1	425	212.90	0 Layer 1	1.8	-20.29	0.07
FINAL RESULTS	1	426	213.40	0 Layer 1	1.8	-19.95	0.07
FINAL RESULTS	1	427	213.90	0 Layer 1	1.885	-20.03	0.05
FINAL RESULTS	1	480	240.45	0 Layer 1	1.861	-20.96	0.1
FINAL RESULTS	1	483	241.95	0 Layer 1	1.861	-20.23	0.06
FINAL RESULTS	**1**	**484**	**242.46**	**0 Layer 1**	**1.861**	**-20.7**	**0.01**
FINAL RESULTS	1	488	244.46	0 Layer 1	1.861	-20.81	0.04
FINAL RESULTS	1	489	244.96	0 Layer 1	1.861	-20.44	0.08
FINAL RESULTS	1	490	245.46	0 Layer 1	1.861	-19.96	0.04
FINAL RESULTS	1	491	245.96	0 Layer 1	1.861	-20.61	0.01
FINAL RESULTS	1	536	268.50	0 Layer 1	1.805	-20.12	0.08
FINAL RESULTS	1	538	269.51	0 Layer 1	1.89	-20.41	0
FINAL RESULTS	1	539	270.01	0 Layer 1	1.805	-20.08	0.12
FINAL RESULTS	1	540	270.51	0 Layer 1	1.89	-20.65	0
FINAL RESULTS	1	543	272.01	0 Layer 1	1.805	-19.89	0.07
FINAL RESULTS	**1**	**544**	**272.51**	**0 Layer 1**	**1.89**	**-20.11**	**0.06**
FINAL RESULTS	1	545	273.01	0 Layer 1	1.89	-20.61	0.02
FINAL RESULTS	1	546	273.51	0 Layer 1	1.89	-20.89	0.1
FINAL RESULTS	1	547	274.01	0 Layer 1	1.805	-20.07	0.06
FINAL RESULTS	1	549	275.02	0 Layer 1	1.89	-20.87	0.07
FINAL RESULTS	1	550	275.52	0 Layer 1	1.805	-20.58	0.05
FINAL RESULTS	1	600	300.56	0 Layer 1	1.87	-20.56	0
FINAL RESULTS	1	601	301.06	0 Layer 1	1.87	-20.43	0.04
FINAL RESULTS	1	602	301.57	0 Layer 1	1.958	-21.47	0.04
FINAL RESULTS	1	603	302.07	0 Layer 1	1.87	-21.46	0.08
FINAL RESULTS	1	604	302.57	0 Layer 1	1.87	-20.94	0.04
FINAL RESULTS	**1**	**606**	**303.57**	**0 Layer 1**	**1.87**	**-21.01**	**0.08**
FINAL RESULTS	1	607	304.07	0 Layer 1	1.87	-20.99	0.08
FINAL RESULTS	1	608	304.57	0 Layer 1	1.958	-22.32	0.04
FINAL RESULTS	1	609	305.07	0 Layer 1	1.958	-21.98	0.04
FINAL RESULTS	1	610	305.57	0 Layer 1	1.958	-21.12	0.07
FINAL RESULTS	1	611	306.07	0 Layer 1	1.958	-20.91	0.03
FINAL RESULTS	1	658	329.62	0 Layer 1	1.654	-20.47	0.15
FINAL RESULTS	1	659	330.12	0 Layer 1	1.58	-19.96	0.01
FINAL RESULTS	1	660	330.62	0 Layer 1	1.58	-20.31	0.05
FINAL RESULTS	1	661	331.12	0 Layer 1	1.58	-20.41	0.01
FINAL RESULTS	1	662	331.62	0 Layer 1	1.58	-20.34	0.09
FINAL RESULTS	**1**	**663**	**332.12**	**0 Layer 1**	**1.58**	**-20.25**	**0.01**
FINAL RESULTS	1	664	332.62	0 Layer 1	1.58	-20.15	0.09
FINAL RESULTS	1	665	333.13	0 Layer 1	1.654	-21.37	0.07
FINAL RESULTS	1	666	333.63	0 Layer 1	1.58	-20.7	0.05
FINAL RESULTS	1	667	334.13	0 Layer 1	1.58	-19.93	0.01
FINAL RESULTS	1	668	334.63	0 Layer 1	1.58	-20.47	0.09

365	$182.84	90 Core Data	4.276	0.828	108610400	7.63	4.50
366	$183.34	90 Core Data	4.276	0.906	108610400	7.63	4.92
367	$183.85	90 Core Data	4.276	0.867	108610400	7.63	4.71
417	$208.89	67 Core Data	4.346	0.828	110388400	7.39	4.57
419	$209.89	67 Core Data	4.346	0.828	110388400	7.39	4.57
421	$210.90	64 Core Data	4.346	0.828	110388400	7.39	4.57
422	$211.40	64 Core Data	4.346	0.828	110388400	7.39	4.57
423	$211.90	64 Core Data	4.346	0.828	110388400	7.39	4.57
424	$212.40	64 Core Data	4.346	0.828	110388400	7.39	4.57
425	$212.90	64 Core Data	4.346	0.828	110388400	7.39	4.57
426	$213.40	64 Core Data	4.346	0.828	110388400	7.39	4.57
427	$213.90	64 Core Data	4.346	0.867	110388400	7.39	4.79
480	$240.45	73 Core Data	4.291	0.867	108991400	7.58	4.73
483	$241.95	75 Core Data	4.291	0.867	108991400	7.58	4.73
484	$242.46	76 Core Data	4.291	0.867	108991400	7.58	4.73
488	$244.46	76 Core Data	4.291	0.867	108991400	7.58	4.73
489	$244.96	76 Core Data	4.291	0.867	108991400	7.58	4.73
490	$245.46	76 Core Data	4.291	0.867	108991400	7.58	4.73
491	$245.96	76 Core Data	4.291	0.867	108991400	7.58	4.73
536	$268.50	81 Core Data	4.358	0.828	110693200	7.35	4.58
538	$269.51	81 Core Data	4.358	0.867	110693200	7.35	4.80
539	$270.01	81 Core Data	4.358	0.828	110693200	7.35	4.58
540	$270.51	79 Core Data	4.358	0.867	110693200	7.35	4.80
543	$272.01	79 Core Data	4.358	0.828	110693200	7.35	4.58
544	$272.51	79 Core Data	4.358	0.867	110693200	7.35	4.80
545	$273.01	79 Core Data	4.358	0.867	110693200	7.35	4.80
546	$273.51	79 Core Data	4.358	0.867	110693200	7.35	4.80
547	$274.01	79 Core Data	4.358	0.828	110693200	7.35	4.58
549	$275.02	79 Core Data	4.358	0.867	110693200	7.35	4.80
550	$275.52	79 Core Data	4.358	0.828	110693200	7.35	4.58
600	$300.56	92 Core Data	4.516	0.828	114706400	6.84	4.75
601	$301.06	92 Core Data	4.516	0.828	114706400	6.84	4.75
602	$301.57	92 Core Data	4.516	0.867	114706400	6.84	4.97
603	$302.07	93 Core Data	4.516	0.828	114706400	6.84	4.75
604	$302.57	93 Core Data	4.516	0.828	114706400	6.84	4.75
606	$303.57	93 Core Data	4.516	0.828	114706400	6.84	4.75
607	$304.07	93 Core Data	4.516	0.828	114706400	6.84	4.75
608	$304.57	93 Core Data	4.516	0.867	114706400	6.84	4.97
609	$305.07	93 Core Data	4.516	0.867	114706400	6.84	4.97
610	$305.57	93 Core Data	4.516	0.867	114706400	6.84	4.97
611	$306.07	93 Core Data	4.516	0.867	114706400	6.84	4.97
658	$329.62	90 Core Data	3.815	0.867	96901000	9.58	4.20
659	$330.12	89 Core Data	3.815	0.828	96901000	9.58	4.01
660	$330.62	89 Core Data	3.815	0.828	96901000	9.58	4.01
661	$331.12	87 Core Data	3.815	0.828	96901000	9.58	4.01
662	$331.62	87 Core Data	3.815	0.828	96901000	9.58	4.01
663	$332.12	85 Core Data	3.815	0.828	96901000	9.58	4.01
664	$332.62	85 Core Data	3.815	0.828	96901000	9.58	4.01
665	$333.13	85 Core Data	3.815	0.867	96901000	9.58	4.20
666	$333.63	85 Core Data	3.815	0.828	96901000	9.58	4.01
667	$334.13	85 Core Data	3.815	0.828	96901000	9.58	4.01
668	$334.63	85 Core Data	3.815	0.828	96901000	9.58	4.01

WARNING: Modification of this ASCII file outside of RADAN may cause
Version = 5   unpredictable behavior when this file is reloaded
Data Filename = 1&2PERP.DZT   into RADAN.
Layer threshold distance = 32.807999 ft
Number of layers = 2
Amplitude Units = Data Units
Last Pick Settings:
Layer 1   Specify   150   0   1   3
Layer 2   Specify   110   0   2   3
Calibration file =

File	Ch#	Scan#	x(ft)	y(ft)	Layer 1	z(in)	Amp
1&2 REFL	1	550	550	0 Layer 1		0.415	2.00E+04
1&2 REFL	1	551	551	0 Layer 1		0.415	1.98E+04
1&2 REFL	1	552	552	0 Layer 1		0.415	1.98E+04
1&2 REFL	1	553	553	0 Layer 1		0.415	1.97E+04
1&2 REFL	1	554	554	0 Layer 1		0.415	1.96E+04
1&2 REFL	1	555	555	0 Layer 1		0.415	1.94E+04
1&2 REFL	1	556	556	0 Layer 1		0.415	1.93E+04
1&2 REFL	1	557	557	0 Layer 1		0.415	1.91E+04
1&2 REFL	1	558	558	0 Layer 1		0.415	1.89E+04
1&2 REFL	1	559	559	0 Layer 1		0.415	1.88E+04
1&2 REFL	1	560	560	0 Layer 1		0.415	1.87E+04

File	Ch#	Scan#	x(ft)	y(ft)	Layer 1	z(in)	Amp
1&2 REFL	1	810	810	0 Layer 2		3.559	1.29E+04
1&2 REFL	1	811	811	0 Layer 2		3.559	1.28E+04
1&2 REFL	1	812	812	0 Layer 2		3.559	1.28E+04
1&2 REFL	1	813	813	0 Layer 2		3.559	1.28E+04
1&2 REFL	1	814	814	0 Layer 2		3.559	1.28E+04
1&2 REFL	1	815	815	0 Layer 2		3.559	1.28E+04
1&2 REFL	1	816	816	0 Layer 2		3.559	1.28E+04
1&2 REFL	1	817	817	0 Layer 2		3.559	1.28E+04
1&2 REFL	1	818	818	0 Layer 2		3.559	1.27E+04
1&2 REFL	1	819	819	0 Layer 2		3.559	1.28E+04
1&2 REFL	1	820	820	0 Layer 2		3.559	1.28E+04

Dev(ft)	Scan#	x(ft)	% Scans	Vel. Type	v(in/ns)	t(ns)	V(m/s)	ε
0.03	550	550	100	Specify	5.906	-0.141	1.50E+08	4.00
0.03	551	551	100	Specify	5.906	-0.141	1.50E+08	4.00
0.02	552	552	100	Specify	5.906	-0.141	1.50E+08	4.00
0.02	553	553	100	Specify	5.906	-0.141	1.50E+08	4.00
0.02	554	554	100	Specify	5.906	-0.141	1.50E+08	4.00
0.01	555	555	100	Specify	5.906	-0.141	1.50E+08	4.00
0.01	556	556	100	Specify	5.906	-0.141	1.50E+08	4.00
0.01	557	557	100	Specify	5.906	-0.141	1.50E+08	4.00
0.01	558	558	100	Specify	5.906	-0.141	1.50E+08	4.00
0.01	559	559	100	Specify	5.906	-0.141	1.50E+08	4.00
0.01	560	560	100	Specify	5.906	-0.141	1.50E+08	4.00

Dev(ft)	Scan#	x(ft)	% Scans	Vel. Type	v(in/ns)	t(ns)	V(m/s)	ε
0.01	810	810	100	Specify	4.331	1.578	1.10E+08	7.44
0.01	811	811	100	Specify	4.331	1.578	1.10E+08	7.44
0.02	812	812	100	Specify	4.331	1.578	1.10E+08	7.44
0.02	813	813	100	Specify	4.331	1.578	1.10E+08	7.44
0.02	814	814	100	Specify	4.331	1.578	1.10E+08	7.44
0.02	815	815	100	Specify	4.331	1.578	1.10E+08	7.44
0.03	816	816	100	Specify	4.331	1.578	1.10E+08	7.44
0.03	817	817	100	Specify	4.331	1.578	1.10E+08	7.44
0.03	818	818	100	Specify	4.331	1.578	1.10E+08	7.44
0.03	819	819	100	Specify	4.331	1.578	1.10E+08	7.44
0.03	820	820	100	Specify	4.331	1.578	1.10E+08	7.44

WARNING: Modification of this ASCII file outside of RADAN may
Version = 5   cause unpredictable behavior when this file is reloaded
Data Filename = 1&2PERP.DZT   into RADAN.
Layer threshold distance = 32.807999 ft
Number of layers = 2
Amplitude Units = Data Units
Last Pick Settings:

| Layer 1 | Core Data | 150 | 0 | 1 | 3 |
| Layer 2 | Core Data | 110 | 0 | 2 | 3 |

Calibration file =

File	Ch#	Scan#	x(ft)	y(ft)	Layer 1	z(in)	Amp	Dev(ft)
1&2 THICK	1	475	475	0 Layer 1		2.91	1.30E+04	0.02
1&2 THICK	1	476	476	0 Layer 1		2.91	1.31E+04	0.03
1&2 THICK	1	477	477	0 Layer 1		2.91	1.31E+04	0.03
1&2 THICK	1	478	478	0 Layer 1		2.91	1.31E+04	0.04
1&2 THICK	1	479	479	0 Layer 1		2.91	1.32E+04	0.05
1&2 THICK	1	480	480	0 Layer 1		2.91	1.32E+04	0.05
1&2 THICK	1	481	481	0 Layer 1		2.91	1.32E+04	0.06
1&2 THICK	1	482	482	0 Layer 1		2.839	1.32E+04	0.06
1&2 THICK	1	483	483	0 Layer 1		2.839	1.33E+04	0.05
1&2 THICK	1	484	484	0 Layer 1		2.839	1.33E+04	0.05
1&2 THICK	1	485	485	0 Layer 1		2.839	1.34E+04	0.05

File	Ch#	Scan#	x(ft)	y(ft)	Layer 1	z(in)	Amp	Dev(ft)
1&2 THICK	1	835	835	0 Layer 2		2.911	1.30E+04	0.05
1&2 THICK	1	836	836	0 Layer 2		2.985	1.30E+04	0.03
1&2 THICK	1	837	837	0 Layer 2		2.985	1.30E+04	0.03
1&2 THICK	1	838	838	0 Layer 2		2.985	1.30E+04	0.03
1&2 THICK	1	839	839	0 Layer 2		2.985	1.29E+04	0.03
1&2 THICK	1	840	840	0 Layer 2		2.985	1.29E+04	0.03
1&2 THICK	1	841	841	0 Layer 2		2.985	1.29E+04	0.02
1&2 THICK	1	842	842	0 Layer 2		2.985	1.28E+04	0.02
1&2 THICK	1	843	843	0 Layer 2		2.985	1.27E+04	0.02
1&2 THICK	1	844	844	0 Layer 2		2.985	1.28E+04	0.02
1&2 THICK	1	845	845	0 Layer 2		2.985	1.28E+04	0.02

Scan#	Vel. Type	v(in/ns)	t(ns)	V(m/s)	ε
475	Core Data	3.60E+00	1.617	9.14E+07	10.78
476	Core Data	3.60E+00	1.617	9.14E+07	10.78
477	Core Data	3.60E+00	1.617	9.14E+07	10.78
478	Core Data	3.60E+00	1.617	9.14E+07	10.78
479	Core Data	3.60E+00	1.617	9.14E+07	10.78
480	Core Data	3.60E+00	1.617	9.14E+07	10.78
481	Core Data	3.60E+00	1.617	9.14E+07	10.78
482	Core Data	3.60E+00	1.578	9.14E+07	10.78
483	Core Data	3.60E+00	1.578	9.14E+07	10.78
484	Core Data	3.60E+00	1.578	9.14E+07	10.78
485	Core Data	3.60E+00	1.578	9.14E+07	10.78

Scan#	Vel. Type	v(in/ns)	t(ns)	V(m/s)	ε
835	Core Data	3.78E+00	1.539	9.61E+07	9.75
836	Core Data	3.78E+00	1.578	9.61E+07	9.75
837	Core Data	3.78E+00	1.578	9.61E+07	9.75
838	Core Data	3.78E+00	1.578	9.61E+07	9.75
839	Core Data	3.78E+00	1.578	9.61E+07	9.75
840	Core Data	3.78E+00	1.578	9.61E+07	9.75
841	Core Data	3.78E+00	1.578	9.61E+07	9.75
842	Core Data	3.78E+00	1.578	9.61E+07	9.75
843	Core Data	3.78E+00	1.578	9.61E+07	9.75
844	Core Data	3.78E+00	1.578	9.61E+07	9.75
845	Core Data	3.78E+00	1.578	9.61E+07	9.75

WARNING: Modification of this ASCII file outside of RADAN may cause

Version = 5   unpredictable behavior when this file is reloaded into RADAN.

Data Filename = 3&4PERP.DZT

Layer threshold distance = 32.807999 ft

Number of layers = 2

Amplitude Units = Data Units

Last Pick Settings:

Layer 1	Core Data	150	0	1	3
Layer 2	Core Data	110	0	2	3

Calibration file =

File	Ch#	Scan#	x(ft)	y(ft)	Layer 1	z(in)	Amp	Dev(ft)
3&4 THICK	1	345	345	0 Layer 1		3.191	1.12E+04	-6.54E+33
3&4 THICK	1	346	346	0 Layer 1		3.126	1.12E+04	-6.54E+33
3&4 THICK	1	347	347	0 Layer 1		3.126	1.12E+04	-6.54E+33
3&4 THICK	1	348	348	0 Layer 1		3.126	1.13E+04	-6.54E+33
3&4 THICK	1	349	349	0 Layer 1		3.126	1.13E+04	-6.54E+33
3&4 THICK	1	350	350	0 Layer 1		3.126	1.15E+04	-6.54E+33
3&4 THICK	1	351	351	0 Layer 1		3.126	1.14E+04	-6.54E+33
3&4 THICK	1	352	352	0 Layer 1		3.126	1.16E+04	-6.54E+33
3&4 THICK	1	353	353	0 Layer 1		3.126	1.17E+04	-6.54E+33
3&4 THICK	1	354	354	0 Layer 1		3.126	1.18E+04	-6.54E+33
3&4 THICK	1	355	355	0 Layer 1		3.126	1.17E+04	-6.54E+33

File	Ch#	Scan#	x(ft)	y(ft)	Layer 1	z(in)	Amp	Dev(ft)
3&4 THICK	1	595	595	0 Layer 2		3.018	1.09E+04	-6.54E+33
3&4 THICK	1	596	596	0 Layer 2		3.018	1.10E+04	-6.54E+33
3&4 THICK	1	597	597	0 Layer 2		3.018	1.11E+04	-6.54E+33
3&4 THICK	1	598	598	0 Layer 2		3.018	1.11E+04	-6.54E+33
3&4 THICK	1	599	599	0 Layer 2		3.018	1.12E+04	-6.54E+33
3&4 THICK	1	600	600	0 Layer 2		3.018	1.14E+04	-6.54E+33
3&4 THICK	1	601	601	0 Layer 2		3.018	1.14E+04	-6.54E+33
3&4 THICK	1	602	602	0 Layer 2		3.018	1.15E+04	-6.54E+33
3&4 THICK	1	603	603	0 Layer 2		3.018	1.15E+04	-6.54E+33
3&4 THICK	1	604	604	0 Layer 2		3.018	1.16E+04	-6.54E+33
3&4 THICK	1	605	605	0 Layer 2		3.018	1.17E+04	-6.54E+33

Scan#	Vel. Type	v(in/ns)	t(ns)	V(m/s)	ε
345	Core Data	3.307	1.93	8.40E+07	12.76
346	Core Data	3.307	1.891	8.40E+07	12.76
347	Core Data	3.307	1.891	8.40E+07	12.76
348	Core Data	3.307	1.891	8.40E+07	12.76
349	Core Data	3.307	1.891	8.40E+07	12.76
350	Core Data	3.307	1.891	8.40E+07	12.76
351	Core Data	3.307	1.891	8.40E+07	12.76
352	Core Data	3.307	1.891	8.40E+07	12.76
353	Core Data	3.307	1.891	8.40E+07	12.76
354	Core Data	3.307	1.891	8.40E+07	12.76
355	Core Data	3.307	1.891	8.40E+07	12.76

Scan#	Vel. Type	v(in/ns)	t(ns)	V(m/s)	ε
595	Core Data	3.331	1.813	8.46E+07	12.57
596	Core Data	3.331	1.813	8.46E+07	12.57
597	Core Data	3.331	1.813	8.46E+07	12.57
598	Core Data	3.331	1.813	8.46E+07	12.57
599	Core Data	3.331	1.813	8.46E+07	12.57
600	Core Data	3.331	1.813	8.46E+07	12.57
601	Core Data	3.331	1.813	8.46E+07	12.57
602	Core Data	3.331	1.813	8.46E+07	12.57
603	Core Data	3.331	1.813	8.46E+07	12.57
604	Core Data	3.331	1.813	8.46E+07	12.57
605	Core Data	3.331	1.813	8.46E+07	12.57

WARNING: Modification of this ASCII file outside of RADAN may cause
Version = 5　　　　　　unpredictable behavior when this file is reloaded into RADAN.
Data Filename = 5&6PERP.DZT
Layer threshold distance = 32.807999 ft
Number of layers = 2
Amplitude Units = Data Units
Last Pick Settings:
Layer 1　　Vel. Analys　　150　　　　0　　　　1　　　3
Layer 2　　Vel. Analys　　110　　　　0　　　　2　　　3
Calibration file =

File	Ch#	Scan#	x(ft)	y(ft)	Layer 1		z(in)	Amp	Dev(ft)
5&6 REFL	1	665	665	0	Layer 1	0.185	1.06E+04	0
5&6 REFL	1	666	666	0	Layer 1	0.185	1.09E+04	0
5&6 REFL	1	667	667	0	Layer 1	0.185	1.13E+04	0
5&6 REFL	1	668	668	0	Layer 1	0.185	1.17E+04	0
5&6 REFL	1	669	669	0	Layer 1	0.185	1.20E+04	0
5&6 REFL	1	670	670	0	Layer 1	0.185	1.23E+04	0
5&6 REFL	1	671	671	0	Layer 1	0.185	1.26E+04	0
5&6 REFL	1	672	672	0	Layer 1	0.185	1.29E+04	0
5&6 REFL	1	673	673	0	Layer 1	0.185	1.31E+04	0
5&6 REFL	1	674	674	0	Layer 1	0.185	1.34E+04	0
5&6 REFL	1	675	675	0	Layer 1	0.185	1.38E+04	0

File	Ch#	Scan#	x(ft)	y(ft)	Layer 1		z(in)	Amp	Dev(ft)
5&6 REFL	1	535	535	0	Layer 2	3.999	1.25E+04	0.06
5&6 REFL	1	536	536	0	Layer 2	3.999	1.25E+04	0.06
5&6 REFL	1	537	537	0	Layer 2	3.999	1.24E+04	0.05
5&6 REFL	1	538	538	0	Layer 2	3.999	1.25E+04	0.05
5&6 REFL	1	539	539	0	Layer 2	3.999	1.25E+04	0.05
5&6 REFL	1	540	540	0	Layer 2	3.999	1.24E+04	0.05
5&6 REFL	1	541	541	0	Layer 2	3.999	1.24E+04	0.05
5&6 REFL	1	542	542	0	Layer 2	4.083	1.22E+04	0.04
5&6 REFL	1	543	543	0	Layer 2	4.083	1.23E+04	0.04
5&6 REFL	1	544	544	0	Layer 2	4.083	1.22E+04	0.04
5&6 REFL	1	545	545	0	Layer 2	4.114	1.22E+04	0.07

Scan#	% Scans	Vel. Type	v(in/ns)	t(ns)	V(m/s)	ε
665	63.64	Vel. Analys	5.906	-0.063	1.50E+08	4.00
666	66.67	Vel. Analys	5.906	-0.063	1.50E+08	4.00
667	69.7	Vel. Analys	5.906	-0.063	1.50E+08	4.00
668	72.73	Vel. Analys	5.906	-0.063	1.50E+08	4.00
669	75.76	Vel. Analys	5.906	-0.063	1.50E+08	4.00
670	78.79	Vel. Analys	5.906	-0.063	1.50E+08	4.00
671	81.82	Vel. Analys	5.906	-0.063	1.50E+08	4.00
672	84.85	Vel. Analys	5.906	-0.063	1.50E+08	4.00
673	87.88	Vel. Analys	5.906	-0.063	1.50E+08	4.00
674	90.91	Vel. Analys	5.906	-0.063	1.50E+08	4.00
675	93.94	Vel. Analys	5.906	-0.063	1.50E+08	4.00

Scan#	% Scans	Vel. Type	v(in/ns)	t(ns)	V(m/s)	ε
535	81.82	Vel. Analys	4.331	1.813	1.10E+08	7.44
536	78.79	Vel. Analys	4.331	1.813	1.10E+08	7.44
537	75.76	Vel. Analys	4.331	1.813	1.10E+08	7.44
538	72.73	Vel. Analys	4.331	1.813	1.10E+08	7.44
539	69.7	Vel. Analys	4.331	1.813	1.10E+08	7.44
540	66.67	Vel. Analys	4.331	1.813	1.10E+08	7.44
541	63.64	Vel. Analys	4.331	1.813	1.10E+08	7.44
542	60.61	Vel. Analys	4.331	1.852	1.10E+08	7.44
543	57.58	Vel. Analys	4.331	1.852	1.10E+08	7.44
544	54.55	Vel. Analys	4.331	1.852	1.10E+08	7.44
545	51.52	Vel. Analys	4.331	1.852	1.10E+08	7.44

APPENDIX C

Appendix C contains the MATLAB programs used to calculate the dielectric constant values for each of the surveys, along with the thin bed, GPR wavelet, and TDR analysis programs.

```
% Baron Colbert
% Thesis Project

% The name of this file is combo5.m

% This program uses a typical GPR file from the Lac La Belle Site

% This program will take a GPR wavelet and create an estimated
% reflection coefficient graph before and using the GPR wavelet &
% reflection coefficient to make a
% composite wavelet
Figure
a = .039 * (1:512); % Sample time 39 picoseconds and there are 512
traces per GPR scan(time scale)
load waveletLAC.mat
b = wtLAC;
subplot(3,1,1);
plot(a(1:length(wtLAC)),wtLAC)
axis([0 7 -50000 50000])
xlabel('time(picoseconds)')
ylabel('amplitude')
title('Actual GPR Wavelet')% plot of GPR trace with a timescale

% REFLECTION COEFFICIENTS
dc=5; % dielectric constant
deltat= .039; % delta t ns/point
v = 30/sqrt(dc);% velocity in cm/nanoseconds
count = 0;
for x = 1:.5:30,
count = count + 1;
    pc = round((2*x/v)/deltat);

h = zeros(1,pc); % creating an array of 1 row by 512 columns of
zeroes
h(1)=1; % changing the 1st row and 1st column to 1
h(pc)=-1; % changing the 1 row and bth column to -1
subplot(3,1,2);
bar(a(1:length(h)),h,xlabel('time(picoseconds)'),ylabel('amplitude'
),title('Reflection Coefficient')
axis([0 7 -2 2])

% Synthetic GPR Wavelet

final = conv(wtLAC,h); % convolving the bth trace of the GPR data by
the synthetic trace h
Lfinal = length(final); % finds the length of the convolved GPR
trace(number of samples)
deltat2 =(1:Lfinal); % creating a linear matrix for the number of
samples
deltat2 = .039 * deltat2; % changing the matrix into time series (#
of samples by 39 ps per sample)
subplot(3,1,3);
plot(deltat2,final),xlabel('time(nanoseconds)'),ylabel('amplitude'),
title('Composite Waveform')
```

```
axis([0 7 -50000 50000])
text(.5,-30000, 'thickness in cm =')
text(2.2, -30000, num2str(x))
pause(.5)
end
```

```
% Baron Colbert
% Thesis Project

% The name of this file is tdrdata.m


t = 1;
t2 = 1;
t3 = 1;
t4 = 1;

load print32.mat

disp('choose coodinates for viewing')

disp('to end press zero')

plot(print33(:,2)),xlabel('data
number'),ylabel('voltage'),title('TDR Plot of Data')

while t == 1

y1 = input('input start value for x:      ')

y2 = input('input end value for x:        ')

x1 = [y1:y2]';

a = print33(y1:y2,2);

plot(x1,a),xlabel('data number'),ylabel('voltage'),title('TDR Plot
of Data')

t = input('satisfied press 0 if not press 1:                ')

end

disp('minimum voltage is')

plotmin = min(a) ;

disp('maximum voltage is')

time = .01 .* x1 ;

tdrtime = time./7.61 ;

realt = tdrtime .* 10^-9 ;

voltchange = a - plotmin ;
```

```matlab
plotmax = max(voltchange)

close

Figure

plot(x1,voltchange),xlabel('data
number'),ylabel('voltage'),title('plot of data from TDR')

volt68 = ((plotmax - voltchange) .* .68) + voltchange ;

hold on

plot(x1,volt68,'r')

hold off

disp('choose x coodinates to start red chart')

disp('to end press zero')


while t2 == 1

    y2 = input('input start value for x:           ')

    l = length(x1);

    x2 = [y2:(l+y2)-1]' ;

    o = max(x2);

    plot(x1,voltchange,x2,volt68,'r'),xlabel('data
number'),ylabel('voltage'),title('TDR Data Comparison'),legend('TDR
Data','Voltage Change @ 68%')

    t2 = input('satisfied press 0 if not press 1               ')

end

taureal = realt(y2:y2 + (l-y2));

C = taureal./50 ;

close

 flipvolt = -voltchange + -min(-voltchange);

 flip68 = -volt68 + flipvolt(1,1) ;

  disp('choose y coodinate to place data at above zero')
```

104

```matlab
    disp('1 continues choice when satisfied press zero')


plot(x1,flipvolt,x2,flip68,'r'),xlabel('sample
number'),ylabel('Voltage'),title('Plot of Flipped TDR Data vs
Numerical Data'),legend('Voltage Change','Voltage Change @ 68%')

 while t3 == 1

M = input('input y value for  voltage change input 0 for no change:
')

if M == 0
    M = -min(-voltchange)
end

N = input('input addition value for y in the voltage @ 68% red
graph:    ')

N1 = N + flipvolt(1,1)

flipvolt = -voltchange + M;

flip68 = -volt68 + N1;


plot(x1,flipvolt,x2,flip68,'r'),xlabel('sample
number'),ylabel('Voltage'),title('Plot of Flipped TDR Data vs
Numerical Data'),legend('Voltage Change','Voltage Change @ 68%')

t3 = input('satified press 0 if not press 1:               ' )

 end

 while t4 == 1

y3 = input('input start value of volt68 red chart:             ')

l1 = length(x2);

x3 = [y3:(l1+y3)-1]' ;

plot(x1,flipvolt,x3,flip68,'r'),xlabel('sample
number'),ylabel('Voltage'),title('Plot of Flipped TDR Data vs
Numerical Data'),legend('Voltage Change','Voltage Change @ 68%')

t4 = input('satified press 0 if not press 1:             ' )

 end

 close
```

```
f = log(flipvolt + .0000000000000001)   ;

f1 = f >= mean(f) + 2 .* mean(f);

f2 = f <= mean(f) + 2 .* mean(f);

f1 = f1 .* f;

f2 = f2 .* min(f1) ;

f = f1 + f2 ;

b = log(flip68 + .0000000000000001)    ;

time2 = .01 .* x3 ;

tdrtime3 = time2./7.61 ;

realt2 = tdrtime3 .* 10^-9 ;


plot(realt,f,realt2,b),xlabel('time(seconds)'),ylabel('Ln
Voltage'),title('Log Plot of TDR Data Voltage vs Numerical
Data'),legend('Voltage Change','Voltage Change @ 68%')

Figure

plot(realt(1:length(C)),C),xlabel('time(seconds)'),ylabel('Capacitan
ce farads'),title('Capacitance Vs. Time For Sample')

Figure

plot(x1,flipvolt,x3,flip68,'r'),xlabel('sample
number'),ylabel('Voltage'),title('Plot of Flipped TDR Data vs
Numerical Data'),legend('Voltage Change','Voltage Change @ 68%')

 % place graph here of final product with real time
```

```
% How to use gssi3:

%OUTSIDE of this program I
%define the name of the file,
% for example    name=MTU411.dzt'
% then I run this program (enter gssi3)
% then I run the whos command and check the size of the
% array d. If the data are single channel, I
% enter the command  imagesc(d)
% If the data are two channel I run the program "fixd"
% which gives me a panel of 250 MHz data and a panel of
% 400 MHz data. The default color display is pretty nice,
% but you can convert it to grey by entering colorscale(gray)
%
% CTY 06/07/05

%function data=gssi(name)


fid=fopen(name);
rh.tag=fread(fid,1,'ushort');
rh.data=fread(fid,1,'ushort');
rh.nsamp=fread(fid,1,'ushort');
rh.bits=fread(fid,1,'ushort');


rh.zero=fread(fid,1,'short');


rh.sps=fread(fid,1,'float');
rh.spm=fread(fid,1,'float');
rh.mpm=fread(fid,1,'float');
rh.position=fread(fid,1,'float');
rh.range=fread(fid,1,'float');


rh.npass=fread(fid,1,'ushort');


Create.sec2=fread(fid,1,'ubit5');
Create.min=fread(fid,1,'ubit6');
Create.hour=fread(fid,1,'ubit5');
Create.day=fread(fid,1,'ubit5');
Create.month=fread(fid,1,'ubit4');
Create.year=fread(fid,1,'ubit7');


Modify.sec2=fread(fid,1,'ubit5');
Modify.min=fread(fid,1,'ubit6');
Modify.hour=fread(fid,1,'ubit5');
Modify.day=fread(fid,1,'ubit5');
Modify.month=fread(fid,1,'ubit4');
Modify.year=fread(fid,1,'ubit7');


rh.rgain=fread(fid,1,'ushort');
rh.nrgain=fread(fid,1,'ushort');
rh.text=fread(fid,1,'ushort');
rh.ntext=fread(fid,1,'ushort');
rh.proc=fread(fid,1,'ushort');
rh.nproc=fread(fid,1,'ushort');
```

```
rh.nchan=fread(fid,1,'ushort');

rh.epsr=fread(fid,1,'float');
rh.top=fread(fid,1,'float');
rh.depth=fread(fid,1,'float');

reserved=fread(fid,31,'char');
rh.dtype=fread(fid,1,'char');
rh.antname=fread(fid,14,'char');
rh.chanmask=fread(fid,1,'ushort');
rh.name=fread(fid,12,'char');
rh.chksum=fread(fid,1,'ushort');
%rh.var=setstr(fread(fid,896,'char'));
rh.Gain=fread(fid,1,'ushort');
rh.Gainpoints=fread(fid,rh.Gain,'float');
rh.comments=setstr(fread(fid,rh.ntext,'char'));
rh.proccessing=fread(fid,rh.nproc,'char');

fseek(fid,0,'bof');
fseek(fid,1024,'bof');

d=fread(fid,[rh.nsamp inf],'ushort');
%d(1,:)=d(3,:); %is this a byteswap?
%d(2,:)=d(3,:);
d=d+rh.zero;

data.head=rh;
data.samp=d;
fclose(fid);
```

```matlab
% The name of this program is called cllickerplot.m

% This program finds where the click marks over the roadway cores
% are located

% how to get odometer and clicker marks out of a GSSI file
% for example
name='mtulac2.dzt'; % the 1000 MHz data
gssi3 % read the data
% the odometer click and manual clicker are in the second element of
each trace
clicker=d(2,:)==26624; %the clicker bit
odometer=d(2,:)==25600; %the odometer clickerbit
Figure
subplot(2,1,1)
plot(clicker)
ylabel('clicker location')
subplot(2,1,2)
plot(odometer)
ylabel('odometer click')
xlabel('trace number')
y = clicker .* [1:length(clicker)];
z = find(y);
disp('The specific radar traces for')
disp('')
disp(name)
disp('')
disp('which were marked are:')
disp('')
disp(z)
```

```
% Baron Colbert
% GE 5515
% This is an automatic function selector for the minimum amplitude
for
% each specifically picked trace
% The name of this program is called autopicklayers3.m




name = input('Enter file name : ','s');
    %function data=gssi(name)


fid=fopen(name);
rh.tag=fread(fid,1,'ushort');
rh.data=fread(fid,1,'ushort');
rh.nsamp=fread(fid,1,'ushort');
rh.bits=fread(fid,1,'ushort');

rh.zero=fread(fid,1,'short');

rh.sps=fread(fid,1,'float');
rh.spm=fread(fid,1,'float');
rh.mpm=fread(fid,1,'float');
rh.position=fread(fid,1,'float');
rh.range=fread(fid,1,'float');

rh.npass=fread(fid,1,'ushort');

Create.sec2=fread(fid,1,'ubit5');
Create.min=fread(fid,1,'ubit6');
Create.hour=fread(fid,1,'ubit5');
Create.day=fread(fid,1,'ubit5');
Create.month=fread(fid,1,'ubit4');
Create.year=fread(fid,1,'ubit7');

Modify.sec2=fread(fid,1,'ubit5');
Modify.min=fread(fid,1,'ubit6');
Modify.hour=fread(fid,1,'ubit5');
Modify.day=fread(fid,1,'ubit5');
Modify.month=fread(fid,1,'ubit4');
Modify.year=fread(fid,1,'ubit7');

rh.rgain=fread(fid,1,'ushort');
rh.nrgain=fread(fid,1,'ushort');
rh.text=fread(fid,1,'ushort');
rh.ntext=fread(fid,1,'ushort');
rh.proc=fread(fid,1,'ushort');
rh.nproc=fread(fid,1,'ushort');
rh.nchan=fread(fid,1,'ushort');

rh.epsr=fread(fid,1,'float');
rh.top=fread(fid,1,'float');
```

```
rh.depth=fread(fid,1,'float');

reserved=fread(fid,31,'char');
rh.dtype=fread(fid,1,'char');
rh.antname=fread(fid,14,'char');
rh.chanmask=fread(fid,1,'ushort');
rh.name=fread(fid,12,'char');
rh.chksum=fread(fid,1,'ushort');
%rh.var=setstr(fread(fid,896,'char'));
rh.Gain=fread(fid,1,'ushort');
rh.Gainpoints=fread(fid,rh.Gain,'float');
rh.comments=setstr(fread(fid,rh.ntext,'char'));
rh.proccessing=fread(fid,rh.nproc,'char');

fseek(fid,0,'bof');
fseek(fid,1024,'bof');

d=fread(fid,[rh.nsamp inf],'ushort');
%d(1,:)=d(3,:); %is this a byteswap?
%d(2,:)=d(3,:);
d=d+rh.zero;

data.head=rh;
data.samp=d;
fclose(fid);



whos d

a = input('input number of traces per scan:             ')
b = input('input number of scans:                       ')

lay1 = input('do you want one layer? input 1 for yes 2 for no:     ')

if lay1 == 1



     % Picking Points from AGC Image
u = [1:b]';
     n = 1 ;



m = 1 ;
imagesc(d)
starty = input('where should autopicker start y coord:       ')
close all
for t = 1:b ;
```

111

```
    maxnum(m) = min((d(starty:a,t))); % minimum value function for
files
    tracenum(m) = u(t,1) ;

            y = (d(starty:a,u(t,1))) == maxnum(m);
            z =   (starty:a)' .*y ;
        indices = find(z)
     v =   size(indices);


        if v(1,1) > 1 ;

            figure
            bar(indices)
         pick = input('input index to use:              ')
         zo(m) = pick ;
         close all
        else

            zo(m) = find(z);

        end


  maxamp(m,1) = tracenum(m);

  maxamp(m,2) = maxnum(m);

        m = m + 1;



        maxamp;

end

ab = zo ~= min(zo);
ab = ab .* zo;
bc = find(ab);
ab  = nonzeros(ab);


subplot(3,1,1)
plot(maxamp(:,1),maxamp(:,2)),title('Plot of Maximum Amplitude Value
Vs. Seismic Trace'),xlabel('trace'),ylabel('Amplitude'),grid
subplot(3,1,2)
plot(bc,ab,'*'),title('Plot of Trace Point Vs. Trace Number'),
xlabel('trace'),ylabel('trace point')
subplot(3,1,3)
imagesc(d),title('GPR Image of Pavement Samples'),xlabel('Trace
Number'),ylabel('trace point')
```

```
figure
plot(maxamp(:,1),zo,'*'),title('Original Plot of Trace Point Vs.
Trace Number'), xlabel('trace'),ylabel('trace point')

else

end



% for second layer

lay2 = input('do you want to input two layers?    1 for yes, 2 for no
')

if lay2 == 1

figure

imagesc(d)
disp('zoom in to where second layer is')

disp('input y locations of boundary around second layer')

seconda = input('input top boundary location:              ')
secondb = input('input bottom boundary location:           ')


m = 1;

u2 = [seconda:secondb]' ;

n = 1 ;

for sec = 1:b

    secmax(m) = min(d(seconda:secondb,sec));
    y2 = d(seconda:secondb,sec) == secmax(m);
          z2 =  d(seconda:secondb,sec) .* y2 ;
        indices2 = find(z2)


      v2 =  size(indices2);


          if v2(1,1) > 1 ;

              figure
              bar(indices2)
            pick2 = input('input index to use:              ')
            zo2(m) = pick2 + seconda ;
             close all
            else
```

113

```
                  zo2(m) = find(z2)+ seconda;

          end


          m = m + 1 ;
end

if lay1 == 1

subplot(2,1,1)
plot(bc,ab,1:b,zo2,'*'),title('Plot of Trace Point Vs. Trace
Number'),  xlabel('trace'),ylabel('trace point')
subplot(2,1,2)
imagesc(d),title('GPR Image of Pavement Samples'),xlabel('Trace
Number'),ylabel('trace point')

elseif lay1 == 2

subplot(2,1,1)
plot(1:b,zo2),title('Plot of Trace Point Vs. Trace Number'),
xlabel('trace'),ylabel('trace point')
subplot(2,1,2)
imagesc(d),title('GPR Image of Pavement Samples'),xlabel('Trace
Number'),ylabel('trace point')

else

end

end


layref = input('do you want to use reflection coefficients 1 for yes
2 for no:        ')

% Reflection Coefficint Correction

if layref == 1

    figure

    subplot(2,1,1)
plot(maxamp(:,1),maxamp(:,2)),title('Plot of Maximum Amplitude Value
Vs. Seismic Trace'),xlabel('trace'),ylabel('Amplitude'),grid
subplot(2,1,2)
plot(ab,'*'),title('Plot of Trace Point Vs. Trace Number'),
xlabel('trace'),ylabel('trace point')


whos ab
b1x = input('input start of first sample:            ')
```

```
b2x = input('input end of first sample:                ')

c1x = input('input start of second sample:            ')
c2x = input('input end of second sample:              ')


bx = [b1x:b2x];
cx = [c1x:c2x];

bx = ab(bx)+ starty;
cx = ab(cx)+ starty ;

by = - 0.316.*bx.^(2) - 45.9.*bx + 3.87e+004 ;
cy = - 7.7286e-006.*cx.^(5) + 0.0052152.*cx.^(4) - 1.3747.*cx.^(3) +
176.19.*cx.^(2) - 11059.*cx +  3.0528e+005;


RCb =  maxamp(b1x:b2x,2)./by;

RCc = maxamp(c1x:c2x,2)./cy;

else

end
```

APPENDIX D

Appendix D contains the dielectric constant values of the TDR samples, C_{theory} is capacitance calculated from a parallel plate capacitor assuming an air dielectric $\varepsilon = 1$, $C_{theory} = \dfrac{A\varepsilon}{d}$ where C is capacitance, A is plate area, and d is sample thickness.

TDR capacitance is the value of capacitance taken from the TDR and ε using C/ C_{theory} is dielectric constant calculated by taking the ratio of TDR capacitance vs. the C_{theory} value.

PAVEMENT SAMPLE	ε using C/Ctheory	ε using TDR air dielectric values	Air Dielectric Check $CTDR_{air}/Ctheoretical$
US 127 MASON 3C	4.15	10.17	0.41
US 127 MASON B2	2.35	1.28	1.83
US 127 MASON A	16.36	3.77	4.34
US 131 E	10.42	3.52	2.96
US 127 MASON E	5.86	2.21	2.65
US 127 MASON E	2.82	1.06	2.65
US 12 Mich Ave D	8.91	3.51	2.54
US 12 Mich Ave A	5.57	1.33	4.18
US 12 Mich Ave B	5.33	3.35	1.59
US 12 Mich Ave F	4.52	1.16	3.89
US 12 Mich Ave C	1.43	0.76	1.89
US 12 Mich Ave E	4.92	2.48	1.98
US 131 BG Rapids A	4.99	1.68	2.97
US 131 BG Rapids B	5.17	1.37	3.78
US 131 BG Rapids C	5.31	1.90	2.80
US 131 BG Rapids D	5.47	2.38	2.30
US 127 MASON E	5.04	1.59	3.17
M84 Saginaw 3B	51.28	10.55	4.86
1	1.50	2.49	0.62
2	1.81	2.78	0.62
3	1.32	1.74	0.62
4	1.95	2.38	0.62
5	1.70	2.20	0.62
6	1.16	1.50	0.62
7	1.83	2.95	0.62

PAVEMENT DIELECTRIC	slope	TDR Capacitance	Theoretical Capacitance
US 131 E	8.93E+09	1.12E-10	3.59E-12
US 131 BG Rapids A	9.23E+09	1.08E-10	5.21E-12
US 131 BG Rapids B	7.80E+09	1.28E-10	3.91E-12
US 131 BG Rapids C	9.04E+09	1.11E-10	4.47E-12
US 131 BG Rapids D	5.65E+09	1.77E-10	5.69E-12
M84 Saginaw A	1.15E+10	8.68E-11	2.00E-12
M84 Saginaw 3B	1.37E+10	7.28E-11	1.65E-12
1	9.19E+09	1.09E-10	2.77E-11
2	5.38E+09	1.86E-10	2.57E-11
3	5.01E+09	2.00E-10	2.20E-11
4	6.26E+09	1.60E-10	2.04E-11
5	5.80E+09	1.72E-10	2.16E-11
6	5.75E+09	1.74E-10	2.15E-11
7	7.28E+09	1.37E-10	2.69E-11
US 127 MASON 3C	1.04E+10	9.62E-11	6.26E-12
US 127 MASON B2	1.18E+10	8.44E-11	6.26E-12
US 127 MASON A	8.55E+09	1.17E-10	5.21E-12
US 127 MASON E	1.11E+10	9.02E-11	3.91E-12
US 127 MASON E	6.89E+09	1.45E-10	5.69E-12
US 127 MASON E	1.83E+10	5.46E-11	5.69E-12
US 12 Mich Ave D	8.52E+09	1.17E-10	4.47E-12
US 12 Mich Ave E	8.13E+09	1.23E-10	4.47E-12
US 12 Mich Ave B	8.29E+09	1.21E-10	3.91E-12
US 12 Mich Ave C	1.26E+10	7.93E-11	4.47E-12
US 12 Mich Ave F	9.96E+09	1.00E-10	3.91E-12
US 12 Mich Ave A	8.14E+09	1.23E-10	4.81E-12

| Air Dielectric Sample	Sample Thickness	slope	TDR Air Capacitance Value
US 127 MASON 3C	2.9 cm	7.83E+09	1.28E-10
US 127 MASON B2	3.5 cm	6.96E+09	1.44E-10
US 127 MASON A	3.5 cm	7.61E+09	1.31E-10
US 127 MASON E	3.5 cm	1.11E+10	9.02E-11
US 127 MASON E	3.5 cm	1.14E+10	8.79E-11
US 127 MASON E	3.0 cm	1.03E+10	9.67E-11
US 12 Mich Ave D	3.5 cm	5.02E+08	3.98E-11
US 12 Mich Ave E	4.0 cm	1.47E+10	6.78E-11
US 12 Mich Ave B	4.0 cm	1.27E+10	7.86E-11
US 12 Mich Ave C	4.0 cm	1.18E+10	8.49E-11
US 12 Mich Ave F	3.5 cm	1.21E+10	8.24E-11
US 12 Mich Ave A	3.0 cm	7.49E+09	1.34E-10
US 131 E	4.0 cm	1.40E+10	7.15E-11
US 131 BG Rapids A	4.0 cm	9.23E+09	1.08E-10
US 131 BG Rapids A	4.0 cm	1.65E+10	6.07E-11
US 131BG Rapids B	3.0 cm	5.47E+09	1.83E-10
US 131 BG Rapids C	4.0 cm	1.23E+10	8.13E-11
US 131 BG Rapids D	3.5 cm	8.91E+09	1.12E-10
M84 Saginaw 3B	9.5 cm	2.37E+08	8.44E-11
M84 Saginaw A	7.5 cm	1.71E+08	1.17E-10
Samples 1-7	1.0 cm	4.51E+09	2.22E-10

APPENDIX E

Thin Bed Considerations

The thin roadway layers present at the Lac La Belle and M-26 sites hampered determining the dielectric constant at these sites, therefore I attempted to determine whether the roadway layer was so thin that the reflection from the top and bottom merged, thus making the determination of reflection amplitude inaccurate. This problem is known as the "thin bed problem" in Widess(1973). According to Widess (1973), a thin bed is defined as a bed whose thickness is less than $\lambda_b/8$, where λ_b of a GPR wavelet is the dominant wavelength within the roadway. A sample calculation for the determination of thin pavement layers according to Widess is as follows using the GPR wavelengths, GPR velocity within pavement and in air. For this GPR study

the wavelength in air is $\lambda_b = \dfrac{c}{frequency} = \dfrac{3*10^8 \frac{m}{s}}{1*10^9 \ hz} = 29.98$ cm. Therefore a thin

bed is characterized as any pavement less than about

29.98 cm /8 = 3.75 cm. Using this definition and comparing the pavement thicknesses with those shown in Appendix A, core locations 2,3,5,7,8, & 11 at the M-26 site as well as the Lac La Belle site would qualify as being thin beds since the pavement cores were less than about 3.75 cm. To address this thin bed problem I used metal plate calibration files from the GSSI along with GPR pavement surface amplitudes to find dielectric constant values at these sites. MATLAB was used to automatically determine at what pavement thickness a thin bed would be encountered. This program was implemented using actual GPR waveforms from the M-26 and Lac La Belle sites to determine the roadway thicknesses that would allow reflections from the top and

bottom of the layer to be visible. The computation consists of creating an impulse

response of a thin layer separated by the two way travel time of the layer. This

impulse response is convolved with an actual wavelet taken from a radar trace. The

result of Combo5.m shows the composite waveform which will reveal whether or not

the top and bottom of the layer can be resolved. The wavelets for the Lac La Belle,

M-26, and Five Mile Point Road sites are given in Figures 1 to 3 shown below.
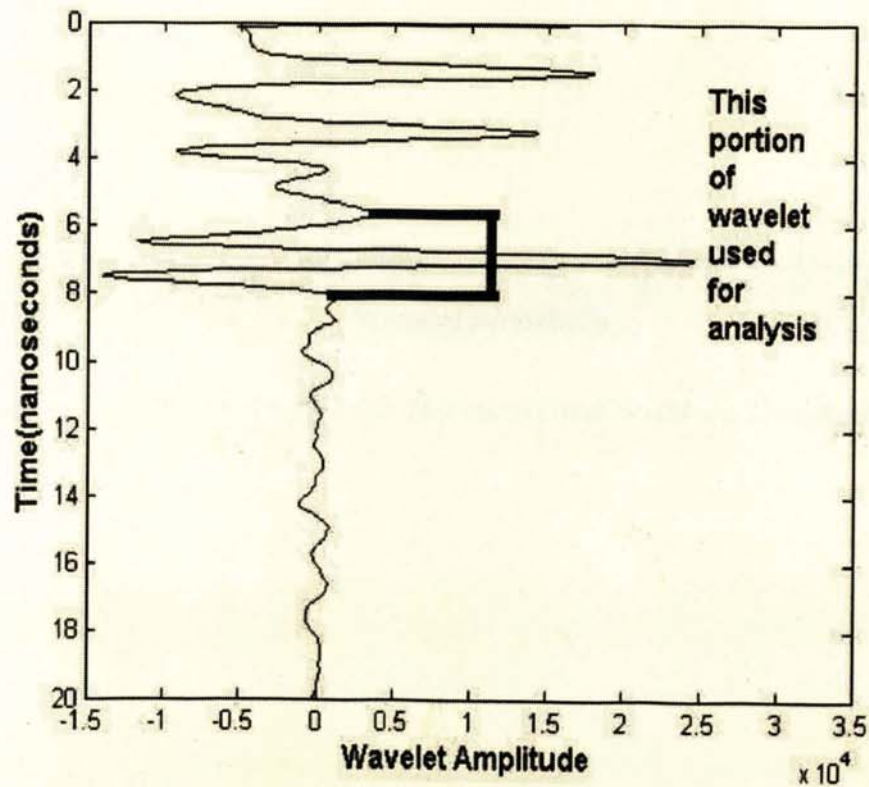
Figure 1: GPR wavelet of trace 540 taken from the Lac La Belle Site
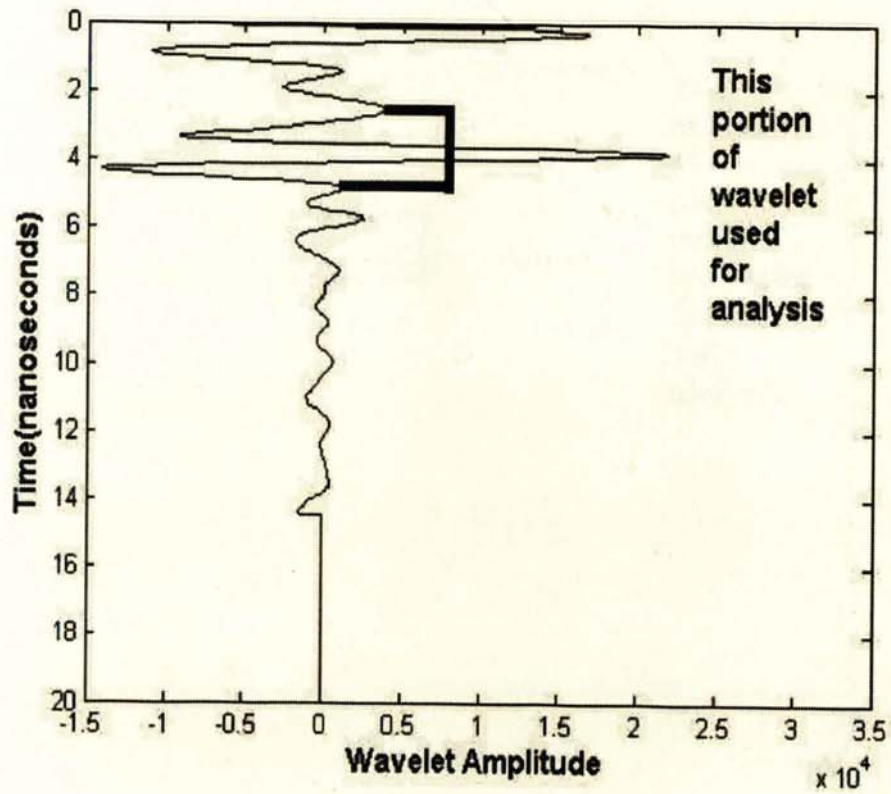
Figure 2: GPR wavelet of trace 540 taken from the M-26 Twin Lakes site
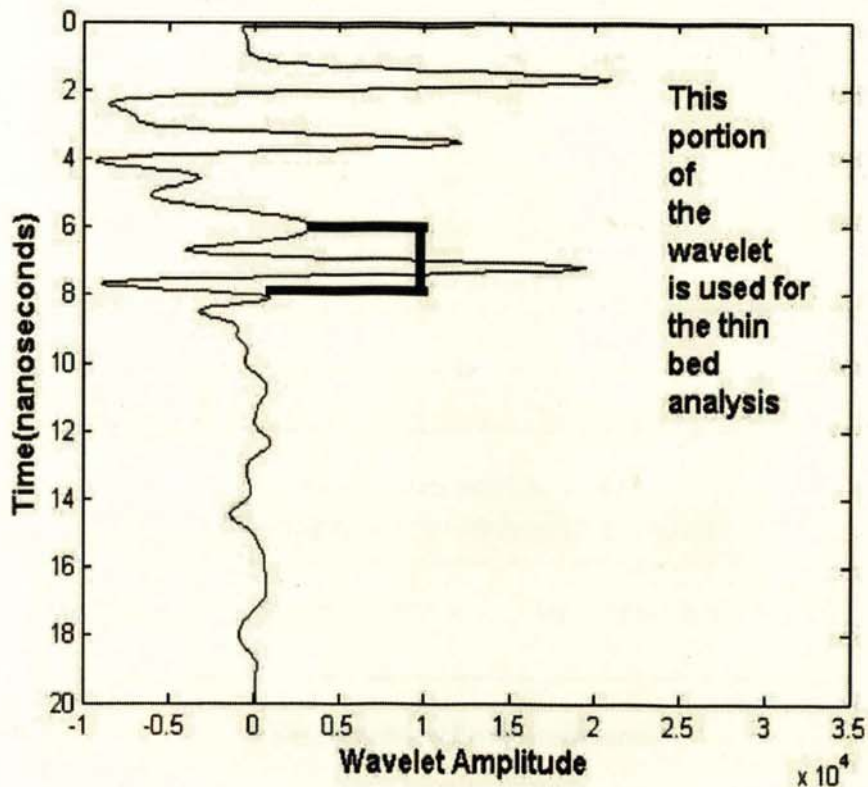
Figure 3: GPR wavelet of trace 362 taken from the Five Mile Point Road

site

Figures 1 to 3 show the sample wavelet taken from each of the sites, the impulse response, and the composite waveforms at each site. Following Widess' example, I created synthetic radargrams using actual radar wavelets from field data. Using the sample rate of the Radan Roadway Software of 39 nanoseconds/sample, the use of actual radar wavelets recorded from each site, and the pavement velocities of nearly 1/3 the speed of light within the pavement, thin bed criterion could be established for each site. Thus, the results from this thin bed analysis program show that the minimum thickness one needs to distinguish a pavement layer from the GPR trace is approximately seven centimeters or 2 ½ inches as shown from Figure 4 to 6.

Figure 4: Composite Wavelet Chart showing the minimum distance where two waveforms are completely separated in time for the Lac La Belle site
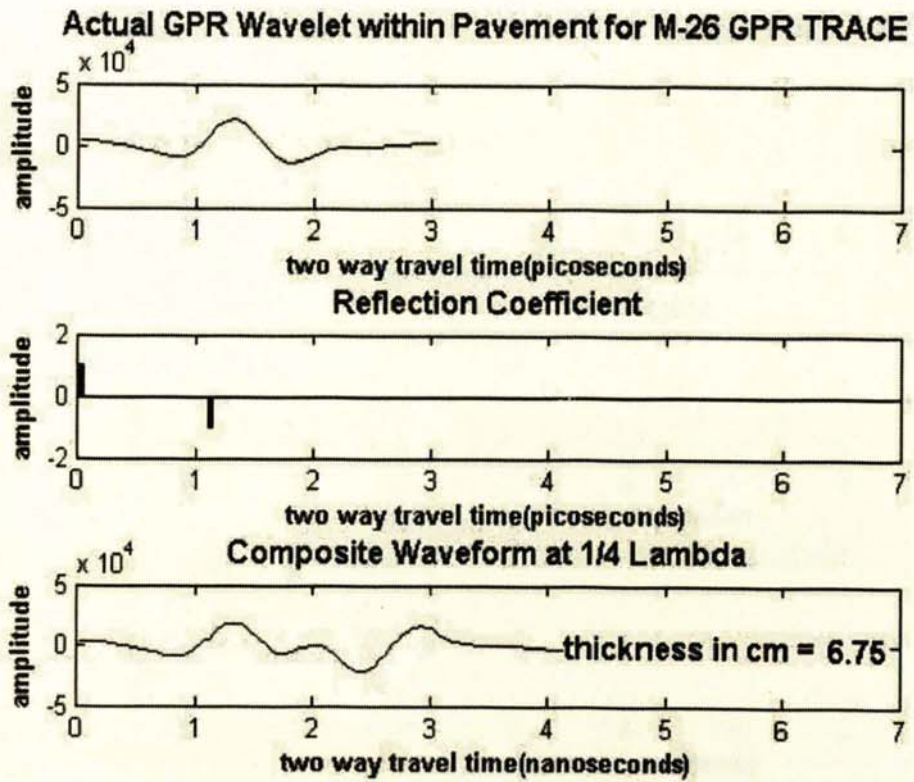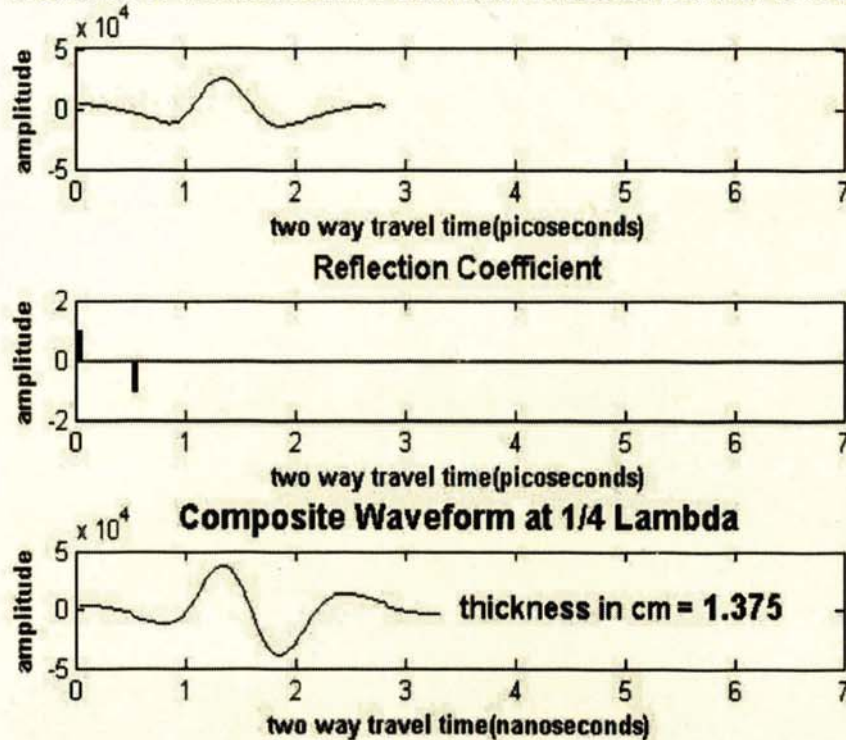
Figure 5: Composite Wavelet Chart showing the minimum distance where two waveforms are completely separated for the M-26 / Twin Lakes site

Actual GPR Wavelet within Pavement for Lac La Belle GPR TRACE

Reflection Coefficient

Composite Waveform at 1/4 Lambda

Figure 6: Composite Wavelet Chart encompassing the entire upper and lower pavement interfaces for greater resolution at the Lac La Belle site.

Thus, the M-26 and the Lac La Belle Road sites would marginally qualify as sites that may have thin bed considerations due to their thickness measurement being less than $\lambda/8$ or $\lambda = \dfrac{c/1*10^9}{8} = \dfrac{}{8} = 3.75cm$. Also the fact the reflections from the top and bottom of the layer are beginning to merge indicates that the bed is "very thin". To overcome this problem the steps taken in the analysis section as suggested in the Widess (1975) study the entire bed encompassing both upper and lower interfaces may have to be considered together in order to greatly increase the resolving power for the GPR trace.